On the Numerical Simulation of Friction-Isolated Structures

A Thesis submitted to the
Civil Engineering Department of
Wuppertal University

In Partial Fulfilment of the Requirements for the
Degree of
Doctor of Philosophy

By

Navid Jamali

2008

Reibungs-Pendelsysteme als Mittel zur Basisisolation von Bauwerken

Dissertation

zur

Erlangung des Akademischen Grades
Doktor-Ingenieur (Dr. –Ing.)

der

Abteilung Bauingenieurwesen
im Fachbereich D an der
Bergischen Universität Wuppertal

von

Navid Jamali

2008

Veröffentlicht als Heft 12 in der Schriftenreihe des
Instituts für Konstruktiven Ingenieurbau
Fachbereich D, Abteilung Bauingenieurwesen
Bergische Universität Wuppertal

Herausgeber

Der Geschäftsführende Direktor
Institut für Konstruktiven Ingenieurbau
Bergische Universität Wuppertal

Fachgebiet

Baumechanik und numerische Methoden
Univ.-Prof. Dr.-Ing. Wolfhard Zahlten
Fachbereich D, Abteilung Bauingenieurwesen
Bergische Universität Wuppertal

Organisation und Verwaltung

Dipl.-Ing. W. Hammer
Institut für Konstruktiven Ingenieurbau
Bergische Universität Wuppertal
Pauluskirchstraße 7
42285 Wuppertal
Telefon: (0202) 439-4209

Gedruckt mit Unterstützung des Deutschen Akademischen Austauschdienstes

ISBN 978-3-940795-11-3

Abstract

In spite of considerable developments and modifications of earthquake-resistant design methods and much more conservative building norms, massive death and destructions have been reported after several great earthquakes in recent years. High developed countries are susceptible to earthquakes as well, as for example the unprecedented economical loss of Kobe earthquake (Japan, 1995).

Seismic building norms are mainly *life-safety* oriented. Providing a sufficient plastic reserve by a ductile design concept to guarantee the structural *serviceability* after a severe shaking has been proved to be very difficult to be implemented. In an alternative method, based on the concept of reduction of the earthquake-induced forces, structural properties are modified, instead of providing additional strength and stiffness. In *friction pendulum isolated systems* this can be done by means of several bearings sliding over concave contact surfaces, which are decoupling the system from its foundation.

In this study a numerical model is developed to simulate the response of such an isolated structure. First, assuming a rigid structural response, a one-degree-of-freedom model has been applied to simulate the response of a sliding bearing. The model is then improved to a two-degree-of-freedom system, to consider the interaction effect between a sliding bearing and the structure over it. Finally, a general multi-degree-of-freedom planar model is developed, in which several extra degrees-of-freedom, regarding the number of the isolators in the set, are activated, as soon as the set starts sliding. By sticking of some bearings, the corresponding degrees of freedom are deactivated. Hence, there are different system configurations in sticking and sliding phases. This makes the exact prediction of all phase changes during an analysis very important. By means of a developed adaptive time digitization algorithm extremely short time steps would be applied only in the case of possibility of a phase change. In this way numerical costs of the analysis can be reduced. As the nonlinearity of the response of such a system is only restricted to phase changes between time steps and in every single time step system properties do not change, modal analysis has been used to solve the set of differential equations, so that only the first few mode shapes governing the main part of the structural response are required to be considered. Results are then transformed back into the original space to be evaluated. To verify the numerical model, several practical cases have been simulated. Results are then compared with those reported in literature.

Zusammenfassung

In den letzten Jahren sind viele Entwicklungen und Fortschritte im Bereich erdbebensicheres Bauen gemacht worden. Trotzdem hat in den vergangenen Jahren manch verheerendes Erdbeben, wie zum Beispiel in Bam (Iran, 2003) oder Kaschmir (Pakistan, 2005) massive Zerstörungen angerichtet. Das geschieht nicht nur in den Entwicklungsländern, sondern auch in den hoch entwickelten Ländern wie Japan, beispielsweise das Erdbeben in Kobe (1995).

Die Normen sind meistens ‘‘*life-safety*’’ orientiert. Das führt dazu, dass die Sanierung wegen des Schadensniveaus unwirtschaftlich oder gar unmöglich ist. Es gibt zwei Strategien um die Funktionalität eines Gebäudes im Falle eines Erdbebens erhalten zu können:

Nach der klassischen Strategie wird versucht durch plastische Reserve die Tragfähigkeit des Systems zu gewährleisten. Zahlreiche Gebäude, die nach diesem Prinzip konzipiert sind, haben in der Vergangenheit einer Erdbebenbelastung nicht standgehalten. Das war zum Beispiel auf Ausführungsmängel und geringe Baustoffqualität zurückzuführen.

Alternativ dazu versucht man durch gezielte konstruktive Maßnahmen die dynamischen Systemeigenschaften zu verändern, so dass die Erdbebenkräfte dissipiert bzw. reduziert werden können. Eine mögliche Maßnahme ist die Basisisolation. Dabei wird das Gebäude durch spezielle Lager, zum Beispiel Elastomerlager oder Reibelemente von den Fundamenten entkoppelt.

Sogenannte *Reibpendelelemente* sind spezielle Lager, die zur Basisisolation von Gebäuden eingesetzt werden. Sie besitzen eine gekrümmte Oberfläche um eine Zwangszentrierung der Lager zu gewährleisten. Ihre Oberfläche ist mit einer speziellen Beschichtung versehen, die den Reibungskoeffizient minimiert. Sobald die durch ein Erdbeben induzierten Kräfte den statischen Reibungswiderstand des Lagers überschreiten, lässt das Lager ein Gleiten des Gebäudes gegenüber dem Baugrund zu. In der vorliegenden Arbeit wird ein numerisches Modell zur Simulation von Systemen mit einem Reibpendellager entwickelt. Zunächst wurde ein einfreiheitsgerades System benutzt, wobei das Verhalten des Gebäudes starr angenommen wird. Um die Wechselwirkung zwischen der Struktur und dem Lager zu berücksichtigen, wurde ein zweifreiheitsgerades System verwendet. Anschließend ist ein MDOF Planarmodell entwickelt worden, in dem mehrere zusätzliche Freiheitsgerade aktiviert werden, sobald das System anfängt zu gleiten. Die zusätzliche Freiheitsgerade dient dazu, die Reibelemente in Gleit-Phasen zu simulieren. Sobald das System wieder haftet, werden diese Elemente deaktiviert. Das Modell wird bezüglich des numerischen Aufwands optimiert. Um das numerische Modell zu verifizieren, mehrere praktische Anwendungen wurden mit diesem Modell simuliert.

Acknowledgements

This research has been conducted as a PhD thesis at the *Bergische Universität Wuppertal* in *Civil Engineering Department*, *Structural Mechanics chair*.

This study has been financed by the *German academic exchange service* (DAAD). I would like to appreciate it gratefully. A six-month language course in Göttingen by Goethe Institute was included in the award as well. It made a pleasant residence and integration in the new society possible.

Professor Georg Pegels was my first contact with Wuppertal University and actually motivated this research. I would like to appreciate his supports. Furthermore, continuous support and contributions of my supervisor Professor Wolfhard Zahlten, head of Structural Mechanics chair are gratefully acknowledged. A great scientific atmosphere in the department was an extra motivation for me during the period that I was doing my PhD thesis.

I would like to express my gratitude to Professor Reinhard Harte and Professor Jamshid Parvizian, members of thesis committee, for their interest and helpful suggestions.

I would like to thank my colleague and friend Christian Neuhaus for sharing his enthusiasm and comments on my work. I am also very grateful to the secretary of the department Beate Nietzold for her willingness to help and kindness.

Last but not the least; I would like to thank especially my parents because of their permanent love and support.

Wuppertal, August 2008

Navid Jamali

Submitted on:	30.01.2008
Oral examination:	20.05.2008
Reviewed by:	Univ.-Prof. Dr.-Ing. W. Zahlten
	Univ.-Prof. Dr.-Ing. R. Harte
	Prof. J. Parvizian
Head of thesis committee:	Univ.-Prof. Dr.-Ing. G. Pegels

Contents

List of Symbols

General

$\{..\}_b$	Base (foundation) property
$\{..\}_s$	Structural property
$\{..\}_{rel}$	Relative value
$\{..\}_{tot}$	Total (absolute) value
c	Damping
γ	Mass ratio
Γ, λ	Participation factor
DE	Dissipated energy
ε	Squared frequency ratio
ξ	Damping ratio
IE	Input seismic energy
KE	Kinetic energy
k	Stiffness
m	Mass
SE	Strain energy
u	Relative sliding displacement
$\dot{u}$	Relative sliding velocity
$\ddot{u}$	Relative sliding acceleration
$\ddot{u}_g$	Gravitational acceleration
$\mathbf{\Phi}$	Matrix of Eigenvectors
ω	Natural circular frequency of vibration
ω_d	Damped circular frequency of vibration

Friction

F_f	Friction force
$f_{\min}$	Maximum friction coefficient (modified Coulomb model)
$f_{\max}$	Minimum friction coefficient (modified Coulomb model)
α	Rate control parameter
μ	Friction coefficient (Coulomb model)
β	Viscoplasticity dimensionless parameter
γ	Viscoplasticity dimensionless parameter
sign(..)	Signum function
tanh(..)	Hyperbolic tangent function
$\dot{u}$	Sliding velocity
W	Weight
Y	Yield displacement
Z	Hysteretic dimensionless parameter (viscoplasticity model)

Friction Pendulum Systems

$\{..\}^{i-1}$	Known value at the previous time step
$\{..\}^{i}$	Unknown value at the current time step
$\{..\}_0$	Initial condition
A	Cross sectional area
α	Mass ratio
$\mathbf{C}$	Damping matrix
δ	Sliding displacement
E	Young's module
F	Resultant force in a sliding bearing
F_R	Restoring (recentering) force
g	Gravitational acceleration
i	Time step
I	Moment of inertia

$\mathbf{K}$	Stiffness matrix
$k_{eq.}$	Equivalent stiffness
L	Length of an element
L_W	Input influence matrix
$\mathbf{M}$	Mass matrix
$\hat{n}$	Normal unitary vector
$\xi_{eq.}$	Equivalent damping
$\mathbf{P}$	Nodal kinetic transformation matrix
$\mathbf{P}(t)$	Load vector in time domain
$\mathbf{P}_g$	Matrix of inertial force due to the ground acceleration
$\mathbf{q}, \mathbf{s}$	Structural degree-of-freedom
$\mathbf{Q}$	Vector of nonlinear restoring force
R	Radius of curvature of the sliding surface
ρ	Density
$\hat{\mathbf{s}}$	Tangent unitary vector
S_a	Spectral relative acceleration
S_d	Spectral relative displacement
S_v	Spectral relative velocity
S_{pa}	Pseudo-acceleration spectral value
S_{pv}	Pseudo-velocity spectral value
Δt	Time step
T	Period of vibration of friction pendulum systems
φ	Oscillation angle
Ω	Load frequency
W_d	Dissipated energy
W_k	Spring potential energy
Z	Vertical displacement of a sliding bearing

Chapter 1

Motivation

In this chapter, firstly a short review of devastating earthquakes in the last century is given. Then, three main design concepts are introduced. Disadvantages of these classical concepts are discussed. In an alternative design concept, active and passive control methods are then introduced. Afterwards, the significance of this study is briefly discussed and the aims of this study are reviewed. Finally, the outline of the dissertation is presented.

1.1 Introduction

Earthquake-resistant design is a challenging task for civil engineers. Although building codes of praxis have become more detailed and conservative, severe damages have been reported to modern buildings after several strong earthquakes in recent years. A list of strong earthquakes with fatalities larger than 1000 is given in Appendix *A*. It shows that an average of almost 19000 persons were killed yearly due to earthquakes. Earthquakes' aftermath are also usually disastrous, namely *conflagrations*, *landslides*, and *tsunamis*.

Building code provisions based on different design methods pursue two main goals: Firstly to provide a low probability of failure under all likely load combinations through prescription of a minimum required level of structural *strength*; and secondly, a minimum *stiffness* must be available to restrict deflections; so that the structure remains *serviceable* [Chen and Scawthorn, 2003].

Main design methods are *conventional*, *capacity*, and *performance-based design methods*. In conventional methods, buildings are designed to remain elastic in their life-time under all possible load combinations. This leads to an uneconomical design for structures in regions with high seismic risk. In capacity design methods, however, some plastic hinges are allowed to be produced in predefined locations. Through plastic deformations (damage) it is possible to dissipate excitation energy to some extent.

Current building code provisions are *prescriptive* in nature. They require that buildings are designed with a minimum specified strength and stiffness. In contrary to them, performance based procedures permit the designer to demonstrate directly that a design is capable of meeting prescriptive strength and stiffness criteria. An acceptable performance may be demonstrated through a variety of means, including prototype testing or analytical simulations [Chen and Scawthorn, 2003].

Seismic codes are mainly *life-safety* oriented. At least for residential buildings they do not define *serviceability* and *functionality* of a structure after an earthquake with the same priority as life-safety. High damage levels in structures after earthquakes make it impossible (or uneconomical) to retrofit them.

To maintain structural functionality after severe shakings different strategies are available. In traditional methods, by providing a reserve stiffness and ductility in the system the serviceability after an earthquake is guaranteed. The collapse ofnumerous modern structures in recent earthquakes showed that it is very difficult to provide such a reserve capacity. Flawed implementations, poor material quality, corruption, and lack of supervision are the main reasons for shortcomings of this strategy. This motivated the designer to develop control systems (active and passive) to modify structural features in case of major ground shakings. The dependency of active systems on additional controlling software and hardware make their application restricted to rare special structures. In contrast to them, passive systems as base isolated systems and tuned mass dampers do not require any additional controlling mechanism, which makes them more attractive for engineers.

1.2 Motivation

Iran's plateau is located in a very active seismic zone along the *Alpine-Himalayan mountain belt* between the *Indian*, *Arabian*, and *Eurasian* plates (Figure 1.1) [Berberian]. Several devastating earthquakes in Iranian history have been registered with tens of thousand casualties and massive destructions (Table 1.1). At least 150000 people have been killed in great earthquakes in Iran in the last 100 years. It was not only as a matter of the national interest of the author, but also as a real engineering concern, which made the motivation to propose a method to solve a part of this problem.

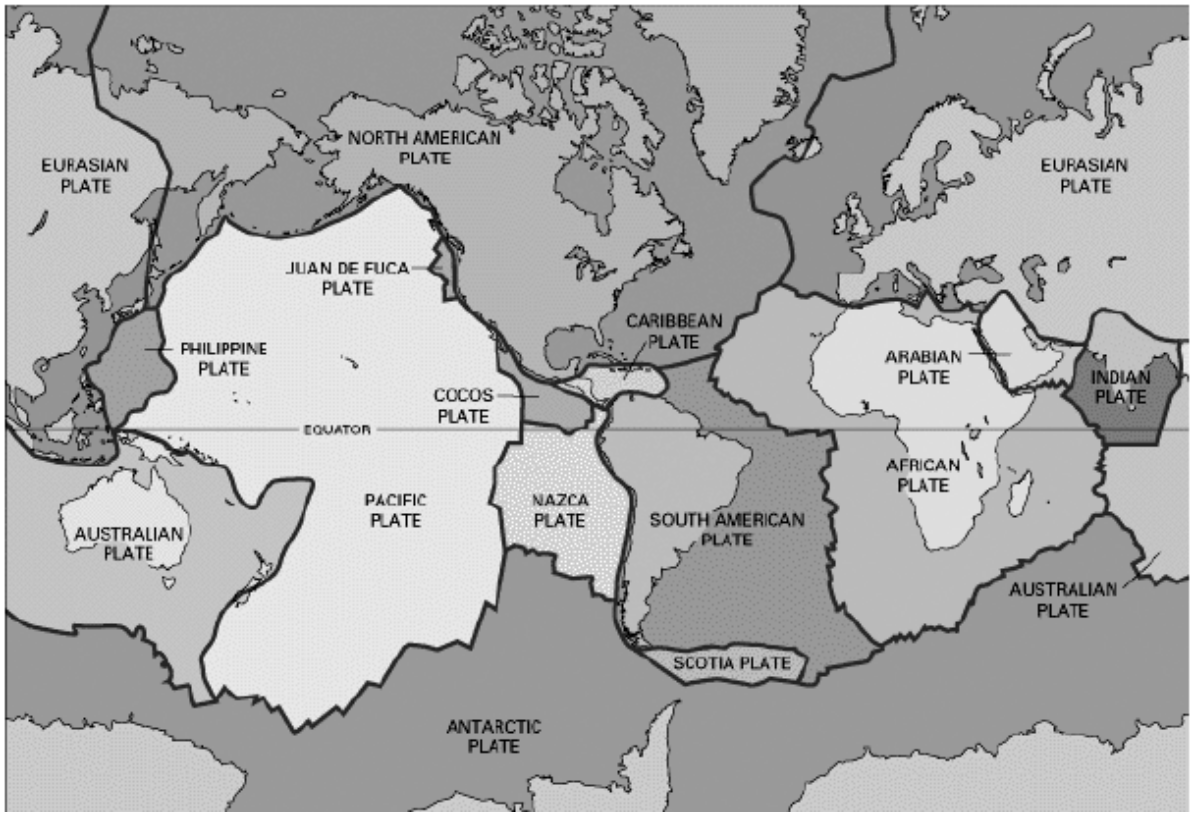

Figure 1.1: Global tectonic plate boundaries [USGS].

Besides, a very rapid population growth, especially in the last century, has resulted in an enormous demand of housing of around one million units per year. Iran's need for an annual investment of 20 billion dollars in the housing sector is out of the capacity of domestic investors [Iran Daily, 2006].

Mass production of affordable earthquake-proof structures is an essential need for the young Iranian generation. It has great economical, social, and political importance for the country as well. *Low-rise buildings* with prefabricated segments equipped with base isolation method against earthquakes have the potential to be considered as a solution for this dilemma.

1.3 Aims

The main aim of this study is to develop a numerical model to simulate the response of friction-based isolated structures. The model is developed in three main stages. Firstly, a single-degree-of-freedom model is applied, in which the structural response is considered to be rigid. Secondly, to simulate the interaction between the isolation block and the structure, a model with two degrees of freedom is developed. Finally, the model is generalized, so that friction-based isolated systems with many degrees-of-freedom can be also simulated. In between, features of such systems are studied and advantages and disadvantages of this method in different situations are discussed.

1.4 Overview

In Chapter two, some basic earthquake principles are introduced. Plate tectonics, different types of faults, and shear waves are briefly reviewed. At last, earthquake magnitude and intensity scales are presented.

In Chapter three, control systems (active, passive, and hybrid) are discussed. The history of the base isolation is then reviewed. Finally, different types of base isolation method are presented.

Friction force and its nature are the main themes of Chapter four. Different models to simulate this force are presented. The response of a single degree-of-freedom model with friction is then studied. Afterwards, frictional properties of a Teflon layer sliding on polished stainless steel plate are studied.

In Chapter five, the concept of base isolation is explained. Using the response spectrum method the period shift effect is described. An arbitrary two-degree-of-freedom model is then used to prove mathematically how isolation decreases earthquake-induced forces in structures.The friction pendulum system as an isolation means is introduced in chapter six. Different configurations of bearing modules are firstly illustrated. Then physical properties of such a system are studied. At last, a stick-slip criterion is presented.

In Chapter seven, after a brief review of classical analysis methods and numerical models, the models developed in this study to simulate the response of an isolated system are presented.

Chapter eight is devoted to case studies done to evaluate the models developed in the previous chapter. Main features of base isolated systems are studied in between.

In Chapter nine, the results are discussed. Advantages and disadvantages of friction base isolation method are explained. Finally, features of the developed numerical model are compared with the classical models.

Table 1.1: Major earthquakes in Iranian history [USGS].

Year	Day-Month	Location	Latitude	Longitude	Deaths	M
856	22-Dec	Iran, Damghan	36.0N	54.0E	200000	
893	23-Mar	Iran, Ardabil	38.0N	48.0E	150000	
1727	18-Nov	Iran, Tabriz	38.0N	46.0E	77000	
1909	23-Jan	Iran, Silakhor	33.4N	49.1E	5500	7.3
1923	25-May	Iran, Torbat e heydaria	35.3N	59.2E	2200	5.7
1929	01-May	Iran, Koppe Dagh	38.0N	58.0E	3300	7.4
1930	06-May	Iran, Salmas	38.0N	44.5E	2500	7.2
1957	02-Jul	Iran, Mazandaran	36.2N	52.7E	1200	7.4
	13-dec	Iran, Sahneh	34.4N	47.6E	1130	7.3
1962	01-Sep	Iran, Qazvin	35.6N	49.9E	12230	7.3
1968	31-Aug	Iran, Dasht e Bayaz	34.0N	59.0E	12000	7.3
1972	10-Apr	Iran, Southern (Fars)	28.4N	52.8E	5054	7.1
1976	24-Nov	Iran	39.1N	44.0E	5000	7.3
1978	16-Sep	Iran, Tabas	33.2N	57.4E	15000	7.8
1981	11-Jun	Iran, Southern	29.9N	57.7E	3000	6.9
	28-Jul	Iran, Southern	30.0N	57.8E	1500	7.3
1990	20-Jun	Iran, western	37.0N	49.4E	40000	7.7
1997	28-Feb	Iran, Ardabil	38.1N	48.1E	1200	6.1
	10-May	Iran, Manjil	33.9N	59.7E	1560	7.5
2002	22-Jun	Iran, Qazwin	35.6N	49.1E	261	6.5
2003	26-Dec	Iran, Bam	29.0N	58.3E	31000	6.6
2005	22-Feb	Iran, Zarand	30.1N	56.8E	612	6.4

Chapter 2

Basic Earthquake Principles

The Lithosphere, the outermost part of the earth interior, is made up of large plates, which are continuously in movement because of forces acting on them. Elastic rebound theory is one of the theories describing this phenomenon. According to it a sudden release of a huge amount of energy as a result of slippage of two plates over each other causes an earthquake. This sudden rupture propagates several types of waves, which are mainly responsible for the devastating damages of earthquakes. In technical literature, earthquakes are usually described quantitatively. Whereas, a qualitative description of earthquakes is more usual in media. In this chapter plate tectonics is briefly reviewed. Then different types of seismic waves are categorized. Finally, quantitative and qualitative measurements of an earthquake are introduced.

2.1 Plate tectonics

The earth consists of several layers of different compositions, which can be divided in an inner solid core, an outer molten core, the mantle, and the crust. The combination of the crust and the rigid part of the mantel is called *lithosphere* [Suy, 2005]. The Lithosphere's large plates are driven by the convective motion of the material in the earth's mantle. Relative plate motions are constrained by friction and asperities between adjacent plates (Figure 2.1). According to the e*lastic rebound theory,* the strain energy accumulated in the plates eventually overcomes the friction force between plates and causes a slippage between two adjacent plates. This sudden slippage releases a large amount of energy, which causes an earthquake [Chen, 1999].

The fractured zone between two plates along which a rupture has happened is called *fault.* The *Hypocenter* is the point, where the rupture in a fault during an earthquake has been initiated. Its projection on the surface of the ground is called *Epicenter*. There are several different types of faults. The most common ones are:

- *Strike-slip fault*, in which the movement between faults is parallel to the strike[1] of the fault (Figure 2.2).
- *Normal fault*, in which the hanging wall block, that is the part of the ground on the right hand side of a fault's block, has moved downward with respect to the foot wall block, which is the block located on the left side of a fault (Figure 2.3).
- Reverse fault, in which the hanging wall block has moved upwardly with respect to the foot wall [Day, 2002].

[1] The orientation of a fault on the earth's surface, which is usually measured clockwise from the north.

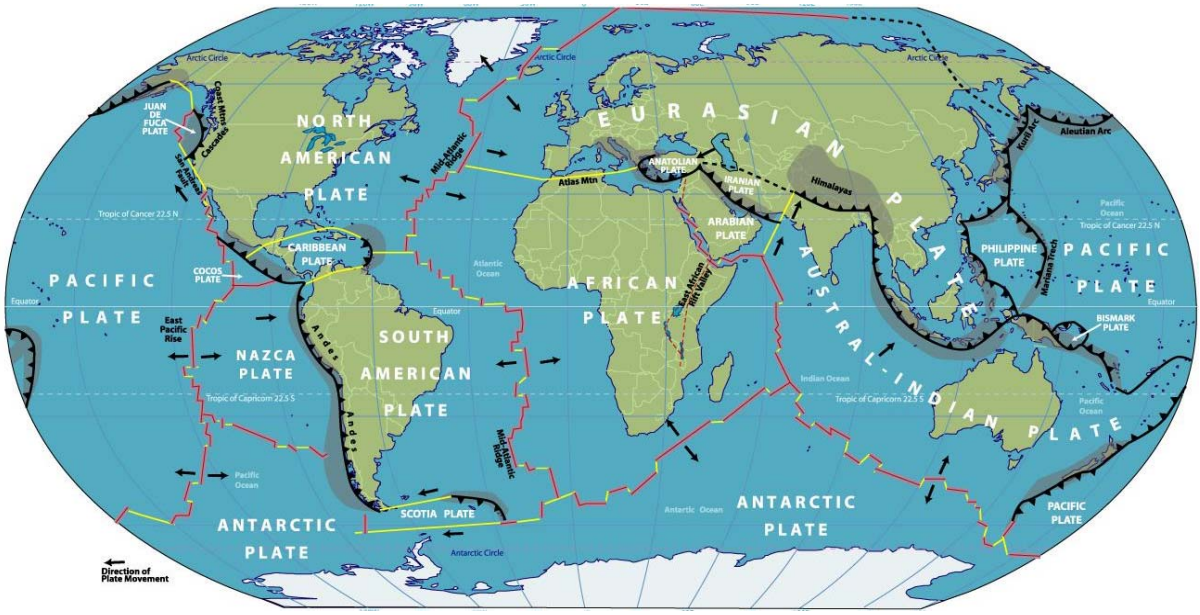

Figure 2.1 World tectonic plates [USGS].

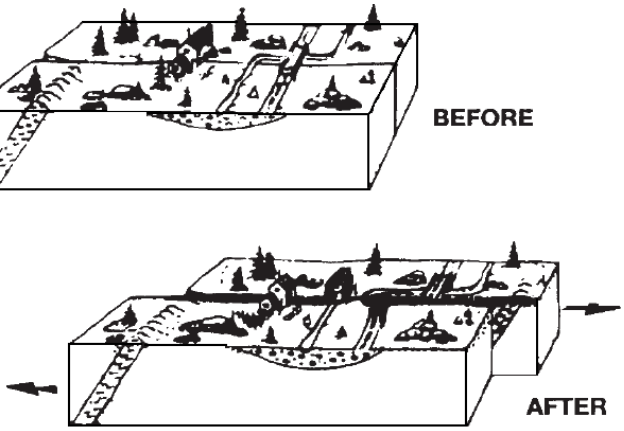

Figure 2.2 Schematic view of a strike-slip fault [Namson and Davis, 1988].

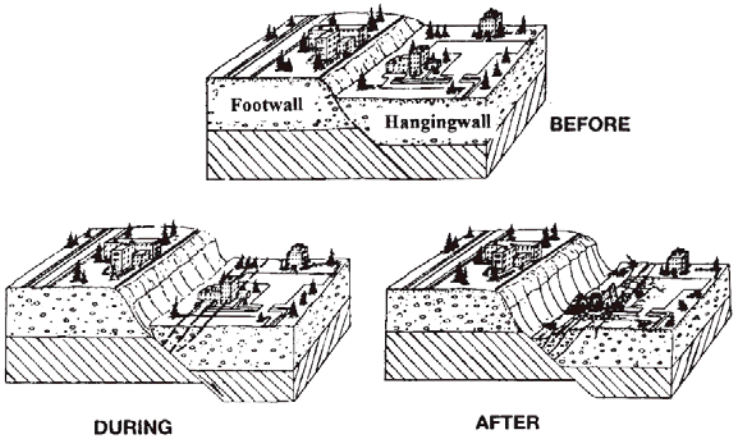

Figure 2.3 Schematic view of a normal fault [Namson and Davis, 1988].

2.2 Seismic waves

Most earthquakes are caused by stress build-up between the asperities of the plates and then a sudden release of energy, as a fault ruptures. To explain features of an earthquake it is of great importance to record the motion of the ground surface due to seismic waves generated by an earthquake. The S*eismograph* is an instrument recording the ground motions. Its record of ground shakings is known as *seismogram*, which can be acceleration, velocity, or displacement of a point on the ground during shakings (Figure 2.4).

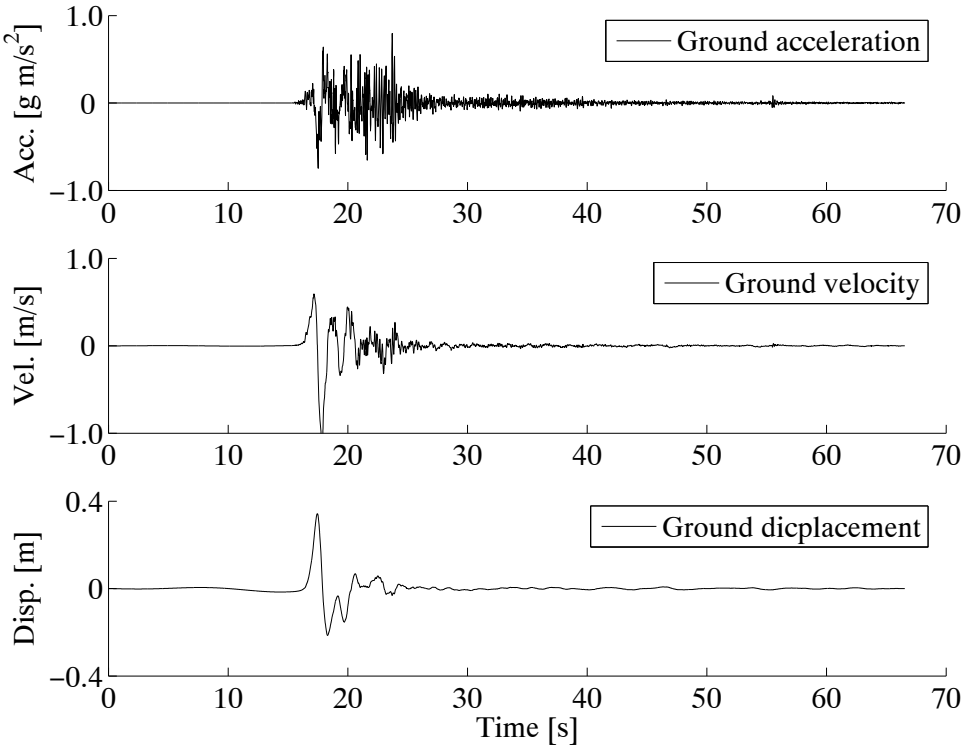

Figure 2.4 Acceleration, velocity, and displacement seismograms of the Bam Earthquake, Iran, 2003.

Seismograms contain valuable information used in seismic analysis and design of structures. Parameters such as acceleration, velocity, displacement, frequency content of the ground motion, duration of strong shakings, and various intensity measures play important roles in seismic evaluation of existing facilities and design of new systems.

Ground motions recorded at different sites vary significantly due to several factors, including, but not limited to, earthquake magnitude, faulting mechanism, distance from the recording site to the earthquake source, local site condition, depth of sediments, basin features, and source directivity effects (Figure 2.5).

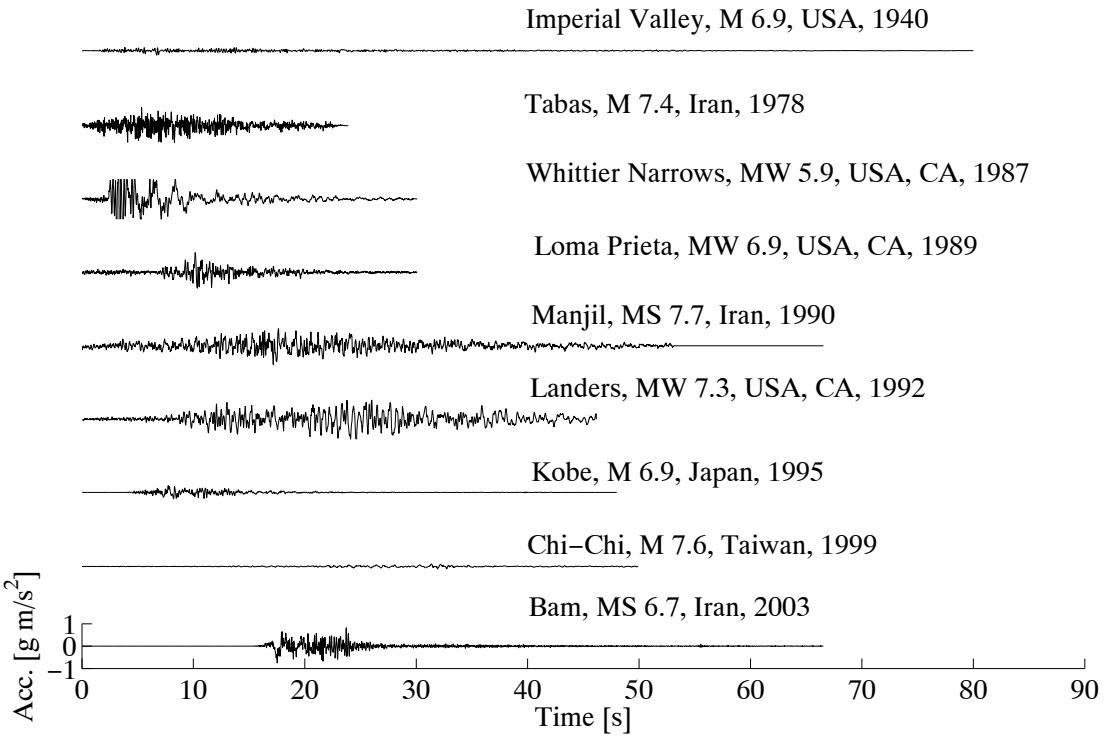

Figure 2.5 Acceleration seismograms of some strong earthquakes [USGS and PEER].

An earthquake produces several types of waves, mainly categorized as body waves and shear waves. Body waves can pass through the interior of the earth, as for example *P-waves* (compression waves). Shear waves, however, can only be observed close to the surface of the ground, as *Love* and *Rayleigh* waves. As a result of the interaction between body waves and the material near the earth's surface, surface waves are produced. They are normally categorized as shear waves. Main seismic waves are (Figure 2.6):

- *P-Wave*: known as primary or compressional wave. It causes a series of compressions and dilations of the material through which it travels. As the P-wave is the fastest wave produced by an earthquake, its detection is for early warning systems of great importance.
- *S-wave*: known as secondary, shear, or transverse wave. The s-wave causes shear deformation in the material through which it travels and is the most destructive seismic wave produced by an earthquake.
- *Love wave*, which is analogous to the S-wave. In contrast to the S-wave, which has vertical and horizontal components, Love waves have no vertical components.
- *Rayleigh waves*, which are like ocean waves. Particles are displaced by Rayleigh waves both vertically and horizontally in a vertical plane oriented in the direction in which the wave is travelling [Bozorgnia and Bertero, 2004].

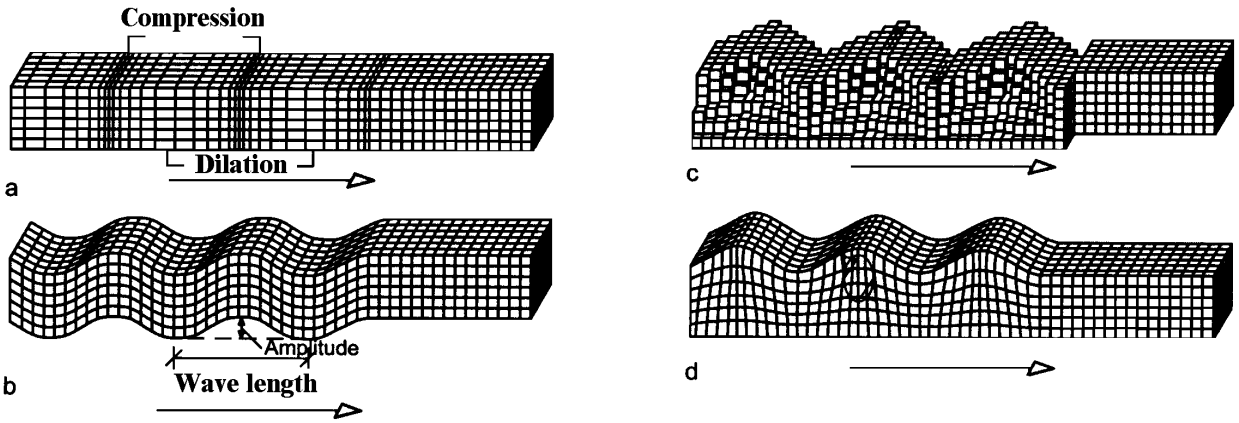

Figure 2.6 (a) P-Wave, (b) S-Wave, (c) Love Wave, and (d) Rayleigh wave [Pocanschi and Phocas, 2003].

2.3 Magnitude and intensity of an earthquake

There are two basic ways to measure the strength of an earthquake: either with a quantitative observation, based on the amount of energy released by an earthquake, that is *magnitude*, or with a qualitative observation, based on damages to buildings and reactions of people, which is called *intensity*.

There are several earthquake magnitude scales used by seismologists. Among them the local magnitude scale, the *Richter magnitude scale* (M_L), is the most famous one. In the Richter magnitude scale, mainly used for shallow local earthquakes, the magnitude is calculated as [Richter, 1935]:

$$M_L = \log A / A_0 \tag{2.1}$$

where M_L is the local magnitude in *Richter scale*. A is the maximum trace amplitude (mm) as recorded by a standard *Wood-Anderson* seismograph, located on a firm ground at a distance of exactly 100 kilometres from the epicentre of the earthquake. A_0 is a constant, taken normally to be 0.001 millimetre.

Because of limitations of the Richter magnitude scale, it is more common to use the *moment magnitude scale* (M_W) to describe the magnitude of an earthquake. First the seismic moment (M_0) is calculated [Meskouris and Hinzen, 2003]. It is a function of shear modulus of the material along the fault plane, the area of the fault plane undergoing a slippage, and the average displacement of the rupture. The moment magnitude is calculated as [Kanamori, 1977]:

$$M_W = -6.0 + 0.67 \log M_0 \tag{2.2}$$

In contrast to the magnitude scale, the intensity of an earthquake is based mainly on the observations of damaged structures and the presence of secondary effects as landslides, liquefaction, and ground cracking. It is also based on the degree to which the earthquake is felt by inhabitants. The most common intensity scale is the *modified Mercalli intensity scale* (Appendix *B*).

Chapter 3

Active and Passive Control Systems

There are several methods to protect buildings from damaging earthquakes. Active and passive control systems belong to a younger generation of these methods. Passive systems, in contrast to active systems, have no logically driven external device to control the structural properties. Base isolation methods are classified under passive control systems. Isolation systems are mainly classified to elastomeric and sliding-based types. The main advantage of sliding-based systems is the capability of the system to slide freely over its foundation, which results in a drastic reduction of the transmitted forces to the structure. In this chapter main structural control systems are introduced. A brief review of different types of base isolation methods is then presented.

3.1 Introduction

Protecting structures from the damaging effects of severe earthquakes is one of the oldest challenges in structural engineering. In the last two decades beside conventional methods, additional protective systems are becoming more and more practical [Soong and Constantinou, 1994] and [Chen, 1999].

Structural protective systems against vibration are divided into three main types: *Passive systems*, as base isolation and energy dissipation systems, *active systems*, as smart bracing and damping systems, and *hybrid control systems* [Zhao et al., 2000]. Active systems in contrast to passive systems monitor the structure and incoming ground motion and through a controlling system and actuators control the structural properties such as stiffness and damping (Figure 3.1). In passive systems, however, no logically driven external device is applied, and by means of a specially designed interface at the structural base, as sliding bearing elements, or special components in the structure, e.g. tuned mass dampers (TMD) and bracings, the input energy of an earthquake is diverted or dissipated. In hybrid control systems a combination of passive and active instruments is applied.

Because of a permanent monitoring of structural features, active control systems are functioning more efficiently than passive systems. Nevertheless, the dependency of such systems on an exterior energy source and monitoring software and hardware is a great drawback, which caused this method not to be used as widely as passive control systems. In the rest of this chapter, a brief review of different base isolation systems will be presented.

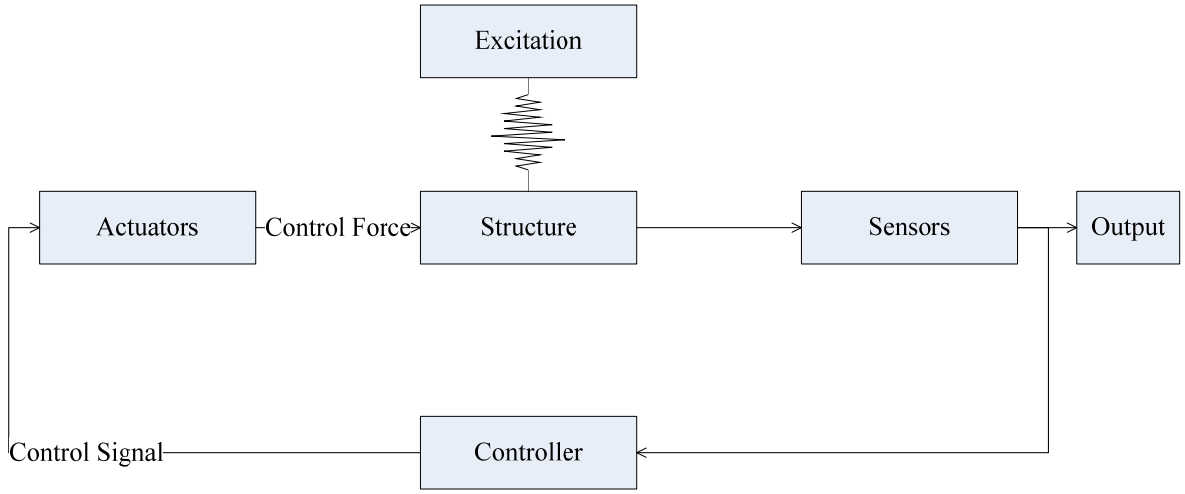

Figure 3.1 Basic elements of an active control system [Soong and Constantinou, 1994].

3.2 Base isolation history

The idea of preventing disastrous damages of strong earthquakes through decoupling a structure from its foundation has a long history. The first documented concept belongs to a Frenchman, named Jules Touaillon [Touaillon, 1870]. To isolate structures, he suggested in his patented work, to use some ball bearings between the base and the foundation of the structure (Figure 3.2).

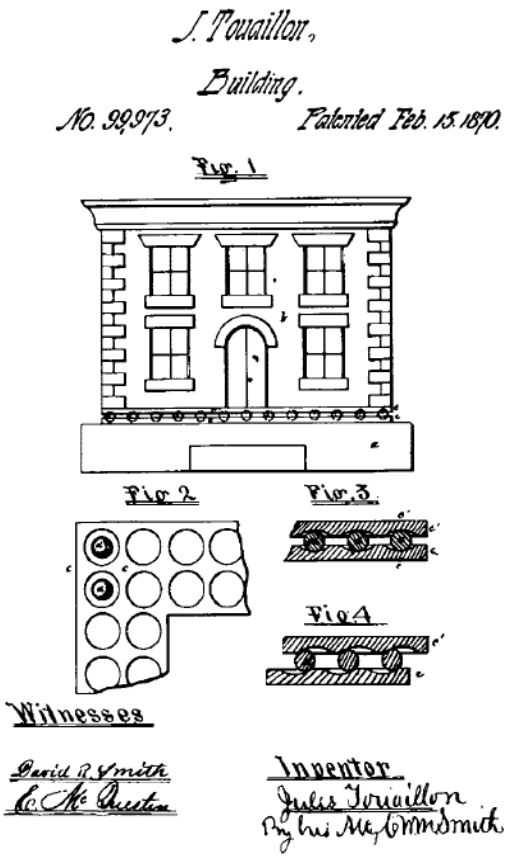

Figure 3.2 Jules Touaillon original patented earthquake-proof building [US Patent Nr. 338240, 1870].

Some years later in 1906, a similar suggestion was proposed by Jakob Bechtold. He suggested a pad of metal spheres as an isolation layer (Figure 3.3) [Bechtold, 1906].

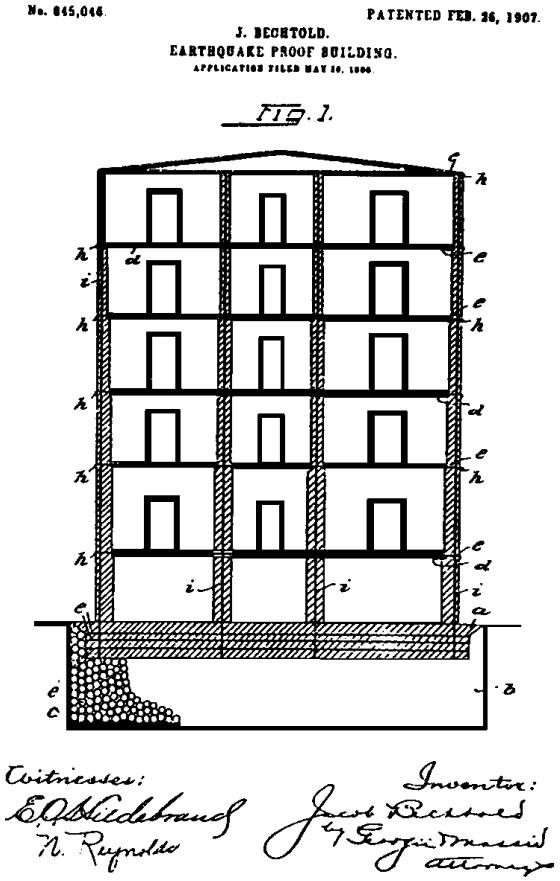

Figure 3.3 Jakob Bechtold patented earthquake-isolated building [US Patent Nr. 845046, 1907].

In 1909, J. A. Calantarients, a medical doctor from England, proposed the construction of buildings on a layer of fine sand, mica, and talc that allows the building to slide in case of severe shakings (Figure 3.4) [Calantarients, 1909]. To withstand large relative displacements he designed a set of ingenious connections for gas lines and sewage pipes (Figure 3.5).

Some local innovative housing techniques can be observed in countries located in regions with high seismic hazards. They are mainly based on the idea of decoupling the structure from its foundation. For example in the north of Iran it is an old tradition to construct the houses over pyramid-shape wooden pedestals (Figure 3.6) [Hosseini, 1999].

Natural rubber was used for the first time to provide an earthquake protection system in 1969 for a school in Skopje, Macedonia [Naeim and Kelly, 1999]. In contrast to modern rubber bearings, the rubber blocks used there are not reinforced, so that the weight of the building caused the bearings to bulge sideways. Some glass blocks are used as seismic fuses to break when the horizontal loading exceeds a certain threshold, to guarantee that under ordinary service loads, such as daily wind load, the structure responds as a classical fixed-base structure.

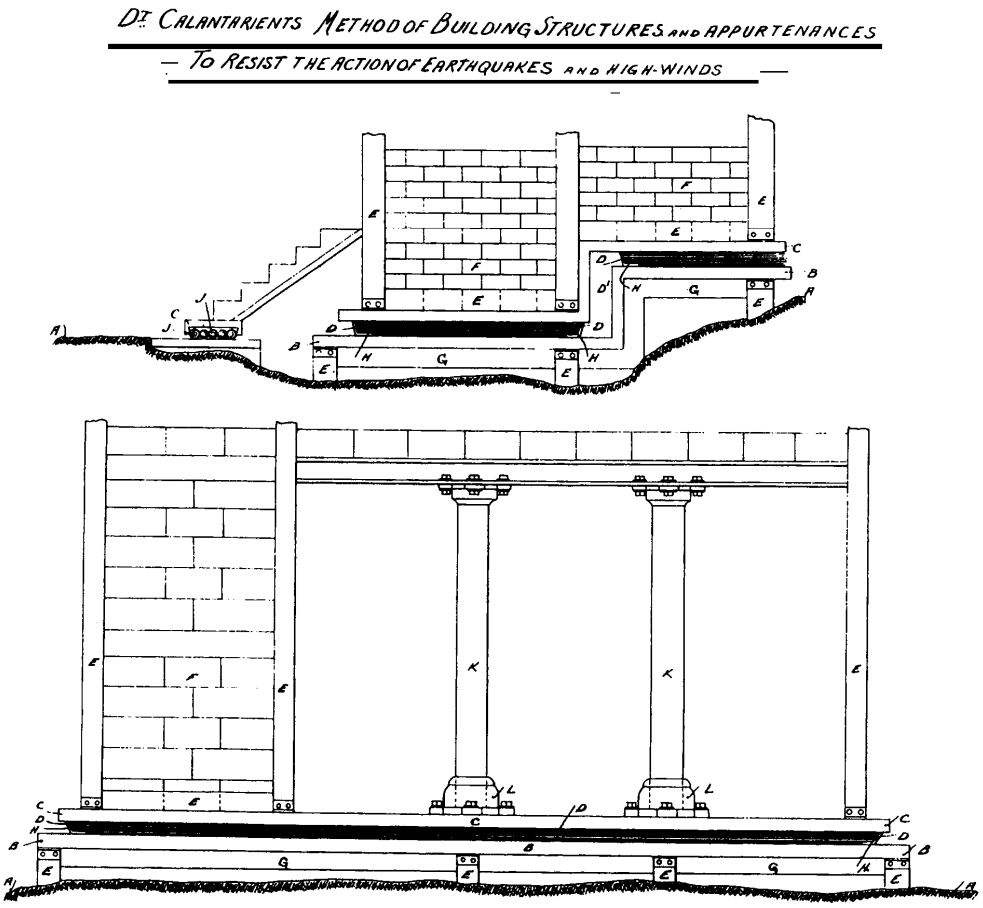

Figure 3.4 Calantarient's base isolation system [Calantarient, 1909].

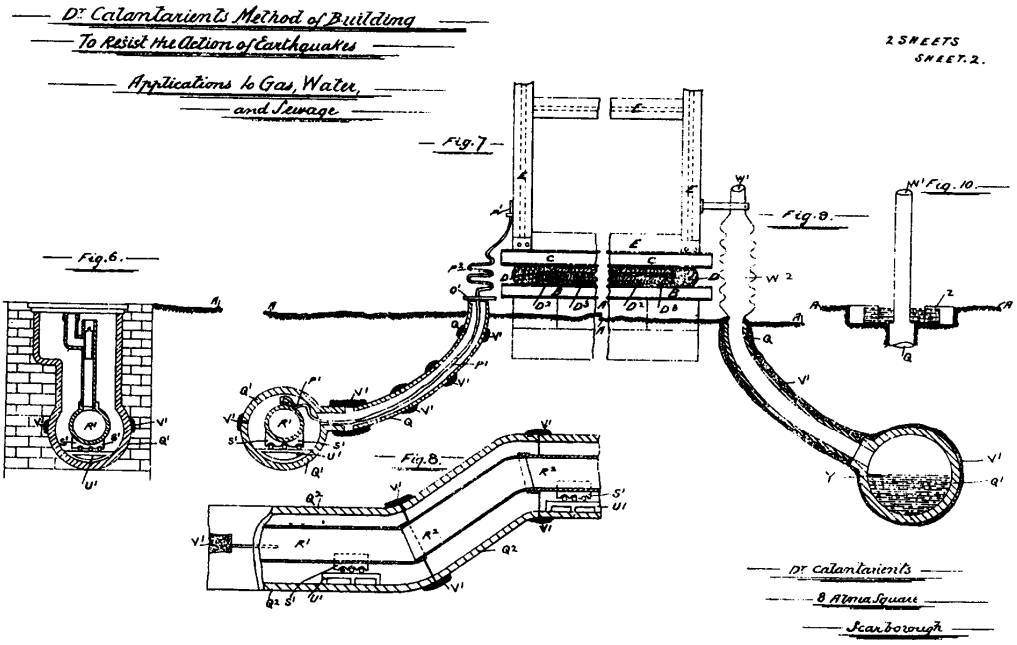

Figure 3.5 Service connection proposed for an isolated structure [Calantarient, 1909].

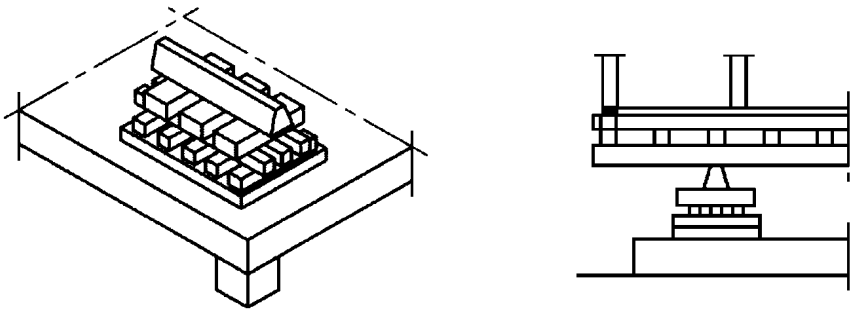

Figure 3.6 Traditional isolated structure, north of Iran [Hosseini, 1999].

3.3 Base isolation types

Base isolation systems are divided into two main groups of systems with a recentering (restoring) mechanism and systems without this mechanism. The recentering mechanism is responsible to push the structure back to its original place to minimize the permanent displacement of the structure in its base. Regarding isolation mechanisms, base isolated systems can be divided into three main groups: elastomeric-based systems, sliding-based types, and spring type systems.

3.3.1 Elastomeric-based systems

In most recent isolated buildings multi-layered laminated rubber bearings with steel reinforcement have been applied (Figure 3.7). Because of steel reinforcements, elastomeric bearings are very stiff in the vertical direction. Because of the low stiffness of rubber, however, the bearings are very soft in the horizontal direction, which guarantees an isolation effect. Laminated elastomeric bearings are categorized into low- and high-damping types.

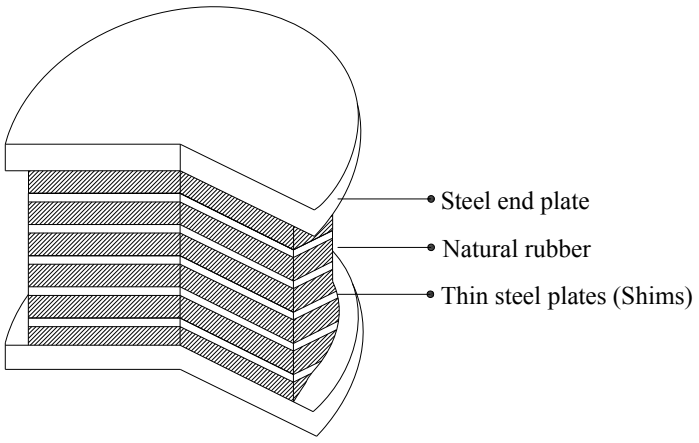

Figure 3.7 A typical elastomeric bearing consisting of two steel end plates, layers of vulcanized low-damping natural rubber, and steel plates.

3.3.1.1 Low-damping rubber systems

A bearing of this type consists of two thick steel endplates and many thin steel plates in between (*shims*), which are vulcanized and bonded to layers of natural rubber in a mold under extreme heat and pressure (Figure 3.7). Steel shims provide the required vertical stiffness without increasing significantly the horizontal stiffness. Such bearings behave under shear

loading quite linearly even up to 100% shear strain with a damping ratio in the range of two to three percent of the critical damping.

This kind of bearing has many advantages, among them an easy manufacturing production process, relatively simple numerical simulation of their response, and a rate independent response under aging and preloading can be mentioned. On the other hand, because of a very low damping rate, they require sometimes a supplementary damping source to restrict lateral displacement.

3.3.1.2 High-damping rubber systems

To avoid supplementary devices, guaranteeing a higher damping ratio for structures isolated with low-damping rubber bearings, the damping properties of natural rubber are improved by adding extra fine carbon blocks, oil, resins, and some other fillers [Derham and Kelly, 1985]. In this way, the damping ratio is increased up to 20% of the critical damping at 100% shear strain. High damping rubber responds strongly nonlinearly, which makes its numerical simulation much more complicated than low-damping rubber systems.

Adding a lead core to such a set serves as an extra source of damping (Figure 3.8). This special kind of bearing was invented in New Zealand and has been used extensively there [Naeim and Kelly, 1999]. The steel plates in the bearing force the lead plug to deform. Because of yielding of the lead core, a bilinear response is produced in the isolator. Buildings isolated with this kind of bearings performed well during the 1994 Northridge and 1995 Kobe earthquakes. Besides, the lead core acts as a seismic fuse. As long as the stress in the core has not reached the yielding stress of the lead, it does not let the elastomeric bearing to be activated. This helps the structure to respond as traditional fixed-base structures to daily service loads.

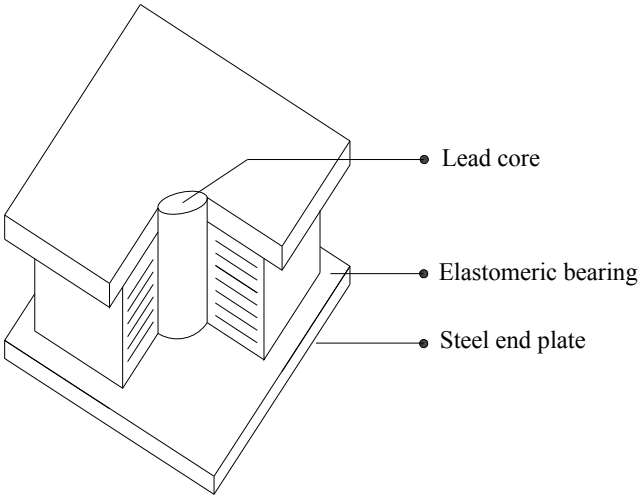

Figure 3.8 Elastomeric bearing with a lead core.

3.3.2 Sliding-based systems

Although initial innovative isolation concepts were mostly of sliding-based type, because of numerous practical problems, this kind of isolation technique was accepted much later than other types in praxis.

Westermo and Udwadia studied the periodic response of a linear isolator with Coulomb friction law [Den Hartog, 1956] and [Westermo and Udwadia, 1983]. The response of a similar model to a general loading was later studied by [Mostaghel et al., 1983 and 1990].

Because of appealing results, many different configurations were suggested, which all were based on the same principle. In the coming section they will be shortly introduced.

3.3.2.1 Electricite-de-France system

This system, developed in the early 1970s, is a combination of the elastomeric isolation with the sliding type one. Laminated neoprene bearings in combination with lead-bronze plates in contact with stainless steel are the main components of this system. The neoprene pad has a limited displacement capacity. If the displacement demand exceeds the displacement capacity of the neoprene pad, the steel plate begins to slide over the lead-bronze plate, guaranteeing the isolation effect for larger displacements (Figure 3.9). There is no restoring mechanism for the sliding part of the bearing. The elastomeric bearing, however, produces a restoring force.

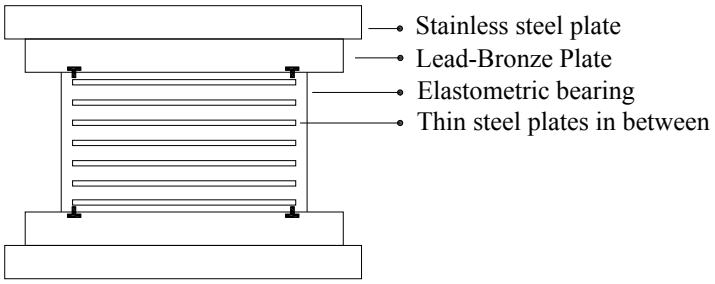

Figure 3.9 Electricite-de-France system.

3.3.2.2 EERC system

This system is also a combination of the introduced methods, in which the interior columns are carried on sliding-based isolators. The exterior columns are isolated with low damping natural rubber bearings. Sliding elements provide the required damping. Elastomeric bearings are responsible for the restoring mechanism [Chalhoub and Kelly, 1990].

With a similar concept the engineers of Taisei corporation in Japan devised a system, in which the entire weight of the structure carried on sliding-based isolators and elastomeric bearings are just providing the restoring force [Kelly, 1988].

3.3.2.3 Resilient-Friction based isolation system (R-FBI)

High sliding velocity between sliding layers, usually Teflon and stainless steel plates, produces high friction coefficients, which is inappropriate for the isolation effect. By using several sliding plates instead of only one layer, it is possible to reduce considerably the sliding velocity and friction coefficient (Figure 3.10). To provide a restoring mechanism a rubber core, which carries no vertical load, is applied [Mostaghel et al., 1987 and 1988] and [Su et al., 1989].

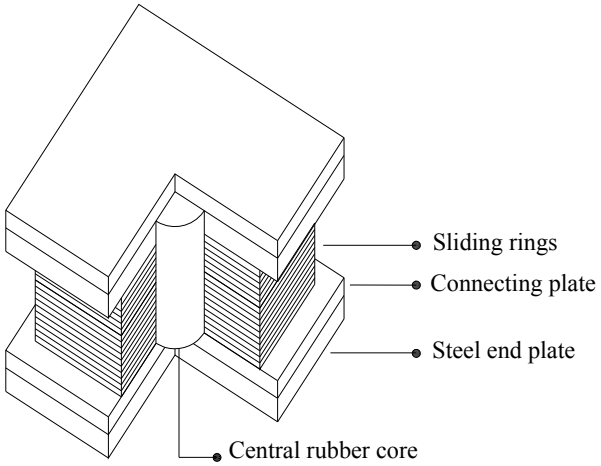

Figure 3.10 Resilient-friction bearing [Mostaghel 1984].

3.3.2.4 Friction pendulum systems

The idea of using an articulated slider on a concave surface, a *friction pendulum system* (FPS), was first proposed by [Zayas et al., 1987]. It combines a sliding action with a restoring mechanism (Figure 3.11). As the slider moves over a spherical surface the supported mass rises and a recentering force is provided because of the concavity of the base plate. At the same time the friction between the spherical surface and the slider produces damping in the set.

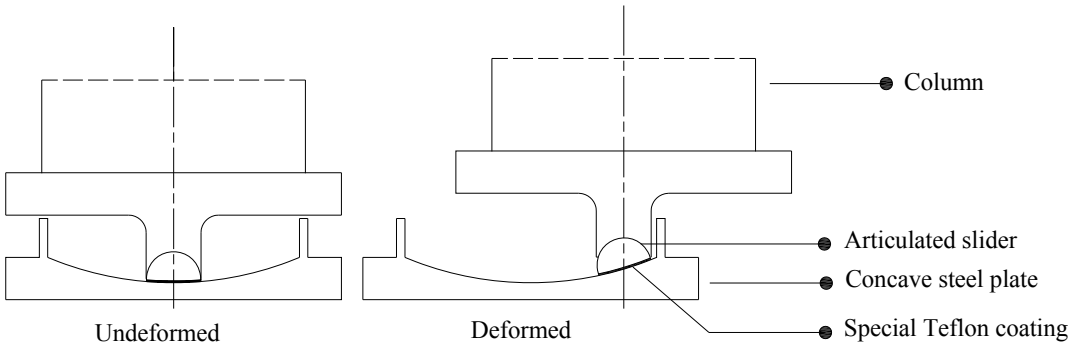

Figure 3.11 Configuration of a friction pendulum bearing [Mokha et al., 1990].

With a similar concept in *sliding concave foundation* (SCF), columns are laid on a concave sliding raft. Bearings can slide over a cylindrical concave foundation. Because of a very large radius of curvature, the system has a longer period of isolation in comparison to FPS, which reduces the possibility of resonance in case of long period waves as in near source earthquakes. From the construction point of view, however, it faces numerous obstacles (Figure 3.12).

The possibility of uplifting is a drawback for all kinds of isolation systems. In recent years some innovative uplift-restraining systems have been proposed [Roussis and Constantinou, 2006], in which tension can be developed in the bearing without any lose of contact between the slider and the sliding surface (Figure 3.13).

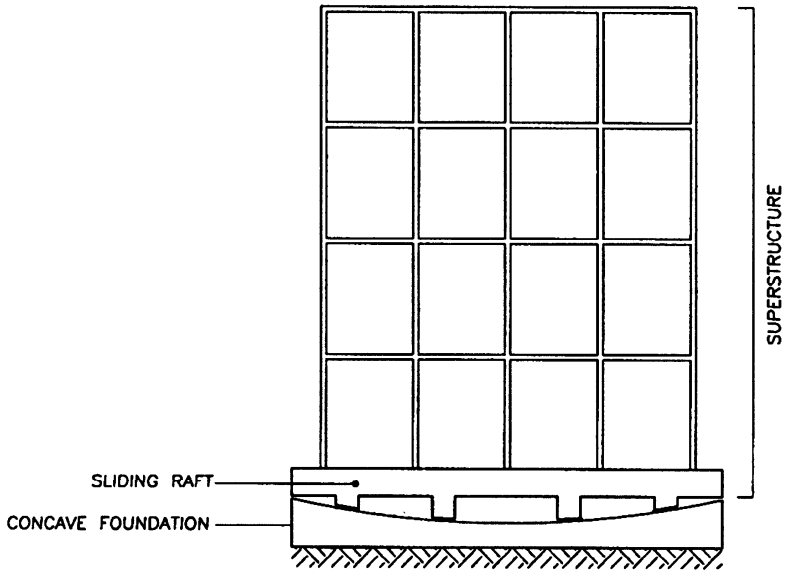

Figure 3.12 Sliding concave foundation [Hamidi at al., 2003].

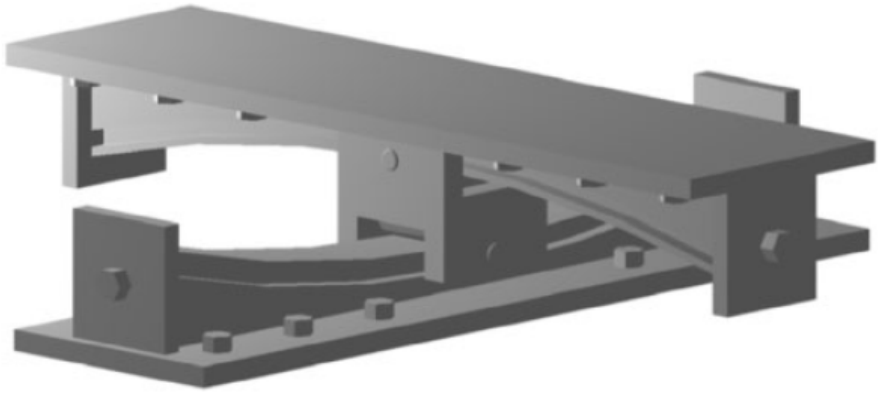

Figure 3.13 Uplift-restraining friction pendulum bearing [Roussis et al., 2006].

3.3.3 Spring-type systems

Spring-type systems, e.g. the Gerb system, are mainly composed of large helical steel springs that are flexible both horizontally and vertically. The system is always used in conjunction with viscodampers (Figure 3.14). The Gerb system was originally developed for vibration isolation of machine foundations such as power plant turbines.

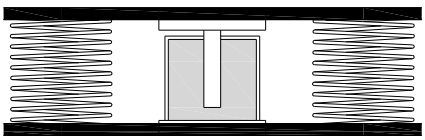

Figure 3.14 Spring-based isolator with viscodamper [Nawrotzki, 2001].

Chapter 4

Friction

The friction force has a complicated nature. It depends on several factors, among them the material of the rubbing surfaces, the contact pressure, the sliding velocity, and the history of loading. There are several models to simulate it. For example, the Coulomb friction law considers a constant friction coefficient during sliding. Whereas, in the viscoplasticity model the friction coefficient is defined as a function of several parameters. In this chapter, after a brief explanation of the nature of friction force, three numerical models, Coulomb, modified Coulomb, and viscoplasticity models, are introduced. Finally, frictional properties of sliding Teflon layers over stainless steel are studied. This will be later used to simulate the friction force in friction pendulum systems.

4.1 Generalities

Friction, the force that opposes the relative motion or the tendency for a movement in a particle, is not considered a fundamental force, as it is made up of electromagnetic forces between atoms. In macro scale, asperities of contact surfaces cause the friction force. The most famous relation used to approximate the friction force between two solid surfaces is the *Coulomb law*:

$$F_f = -\mu W sign(\dot{u}) \tag{4.1}$$

which applies only when sliding has been initiated. μ is the dynamic friction coefficient, W the weight of the sliding particle, and $\dot{u}$ its sliding velocity. In Coulomb friction law the dynamic friction coefficient is considered to be constant.

The friction force has a complicated nature. As long as no sliding has been initiated, it has a passive nature. It opposes the resultant force acting on the body. Only when slippage has occurred and the body starts sliding, the friction force changes its nature and acts on the set independently from other forces in the system.

There are several models to simulate the friction force. They are based on many factors, as for example the sliding velocity, the contact pressure between the rubbing surfaces, and the material of the sliding plates. In the coming sections some of these models will be introduced.

4.2 The Coulomb friction model

To explain how the friction force acts in a dynamic system simulated by the Coulomb model, a simple mass-spring system, with a mass of 100 kg and a spring stiffness of 10 kN/m, laying on a surface with a constant friction coefficient of 0.1, is used. For the sake of simplicity no

other force or damping source has been considered in the system. An initial displacement, u_0 = 0.125 m, is applied as initial condition (Figure 4.1).

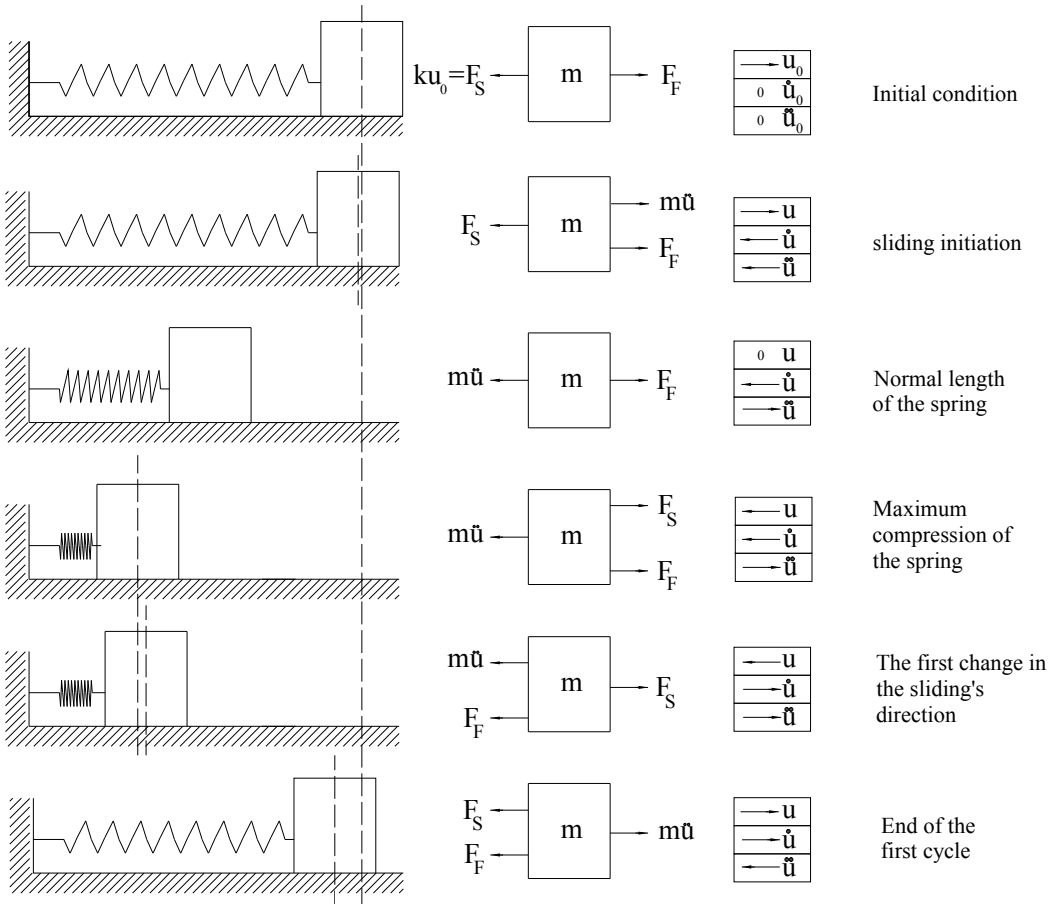

Figure 4.1 Forces acting on the mass in a cycle of oscillation.

When the mass is released, depending on the forces acting on the mass, in this case just the spring force, either the mass remains in its original position, if the spring force cannot overcome the static friction force, or it starts sliding. Supposing that the spring force is large enough to overcome the static friction force, the mass starts sliding. The friction force is simulated by the Coulomb model (Equation 4.1). As the spring force is a restoring force and because of the positive initial displacement, it acts in the negative direction and the friction force works against it according to the equation of equilibrium. As the mass slides further, the spring force gets smaller. The friction force, however, remains constant (Figure 4.3). This decreases the acceleration of the mass. As soon as the spring is compressed, the direction of the spring force changes. It acts in the same direction as the friction force, resulting in an increase of the acceleration of the mass, until the opposing force, the inertial force, is large enough to overcome friction and spring forces and brings the mass to rest (Figures 4.1 and 4.2). At this moment the spring force which is a function of the location of the mass (displacement) and the spring stiffness, is the key factor determining whether the mass starts again sliding in the opposite direction or not (Equation 4.2).

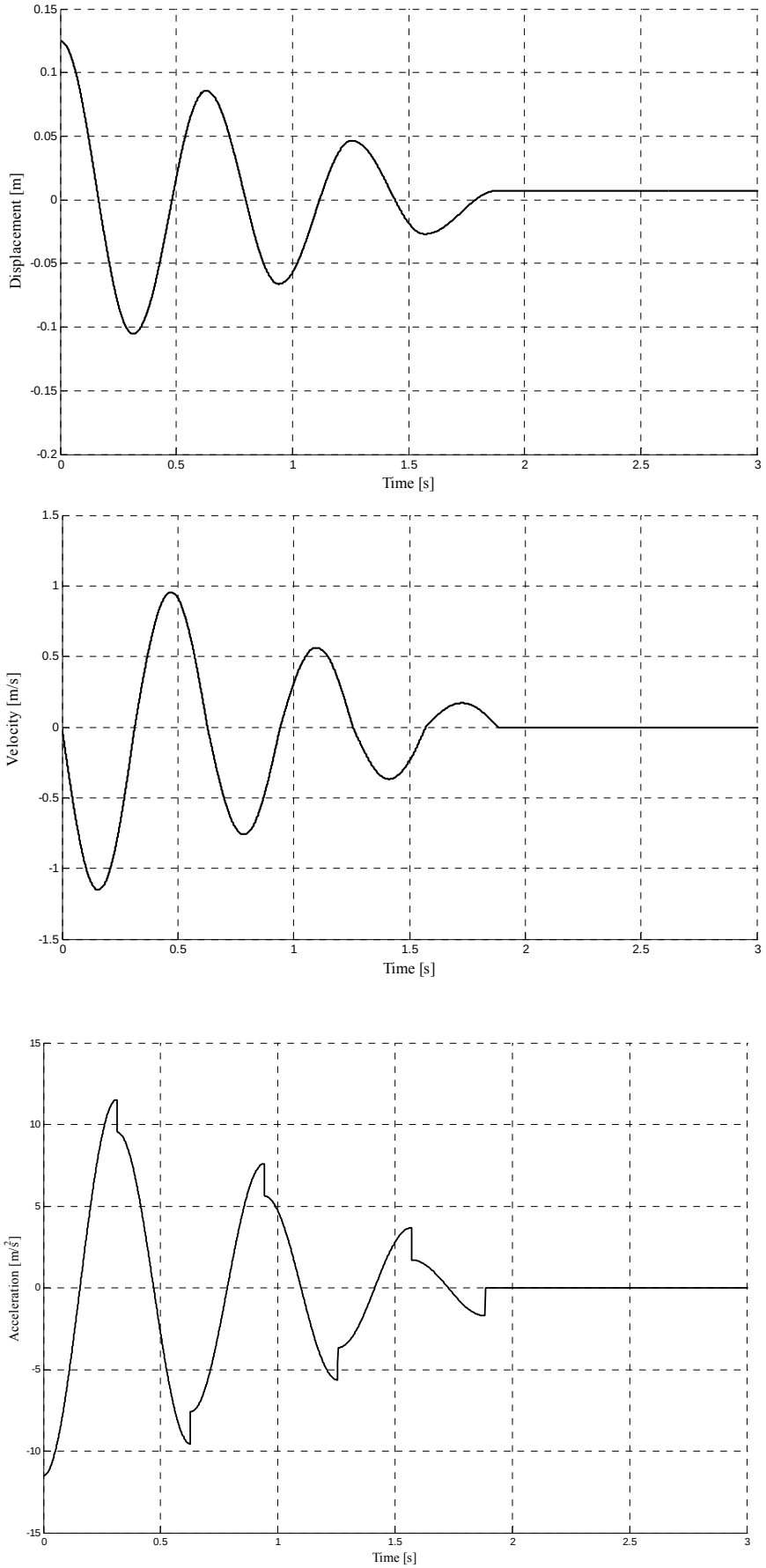

Figure 4.2 Displacement, velocity, and acceleration of the mass during oscillations [Jamali and Zahlten, 2006].

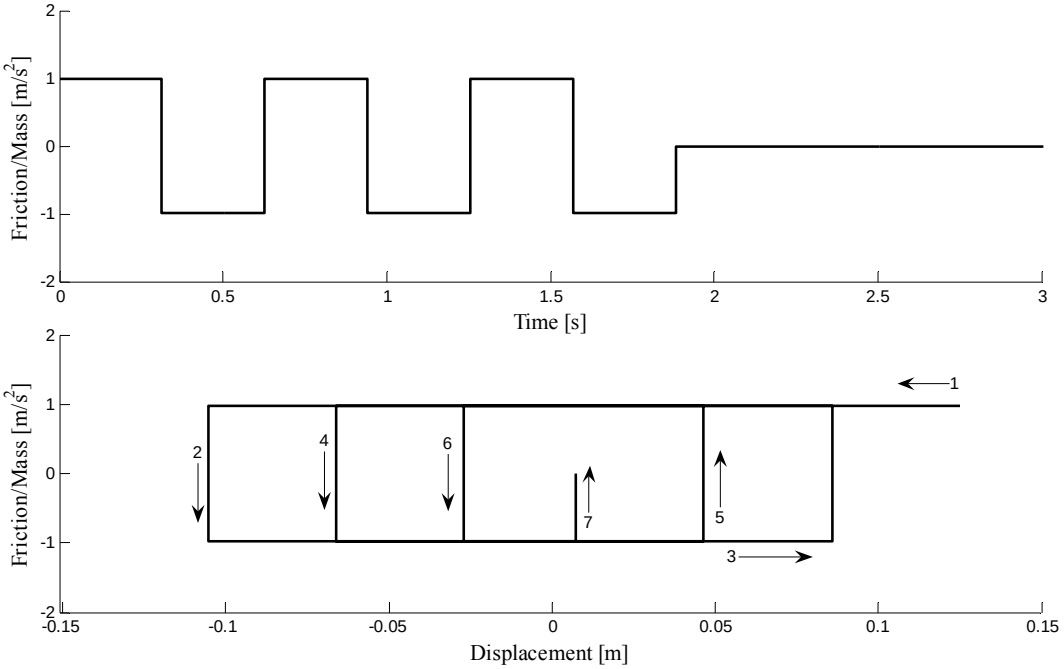

Figure 4.3 Coulomb friction force versus time and sliding displacement.

$$\left|K\,u\right| \overset{?}{\geq} \left|F_f\right| \tag{4.2}$$

The same process is repeated in several cycles until in one of the resting moments the spring force cannot overcome the static friction force. At this moment the mass remains where it is and it will be the end of the oscillation (Figures 4.1 and 4.2) [Jamali and Zahlten, 2006].

The amplitude of oscillation decreases steadily (Figure 4.2). In contrast to hysteretic damping its decreasing rate is linear. Unlike other types of damping, damped and natural frequency of vibration are equal in this case [Petersen, 1996 and 2005] and [Mostaghel and Davis, 1997].

As discussed before, there are two different phases of sticking and sliding in such systems, which are separated by zero crossings of the sliding velocity. There is no analytical solution to find exactly these phase changes. Besides, if there are many sliding devices in a system, keeping track of all phase changes for all sliding elements is too cumbersome. To avoid discontinuities caused by the *signum function* in the Coulomb friction model it is practical to use instead some similar continuous functions, as for instance the *hyperbolic tangent function*.

The signum function is defined as:

$$sign(x) = \begin{cases} +1 & x > 0 \\ 0 & x = 0 \\ -1 & x < 0 \end{cases} \tag{4.3}$$

The hyperbolic tangent function is defined as:

$$\tanh(\alpha\dot{u}) = \frac{e^{\alpha\dot{u}} - e^{-\alpha\dot{u}}}{e^{\alpha\dot{u}} + e^{-\alpha\dot{u}}} \tag{4.4}$$

in which α controls the rate change of the function around zero crossing points. $\dot{u}$ is the relative velocity (Figure 4.4). Larger values of α guarantee a better representation of the signum function.

It must be taken into consideration that a very large coefficient may produce numerical instability.

$$F_f = -\mu W \tanh(\alpha \dot{u}) \tag{4.5}$$

Equation 4.5 is valid only for sliding phases. For sticking phases the friction force must be calculated from the equation of equilibrium.

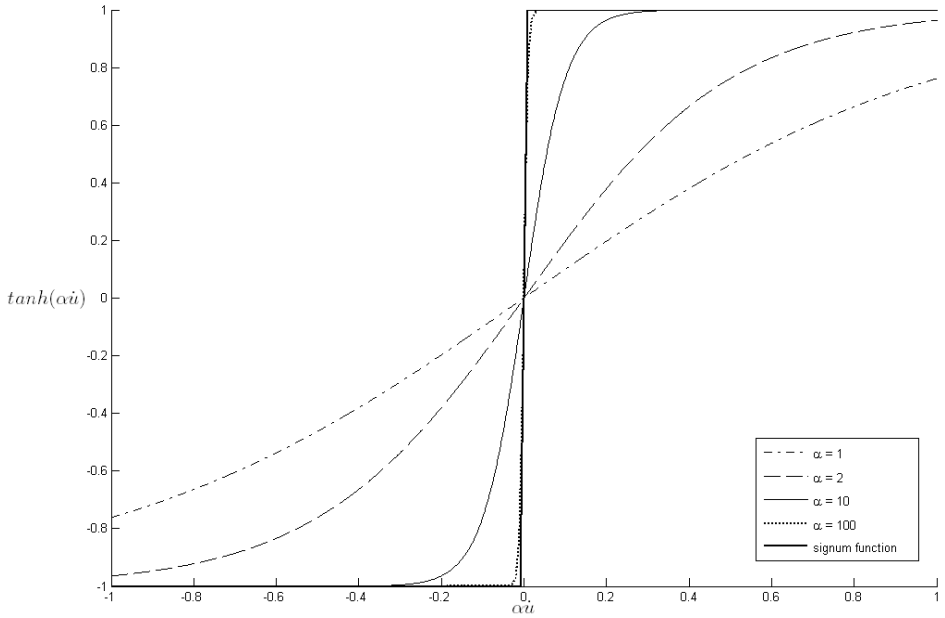

Figure 4.4 comparison of hyperbolic tangent function with signum function.

4.3 The modified Coulomb model

Most of the theoretical works on the seismic performance of sliding isolated systems have been done by utilizing the Coulomb law [Constantinou et al., 1990]. Experimental results, however, show that the material behaviour deviates significantly from that of Coulomb's law of friction [Constantinou, 1987] and [Mokha et al., 1990, 1991, and 1993]. In experiments done on Teflon-steel interfaces, it has been observed that [Mokha et al., 1990] and [Constantinou et al., 1990]:

- the friction force at the initiation of sliding, the breakaway friction force, is substantially larger than the starting (kinetic) value.
- both of these friction coefficients are independent of the sliding acceleration between sliding layers.
- both values depend on the bearing pressure and sliding velocity.
- prestraining of samples reduces the breakaway coefficient. Several cycles of loading with large sliding velocity, however, increase the friction force.

An important factor controlling the friction coefficient in the sliding phase, μ_s, is the sliding velocity.

Velocity-dependent friction coefficient is defined as [Constantinou et al., 1990]:

$$\mu_s = f_{\max} - (f_{\max} - f_{\min})\, e^{-\beta \dot{u}} \tag{4.6}$$

$$F_f = \mu_s W \, sign(\dot{u}) \tag{4.7}$$

in which f_{max} and f_{min} are friction coefficients at high and low sliding velocities, respectively. β is a constant depending on the bearing pressure and condition of the rubbing surfaces. $\dot{u}$ is the sliding velocity. This model is referred to as the *modified Coulomb model*.

4.4 Viscoplasticity model

There are certain complications by applying the modified Coulomb model. For systems with multiple sliding bearings, as in bridges, in which Teflon bearings are placed on top of flexible piers, it is required to apply multiple stick-slip criteria. This makes the model too complicated.

Based on theories of viscoplasticity and random vibration, *the modified viscoplasticity model* has been developed [Wen, 1976], [Park et al., 1986], and [Constantinou et al., 1990]:

$$Y \dot{Z} + \gamma |\dot{u}| Z |\dot{Z}| + \beta \dot{u} Z^2 - \dot{u} = 0 \tag{4.8}$$

$$F_f = \mu_s W Z \tag{4.9}$$

in which $\dot{u}$ stands for the sliding velocity, and Z, as a hysteretic dimensionless quantity, stands for the signum function (Equation 4.1). Y represents the yield displacement, which is in a range of 0.13-0.5 mm. β and γ are model parameters [Constantinou and Adnan, 1987]:

$$\beta + \gamma = 1 \tag{4.10}$$

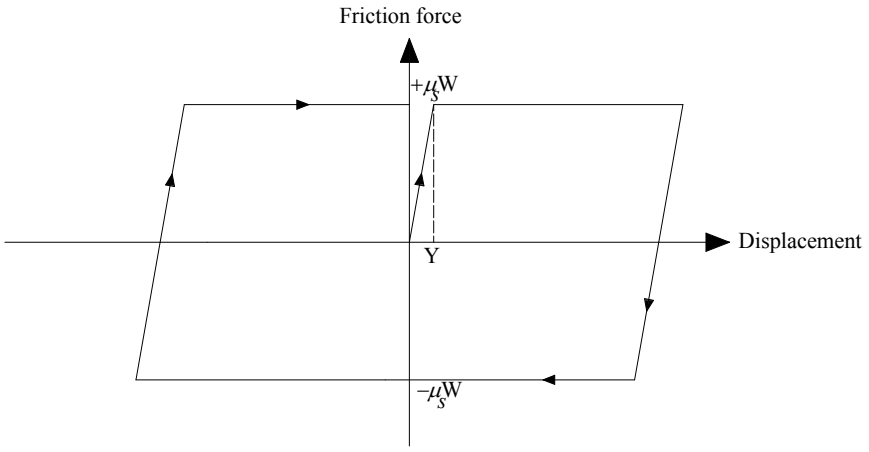

Figure 4.5 Friction force according to the viscoplasticity model in a cycle of loading and unloading, assuming constant sliding velocity.

During sticking phases the absolute value of Z is less than unity and when the set slides, Z takes values of ± 1, depending on the direction of sliding. This model produces a very small elastic displacement, Y, which is consistent with the primary elastic shear deformation of Teflon reported in experimental studies (Figure 4.5).

To account the breakaway friction in the current formulation, μ_s in equation 4.6 is modified for very low sliding velocities as:

$$\mu_s = b\, f_{\min} \qquad for \qquad |Z| \le .999 \tag{4.11}$$

in which *b* is a constant larger than unity taken from experimental studies (Figure 4.6).

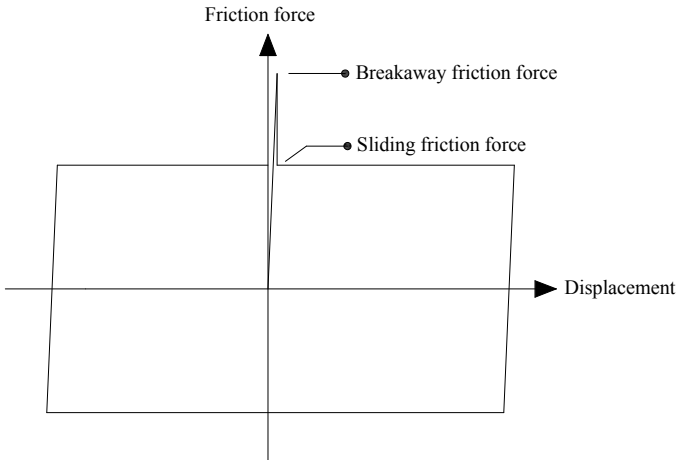

Figure 4.6 Breakaway friction coefficient in viscoplasticity model, assuming constant sliding velocity.

4.5 Frictional properties of Teflon

According to studies on frictional properties of Teflon bearings, the sliding velocity is an important factor controlling the friction coefficient of such bearings. High sliding velocities produce larger friction coefficients. The trend levels off from certain sliding velocities (Figure 4.7).

It has been observed that the sliding acceleration does not have a great effect on the friction coefficient. However, the friction coefficient decreases as the bearing pressure increases (Figure 4.7). At a certain pressure level, this tendency vanishes.

The friction coefficient in the direction perpendicular to the direction of polishing has been reported to be 15%-30% higher than the one in the polishing direction [Mokha et al., 1993].

The friction coefficient of unfilled Teflon layers is reported to be lower than the one of layers filled with glass fibers.

As stated before the friction coefficient at the initiation of sliding, the breakaway coefficient, is substantially larger than the sliding one. This effect has been reported only for the first run of loading and the difference for pre-strained specimens is not that large. According to an experiment by [Mokha et al., 1991] it has been shown that a long period load dwelling has no considerable effect on the breakaway and sliding friction coefficients. In contrast to that, both these two parameters are highly sensitive to contaminations. Therefore, isolation modules must be maintained in a closed environment, to prevent dust and water from gathering in the bearing's module.

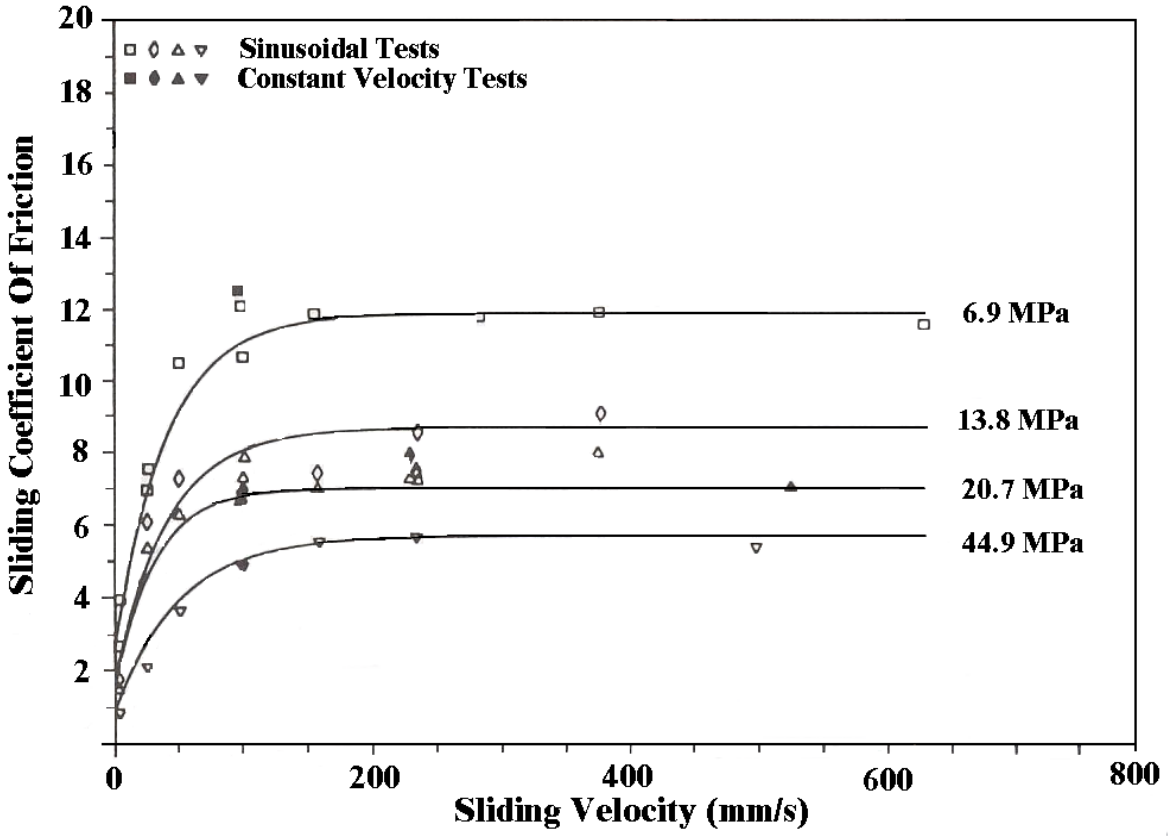

Figure 4.7 Variation of sliding friction coefficient with velocity and pressure of Teflon against polished stainless steel plate [Soong and Constantinou, 1994].

Chapter 5

Concept of Base Isolation

Ductile design concept assumes that part of the seismic input energy of an earthquake will be absorbed by the formation of plastic hinges (damage) in predefined locations. In isolated systems, however, the induced forces are reduced (and in some cases dissipated). As a result of a period shift by isolation it is possible to reduce considerably the forces transmitted to the structure. In addition, higher damping ratios help to some extent to increase the efficiency of the isolation method. In this chapter, the response spectrum analysis is briefly discussed and then the period shift effect is introduced. A simple two-degree-of-freedom system is applied to show how isolation leads to smaller transmitted seismic forces in the structure. Finally, some limitations of this strategy are discussed.

5.1 Philosophy of isolation

The seismic energy transmitted to a structure during an earthquake can be decomposed as [Chen, 1999]:

$$IE = KE + DE + SE \tag{5.1}$$

where *IE* is the input seismic energy, *KE* the kinetic energy, *DE* the dissipated energy, and *SE* the strain energy. By ductile designing of structures, it is possible to form a finite number of plastic hinges in the system in the case of extreme lateral loading without endangering the general stability of the structure. This is the so-called ductility concept for traditional fixed-base structures.

To get an insight into the role of isolation in the seismic protection of structures a single-degree-of-freedom system (SDOF) has been applied. Hence, the structural behaviour is assumed to be rigid. As will be shown later on, this is a reasonable assumption for isolated structures.

The differential equation governing the behaviour of such a set under seismic excitations is:

$$m\ddot{u} + c\dot{u} + ku = -m\ddot{u}_g \tag{5.2}$$

where *m*, *c*, and *k* are mass, damping, and stiffness of the system, respectively. *u* is the relative displacement of the degree of freedom. $\ddot{u}_g$ is the ground acceleration. Defining natural and damped frequencies of vibration as:

$$\omega = \sqrt{\frac{k}{m}} \tag{5.3}$$

$$\omega_d = \omega\sqrt{1-\xi^2} \tag{5.4}$$

where

$$\xi = \frac{c}{2m\omega} \tag{5.5}$$

The response of such a *SDOF* system to an arbitrary earthquake excitation, $\ddot{u}_g$, can be expressed by *Duhamel's integral* as:

$$u(t) = \frac{1}{\omega_d} \int_0^t -\ddot{u}_g(\tau) e^{-\xi\omega(t-\tau)} \sin\left[\omega_d (t-\tau)\right] d\tau \tag{5.6}$$

Applying the Duhamel's integral over a wide range of structural periods and damping ratios, the *response spectrum* can be constructed (Figure 5.1 and Section 7.1.5). It plots the maximum structural response over the structural period. Depending on the type of response acceleration, velocity, and displacement spectra can be generated. For example for a harmonic excitation the pseudo-acceleration response spectrum is computed by two times differentiation of equation 5.6, which is:

$$a(t) = \omega^2 u(t) \tag{5.7}$$

that is used to compute the base shear.

(a)

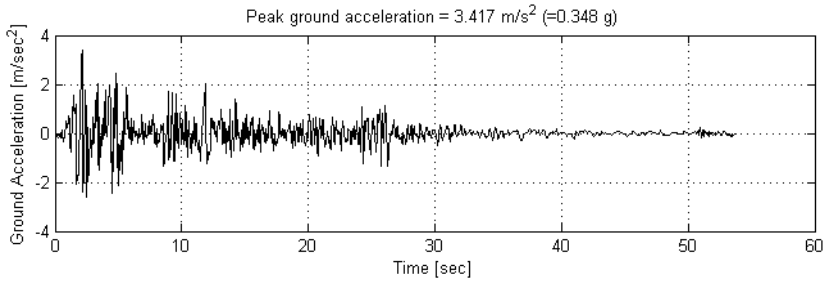

(b)

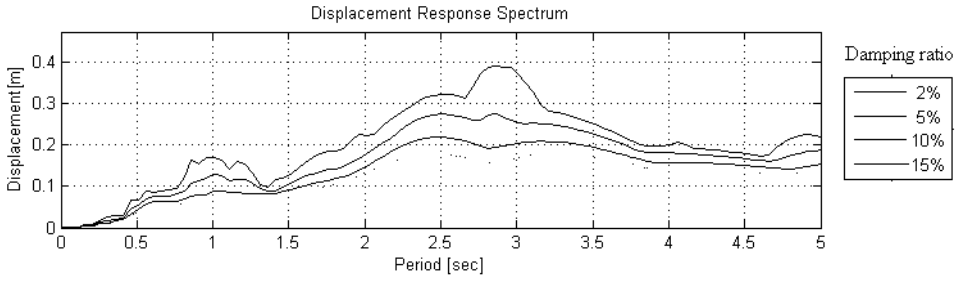

(c)

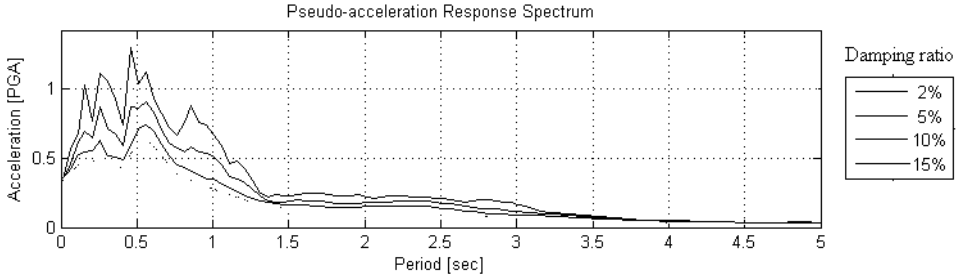

Figure 5.1 (a) El Centro accelerogram, (b) displacement, and (c) acceleration response spectrum.

The response spectrum of a single earthquake cannot be a good representative design criterion for a specified region, as there are numerous factors influencing the structural response. By considering several earthquakes belonging to different local faults in the region and doing probabilistic studies over possible maximum ground accelerations and returning periods of each of them, it is possible to construct a norm response spectrum, which is a safe envelope covering all possible earthquakes (Figure 5.2). The values for T_B, T_C, and T_D, are site-dependent and can be taken for standard cases from engineering codes, e.g. in Europe from Eurocode 8.

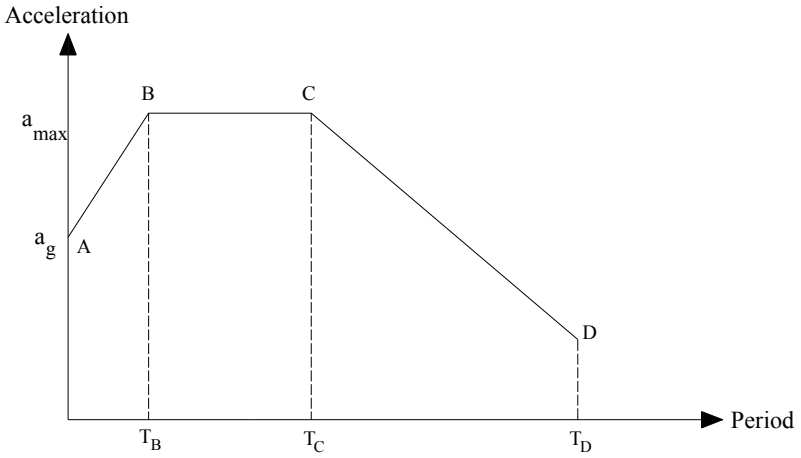

Figure 5.2 Norm response spectrum.

If the structural natural period of vibration is shifted to a higher range with some kind of softer structural design, for instance with a *base isolation method*, it is possible to design the structure for a lower range of seismic forces. Figures 5.3 demonstrates that the period shift reduces the original acceleration of a_1 to the smaller value a_2.

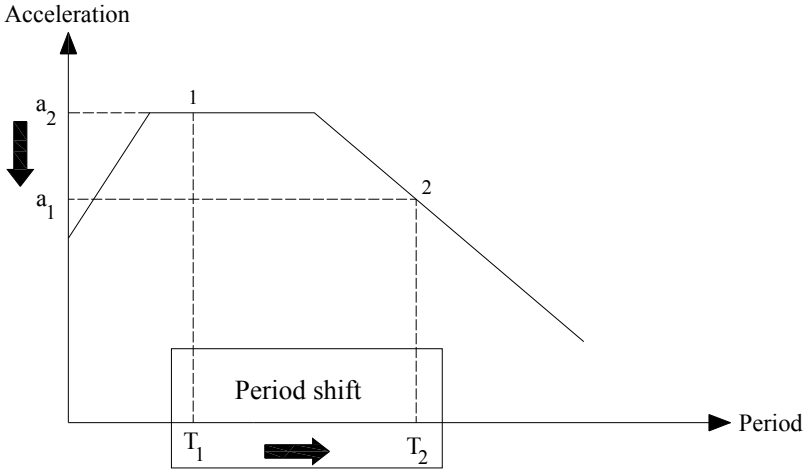

Figure 5.3 The effect of period shifting in the reducing of seismic loads.

Besides, by increasing the damping ratio in a structure it is possible to reduce the seismic forces transmitted to the structure (Figure 5.4). It should be taken into consideration that this effect is restricted and it does not always work. This will be discussed later on.

An appropriate structural period of vibration for isolated structures is in the range of 1.2 to 2.0 seconds. This range is far from the dominant period of vibration of most devastating earthquakes. Isolated structures are susceptible to *resonance* in case of near field earthquakes or against seismic waves, which have traveled a long distance in soft soil layers. Soft soil

layers function the same as a filter medium, producing long period waves, as in the 1985 Mexico City earthquake. Long period waves are dangerous for isolated systems with large period of vibration. They can produce large displacements because of resonance. Therefore a local inappropriate soil layer must be excavated. If sedimentary layers are thick, an extra damping mechanism, among other techniques, can prevent the resonance phenomenon.

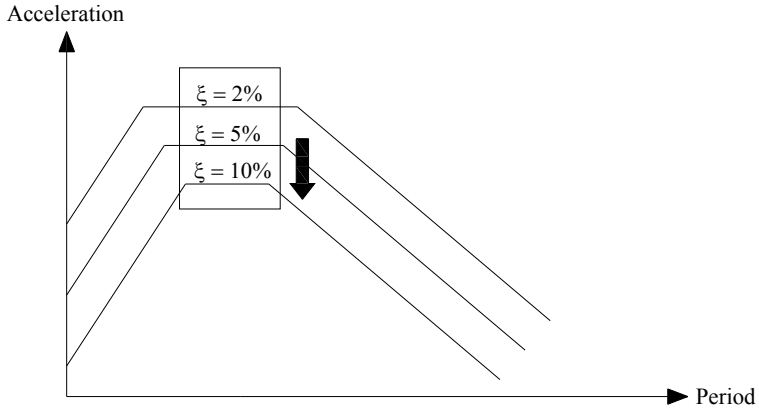

Figure 5.4 The response spectrum regarding structural damping.

5.2 Theory of seismic isolation

To get a better understanding of the concept of *base isolation* a more detailed model rather than the one used in the previous section is needed, in which the structure and the isolation bearings are simulated separately (Figure 5.5).

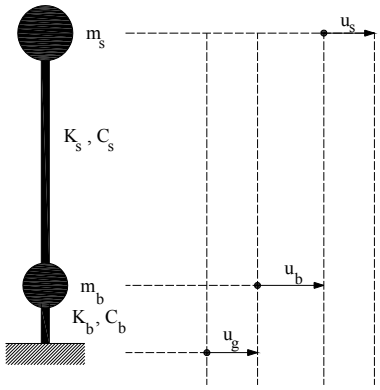

Figure 5.5 A two-degree-of-freedom isolated system and its simplified physical model.

The differential equations governing such a set are [Mostaghel and Khodaverdian, 1988], [Kelly, 1996], and [Jamali and Zahlten, 2006]:

$$\begin{cases} m_s(\ddot{u}_s + \ddot{u}_b + \ddot{u}_g) + m_b(\ddot{u}_b + \ddot{u}_g) + c_b\dot{u}_b + k_b u_b = 0 \\ m_s(\ddot{u}_s + \ddot{u}_b + \ddot{u}_g) \qquad\qquad + c_s\dot{u}_s + k_s u_s = 0 \end{cases} \tag{5.8}$$

where the indices *s*, *b*, and *g* stand for *structure*, *base*, and *ground*, respectively. *m*, *c*, and *k* are the *mass*, *damping*, and *stiffness* of the degrees of freedom. u, $\dot{u}$, and $\ddot{u}$, displacement, velocity, and acceleration of the degrees of freedom, correspondingly, are all written in a relative coordinate system (Figure 5.5). Rearranging the equations and rewriting them in a matrix form:

$$\mathbf{M}\ddot{\mathbf{u}} + \mathbf{C}\dot{\mathbf{u}} + \mathbf{K}\mathbf{u} = -\mathbf{M}\mathbf{r}\ddot{u}_g \tag{5.9}$$

in which

$$\mathbf{u}=\begin{bmatrix}u_b\\u_s\end{bmatrix},\ \mathbf{M}=\begin{bmatrix}m_s+m_b & m_s\\m_s & m_s\end{bmatrix},\ \mathbf{C}=\begin{bmatrix}c_b & 0\\0 & c_s\end{bmatrix},\ \mathbf{K}=\begin{bmatrix}k_b & 0\\0 & k_s\end{bmatrix},\ \mathbf{r}=\begin{bmatrix}1\\0\end{bmatrix} \tag{5.10}$$

Defining the mass and frequency ratios as:

$$\gamma=\frac{m_s}{m_b+m_s} \tag{5.11}$$

$$\varepsilon=(\frac{\omega_b}{\omega_s})^2 \tag{5.12}$$

in which ω_b and ω_s are isolation and structural circular frequencies:

$$\omega_b=\sqrt{\frac{k_b}{m_b+m_s}} \tag{5.13}$$

$$\omega_s=\sqrt{\frac{k_s}{m_s}} \tag{5.14}$$

In this model the structural and base masses are both considered to be in the same order. The structure, however, is much stiffer than the isolators. These are formulated as:

$$\gamma=\mathrm{O}(10^0) \tag{5.15}$$

$$\varepsilon=\mathrm{O}(10^{-2}) \tag{5.16}$$

For further discussion the eigenvalue problem is solved [Chopra, 2001]:

$$[\mathbf{K}-\omega_n{}^2\,\mathbf{M}]\mathbf{\Phi}_n=\mathbf{0} \tag{5.17}$$

where ω_n and Φ_n are the eigenvalue and eigenvector of an arbitrary mode. The characteristic equation as a function of ω_n is:

$$(1-\gamma)\omega_n{}^4-(\omega_b{}^2+\omega_s{}^2)\omega_n{}^2+\omega_b{}^2\omega_s{}^2=0 \tag{5.18}$$

Circular frequencies of the first and second modes are:

$$\omega_1{}^2=\frac{1}{2(1-\gamma)}\left\{\omega_b{}^2+\omega_s{}^2-\left[(\omega_b{}^2+\omega_s{}^2)^2-4(1-\gamma)\omega_b{}^2\omega_s{}^2\right]^{\frac{1}{2}}\right\} \tag{5.19}$$

$$\omega_2{}^2=\frac{1}{2(1-\gamma)}\left\{\omega_b{}^2+\omega_s{}^2+\left[(\omega_b{}^2+\omega_s{}^2)^2-4(1-\gamma)\omega_b{}^2\omega_s{}^2\right]^{\frac{1}{2}}\right\} \tag{5.20}$$

Considering only terms with higher order, mode frequencies are:

$$\omega_1\approx\omega_b\sqrt{1-\gamma\varepsilon} \tag{5.21}$$

$$\omega_2\approx\omega_s\sqrt{\frac{1+\gamma\varepsilon}{1-\gamma}} \tag{5.22}$$

Eigenvectors corresponding to these eigenvalues are (Figure 5.6):

$$\Phi_1 = \begin{bmatrix} 1 \\ \varepsilon \end{bmatrix}$$

$$\Phi_2 = \begin{bmatrix} 1 \\ -\dfrac{1-(1-\gamma)\varepsilon}{\gamma} \end{bmatrix} \tag{5.23}$$

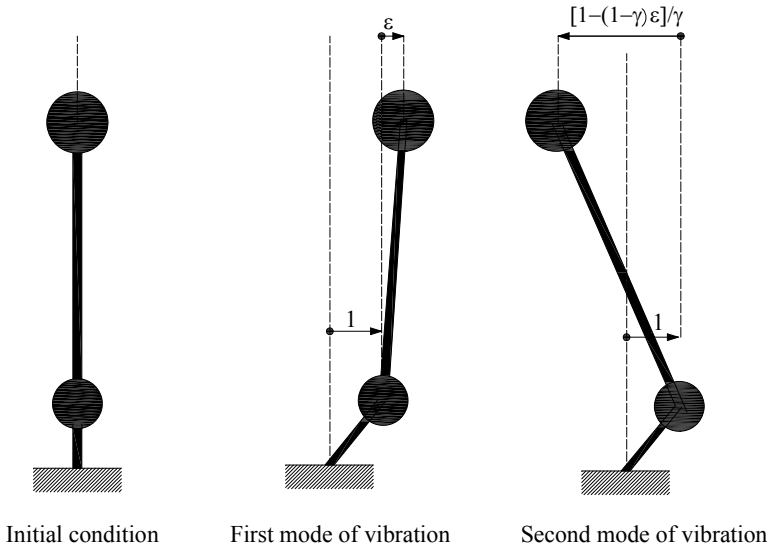

Figure 5.6 Modal shapes of vibration.

It should be noted that eigenvectors are given in the relative coordinate system, as the differential equations were also defined in a relative coordinate system.

The relative displacement of the second degree of freedom in the first mode is negligible in comparison to the relative displacement of the first degree of freedom in this mode, i.e. there is almost a rigid behaviour in the structure. This mode is the favourable excitation mode, explaining the efficiency of the base isolation method. In contrast to the first mode, the response of the second mode is unfavourable, as the relative displacement of the second degree of freedom is much larger than that of the first degree of freedom and in the opposite direction.

Although the second mode is unfavourable, it does not lead to an inefficiency of the base isolation method. To prove it, *the modal participation factor* is firstly defined as:

$$\boldsymbol{\Gamma} = \frac{\boldsymbol{\Phi}^{\mathrm{T}}\mathbf{M}\mathbf{r}}{\boldsymbol{\Phi}^{\mathrm{T}}\mathbf{M}\boldsymbol{\Phi}} \tag{5.24}$$

Using the approximate values of the eigenvectors the participation factors of the first and second modes of vibration are:

$$\Gamma_1 = 1-\gamma\,\varepsilon \tag{5.25}$$

$$\Gamma_2 = \gamma\,\varepsilon \tag{5.26}$$

As long as γ and ε have the orders assumed in this section, the participation factor of the second mode is considerably smaller than the first one. Therefore, the response of such a system is mainly governed by its first mode of vibration.

As far as the structural and isolation natural frequencies of vibration, ω_s and ω_b, respectively, are well separated, i.e. a very stiff structure with a very flexible isolation layer, the argumentation above is valid. Otherwise the frequency ratio, ε, would not be that small, which means a higher participation factor of the unfavourable second mode. This explains why a single-degree-of-freedom model gives a relatively good approximation of the general response of an isolated structure to seismic excitations.

Chapter 6

Friction Pendulum Systems (FPS)

In friction pendulum isolation systems, structures are decoupled from their foundation through special sliding bearings. Because of the concavity of base plates in friction pendulum bearings, a restoring force is produced in the system that constrains the permanent sliding displacement after severe shakings. The FPS has the same frequency of vibration as a simple pendulum, which depends only on its radius of curvature and the gravitational acceleration g. Several possible configurations of the friction pendulum bearing are firstly demonstrated in this chapter. Then the restoring mechanism and forces in such a system are introduced. After introduction of the stick-slip criterion, equivalent damping and stiffness in such systems are derived.

6.1 Introduction

Friction Pendulum Systems (FPS), were first devised by [Zayas et al., 1987], in which isolation, dissipation, and restoring mechanisms are all integrated in one unit. Several numerical and experimental studies have been done in the last two decades on these systems, among them [Al Hussaini et al., 1994] and [Tsai et al., 2005] on small deformations, [Almazan and Llera, 1998 and 2002] on large deformations and $P-\Delta$ effect, [Roussis and Constantinou, 2006] on the uplift prevention, [Mokha et al., 1990], [Al Hussaini et al., 1994], and [Tsai et al., 2003] on full scale tests on the shaking table.

So far friction pendulum systems have been used mainly to retrofit and upgrade historical buildings seismically, as in US Court of Appeals [Mokha et al., 1996], and Oakland, San Francisco, and Los Angeles city halls [Naeim and Kelly, 1999]. Some other great projects as the San Francisco airport international terminal and huge LNG tanks in Greece and Turkey are among other seismically isolated structures with FPS.

6.2 Generalities

A friction pendulum bearing is composed of three main parts: a lower concave plate fixed to the foundation of the structure, an upper pedestal fixed to its top column, and an articulated slider in between (Figure 6.1). The slider is coated with a special Teflon layer (sometimes with other materials such as Techmet-B) to generate a low friction coefficient in the range of 0.05-0.10.

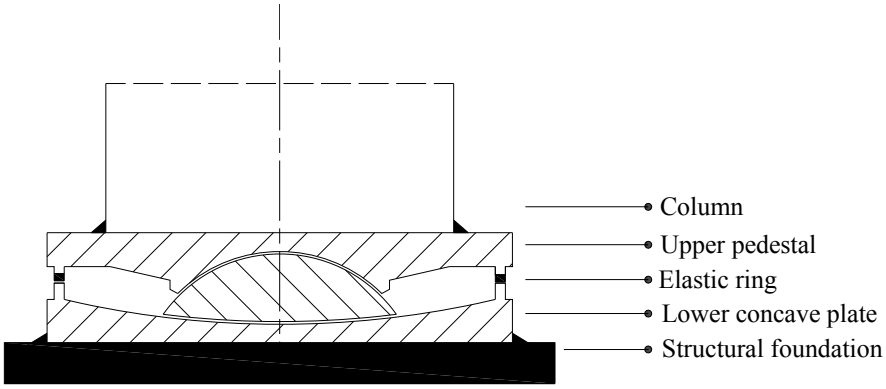

Figure 6.1 A schematic view of a downward friction pendulum isolator.

A bearing element can be installed either downwardly, as in figure 6.1, or upwardly (Figure 6.2). The direction of installation of an element makes no significant difference on the seismic response of the structure. However, in case of large deformations, extra bending moments produced because of $P-\Delta$ effects, will be distributed differently in the super- and sub-structures [Almazan and Llera, 2003].

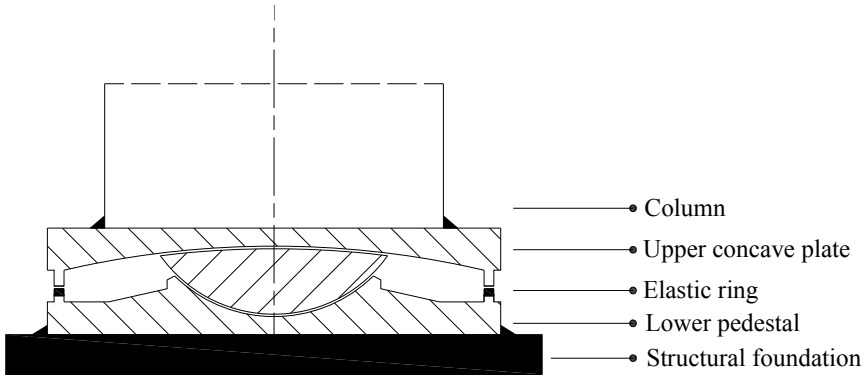

Figure 6.2 A schematic view of an upward friction pendulum isolator.

Where a high sliding displacement capacity is required, as in large-spanned bridges, two-sided isolation bearings are used (Figure 6.3). These bearing have the same features as those stated before. Because of the double curvature of sliding plates, the sliding displacement capacity of the bearing is doubled.

The general geometry of the FPS is the same as a simple pendulum. Hence, they both have the same oscillation frequency. For small deformations, the circular frequency is approximated as:

$$\omega=\sqrt{\frac{g}{R}} \tag{6.1}$$

in which g is the gravitational acceleration (9.81 m/s^2) and R the radius of curvature of the sliding surface. For large deformations the period is:

$$T=2\pi\sqrt{\frac{R}{g}}\left[1+\frac{1}{4}\sin^2(\frac{\hat{\varphi}}{2})+\ldots\right] \tag{6.2}$$

where $\hat{\varphi}$ is the maximum oscillation angle (Figure 6.4). For practical cases, where $\hat{\varphi}$ is relatively small, equation 6.1 has the required accuracy.

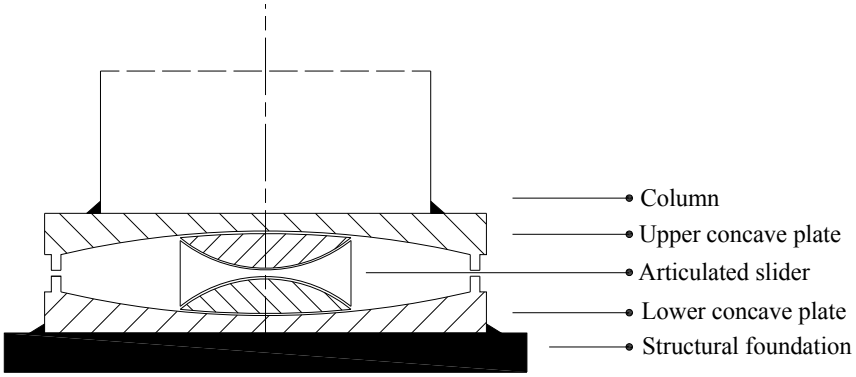

Figure 6.3 A schematic view of a two-sided friction pendulum isolator.

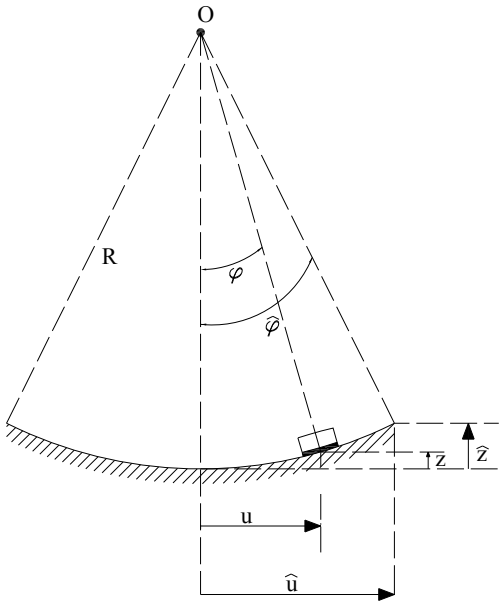

Figure 6.4 Simplified geometrical configuration of FPS.

As a bearing slides on its lower (upper) concave surface the structure rises up. The resulted vertical displacement of the structure is (Figure 6.4):

$$Z = R - \sqrt{R^2 - u^2} \tag{6.3}$$

In comparison to the horizontal displacement, the vertical displacement is negligible. For example the maximum vertical displacement of an isolator with a radius of curvature of 2 meters and a maximum horizontal displacement of 25 centimetres is about 1.6 centimetres (about 6.5% of the horizontal displacement).

Forces acting on an FPS bearing are frictional and gravitational forces (Figure 6.5). Assuming that the isolator is sliding to the right-hand side, for small oscillation angles regarding the equation of equilibrium:

$$F = F_f + \frac{W}{R}u \tag{6.4}$$

in which W is the vertical load over the bearing, F_f the friction force, and F the resultant force in the slider. In the abovementioned formulation, the vertical displacement of the slider is supposed to be small in comparison to its horizontal displacement. The second term is the so-

called restoring (recentering) force, produced because of the concavity of the sliding plate (Equation 6.4). For a bearing sliding on a flat surface this term vanishes. For two-sided bearings the sum of both radii of curvature must be applied as the radius of curvature (Figure 6.3).

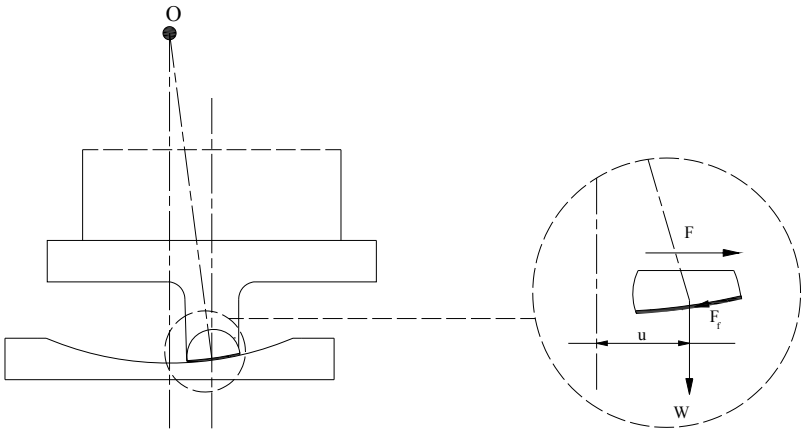

Figure 6.5 Forces acting on the articulated slider (not scaled).

Regarding the definition of stiffness of a degree of freedom, i.e. the force required to produce one unit of displacement in that degree of freedom, the ratio of the weight of the structure to the radius of curvature of the sliding surface (W / R) can be defined as equivalent stiffness of the isolation element (geometrical stiffness).

6.3 Differential equation governing FPS

The simplest model simulating a friction pendulum system is a one-degree-of-freedom system, in which the structural response is assumed to be rigid. The differential equation governing such a set is:

$$m\ddot{u} + \frac{W}{R}u = -F_f - m\ddot{u}_g \tag{6.5}$$

where u and $\ddot{u}$ are the relative displacement and acceleration of the degree of freedom, respectively. W and m are weight and mass of the set. F_f stands for the friction force. $\ddot{u}_g$ is the ground acceleration (Figures 6.6 and 6.7).

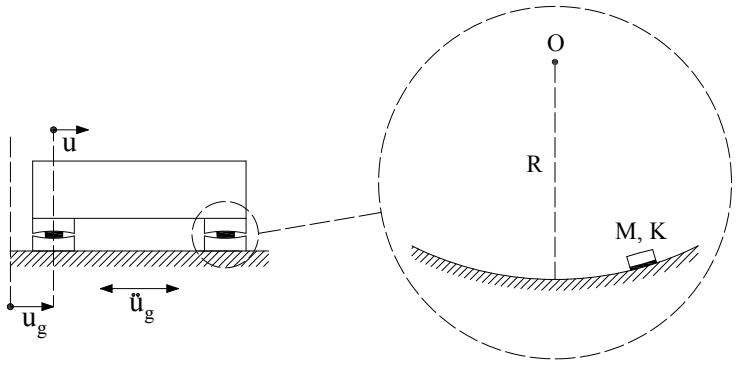

Forces in the system

$m(\ddot{u}_g + \ddot{u})$	Inertial force
$\frac{W}{R}u$	Restoring force (F_R)
F_f	Friction force

Figure 6.6 Simplified physical model of an isolated set assuming a rigid structural response (not scaled).

6.4 Stick-slip Criterion

A prominent factor controlling the numerical accuracy of simulation of such an isolated system is the accurate prediction of phase changes between sticking and sliding. As long as the static friction force has not been overcome, the slider remains sticking. When the resultant force overcomes the static friction force (or the breakaway friction force in the viscoplasticity model) the bearing begins sliding. Therefore, it is of great importance to find the exact time of phase changes.

For a single-degree-of-freedom system the stick-slip criterion is formulated as:

$$\left| m\ddot{u}_g + \frac{W}{R}u \right| \overset{?}{\geq} \left| F_f \right| \tag{6.6}$$

After sliding initiation, the stick-slip criterion is not checked anymore until the sliding velocity vanishes. At this moment if the resultant force in the slider overcomes the static friction force, the slider sticks just for a moment and will slide in the opposite direction, i.e. a change in the direction of sliding. Otherwise the mass sticks where it is.

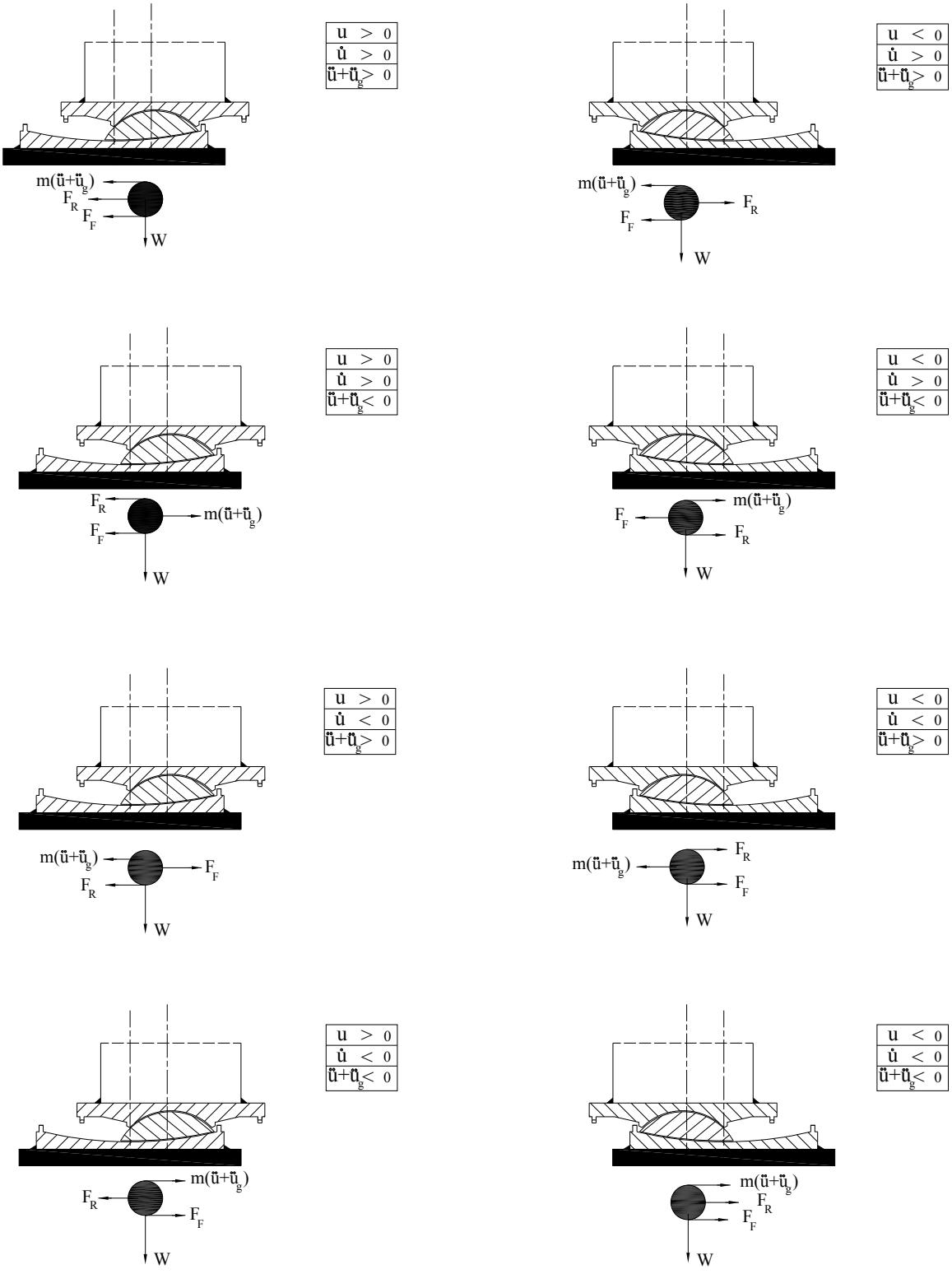

Figure 6.7 Forces acting on an FPS bearing in different configurations.

6.5 Equivalent damping and stiffness

A rough estimate of stiffness and damping of an isolation mechanism is essential for the preliminary steps of the design process. Equivalent damping and stiffness approximated in this way are used to calculate main design factors as base shear and maximum sliding displacement to choose an appropriate isolation bearing. There are numerous methods to estimate equivalent features of such systems [Beucke and Kelly, 1985] and [Petersen, 1996 and 2005].

In friction pendulum systems the resultant force in the isolator is composed of two terms: the friction force, which is a constant term in case of the Coulomb friction model, and the restoring force (F_R), because of the geometrical stiffness (Equation 6.5 and Figure 6.8).

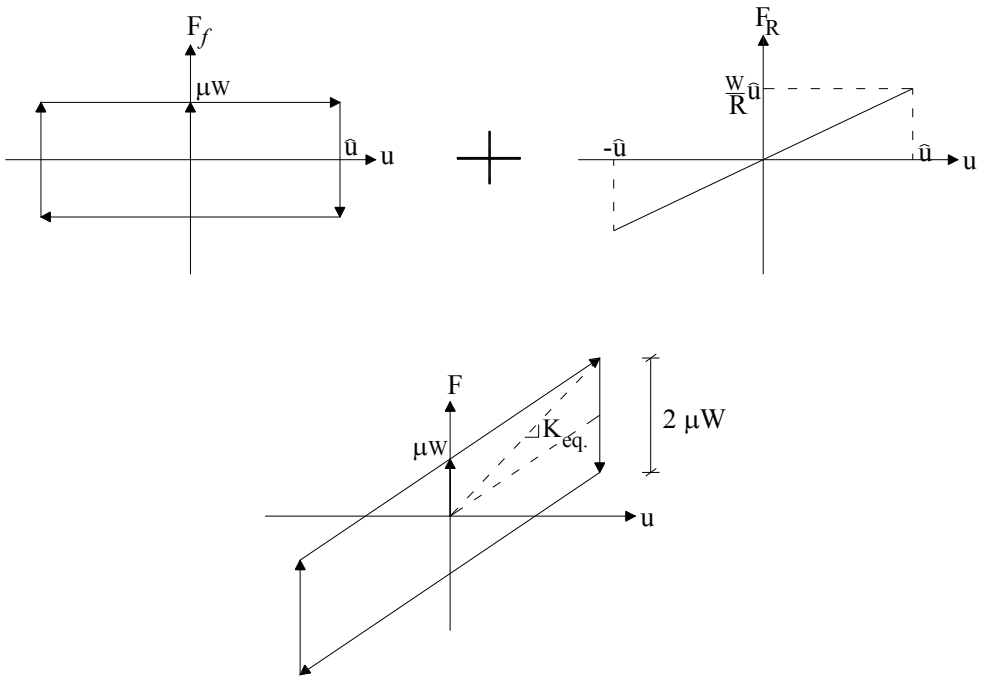

Figure 6.8 Friction, restoring and resultant forces in the isolator in a cycle of loading and unloading.

The energy dissipated by the friction force under periodic forced-displacement with a loading frequency Ω:

$$u = \hat{u}\sin(\Omega t) \tag{6.7}$$

applied to a friction pendulum system is:

$$W_d = 4 F_f \hat{u} \tag{6.8}$$

in which $\hat{u}$ is the maximum displacement and W_d is the surface under the diagram of friction force versus displacement in a full cycle of loading and unloading (Figure 6.8).

Defining an equivalent linear stiffness for such a system as:

$$K_{eq.} = \frac{\hat{F}}{\hat{u}} = \frac{W}{R} + \frac{\mu W}{\hat{u}} \tag{6.9}$$

in which $\hat{F}$ is the maximum resultant force acting on the slider, which occurs at the maximum sliding displacement. The work done by such an artificial spring is:

$$W_k = \frac{1}{2}\hat{F}\hat{u} = \frac{1}{2}\left(\frac{W}{R}\hat{u} + \mu W\right)\hat{u} \tag{6.10}$$

It should be taken into consideration that by increasing the maximum sliding displacement, the equivalent stiffness decreases, which is considered a drawback for such systems.

If the system is assumed to be in resonance, the equivalent damping is then given by:

$$\xi_{eq.} = \frac{1}{4\pi}\frac{W_d}{W_k} = \frac{2}{\pi}\frac{\mu}{\frac{\hat{u}}{R} + \mu} \tag{6.11}$$

in which μ is the friction coefficient, $\hat{u}$ the maximum displacement, and R the radius of curvature of the sliding bearing.

Similar to the equivalent stiffness, the equivalent damping decreases as the maximum sliding displacement increases.

Chapter 7

Numerical Simulation of Dynamic Response of FPS

A numerical simulation of the structural response of friction based-isolated systems to earthquake motions is a time consuming task with existing numerical models. There are several numerical methods to simulate the structural response, namely time stepping methods, modal analysis, response spectrum analysis, frequency domain analysis, and time domain analysis. In this chapter some of them are briefly reviewed. Then a numerical model combined of the constant average acceleration method (time stepping) and modal analysis is developed and applied to simulate the behavior of one degree-of-freedom systems isolated with friction pendulum bearings under earthquake motions. Afterwards, the model is generalized to simulate two and many degree-of-freedom systems as well. The method is based on the activation of an extra element to simulate a sliding bearing as soon as the sliding is initiated in the set. Finally, some considerations about damping are discussed.

7.1 Numerical methods

Considering all forces acting on a body, the dynamic response of a system can be modelled by:

$$\mathbf{M}\ddot{\mathbf{u}}_{tot} + \mathbf{C}\dot{\mathbf{u}}_{rel} + \mathbf{K}\mathbf{u}_{rel} = \mathbf{P}(t) \tag{7.1}$$

in which **M**, **C**, and **K** are the mass, damping, and stiffness matrices, respectively. $\mathbf{u}$, $\dot{\mathbf{u}}$, and $\ddot{\mathbf{u}}$ are the displacement, velocity, and acceleration vectors, respectively. **P**(t) is the load vector acting on the set in the time domain. For damping and stiffness forces, 2nd and 3rd terms of the equation, relative variables (values) are required. To compute inertial forces, however, the absolute acceleration, in case of earthquake loading the sum of the ground acceleration and the relative acceleration of the degree of freedom, must be used. For earthquake excitations there is no explicit form of loading. A part of the inertial force because of the ground acceleration takes this role:

$$\mathbf{M}\ddot{\mathbf{u}}_{rel} + \mathbf{C}\dot{\mathbf{u}}_{rel} + \mathbf{K}\mathbf{u}_{rel} = -\mathbf{M}\ddot{\mathbf{u}}_{g} \tag{7.2}$$

All variables used in this chapter are considered relative, here with subscript $_{rel}$, unless it is explicitly stated that they are total (absolute) values, here with subscripts $_{tot}$.

There are several numerical methods to solve such a differential equation [Meskouris, 1999]. In the coming sections some of them will be briefly reviewed.

7.1.1 Time stepping methods

The step-by-step procedure is a general approach to dynamic response analysis and is mainly used for nonlinear systems. Considering the differential equation governing the dynamic response of a system (Equation 7.1) subjected to initial conditions:

$$u_0 = u(0) \tag{7.3}$$

$$\dot{u}_0 = \dot{u}(0) \tag{7.4}$$

the response of the system is determined in an arbitrary time step t_i relying on its previous time steps' results. Accuracy, efficiency, stability, and the rate of convergency are main factors, considered to compare different algorithms. Algorithms are divided into two main groups of explicit and implicit types, in which in explicit methods just the results of the previous known time steps are required. In implicit methods, however, unknown parameters of the current time step are also needed to compute the unknown variables. *Euler-Cauchy*, *Runge-Kutta*, and *central difference method* are some examples of explicit methods. *Park*, *Newmark*, and *Wilson-Θ methods* are classified among implicit algorithms [Petersen, 1996], [Clough and Penzien, 1993], and [Chopra, 2001].

In this study *Constant Average Acceleration* (CAA) method has been used to solve numerically the differential equation (Equation 7.1). The method is unconditionally stable and it is a self-starting method. In this method it is assumed that the acceleration remains constant in every time step:

$$\ddot{u}(\tau) = \frac{1}{2}(\ddot{u}^{i-1} + \ddot{u}^{i}) \tag{7.5}$$

in which *i* stands for the current time step and *i-1* for the last one, which is already known (Figure 7.1).

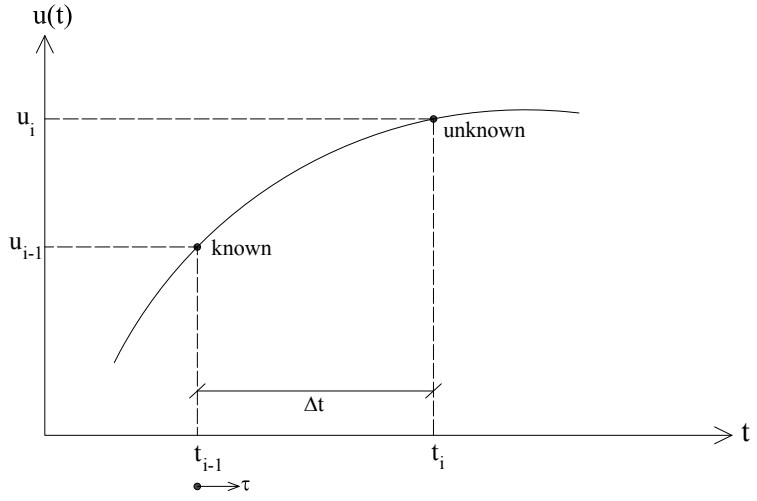

Figure 7.1 Constant average acceleration method.

To compute the unknown displacement, u_i, equation 7.5 must be integrated. Rewriting acceleration and velocity in term of u_i, and replacing them in equation 7.1 leads to the following system of algebraic equations:

$$\mathbf{K}_{\text{eff.}}\,\mathbf{u}^{i} = \mathbf{P}_{\text{eff}} \tag{7.6}$$

in which

$$\mathbf{K}_{eff} = \mathbf{K} + \frac{4}{\Delta t^2}\mathbf{M} + \frac{2}{\Delta t}\mathbf{C} \tag{7.7}$$

$$\mathbf{P}_{eff}(t) = \mathbf{P}(t) + \left(\frac{4}{\Delta t^2}\mathbf{M} + \frac{2}{\Delta t}\mathbf{C}\right)\mathbf{u}^{i-1} + \left(\frac{4}{\Delta t}\mathbf{M} + \mathbf{C}\right)\dot{\mathbf{u}}^{i-1} + \mathbf{M}\ddot{\mathbf{u}}^{i-1} \tag{7.8}$$

Based on the computed displacement at the end of a time step, velocity and acceleration are computed as:

$$\dot{\mathbf{u}}^{i} = \frac{2}{\Delta t}(\mathbf{u}^{i} - \mathbf{u}^{i-1}) - \dot{\mathbf{u}}^{i-1} \tag{7.9}$$

$$\ddot{\mathbf{u}}^{i} = \frac{4}{\Delta t^2}(\mathbf{u}^{i} - \mathbf{u}^{i-1}) - \frac{4}{\Delta t}\dot{\mathbf{u}}^{i-1} - \ddot{\mathbf{u}}^{i-1} \tag{7.10}$$

7.1.2 Modal analysis

For linear-elastic systems with many degrees of freedom (MDOF) it is inefficient, even sometimes not feasible, to solve the coupled set of differential equations of motion. In an alternative process, the system of equations can be transformed to another space so that the coupled set of equations can be decomposed into a set of uncoupled equations, i.e. several single-degree-of-freedom systems (SDOF), which can be solved much more easily. To this end, an eigenvalue problem must be solved to compute eigenvectors and eigenvalues of the system, which are used to transform the set of equations (Equation 7.1) into modal space (Equation 7.11).

$$\tilde{m}_n\ddot{\eta}_n + \tilde{c}_n\dot{\eta}_n + \tilde{k}_n\eta_n = \tilde{p}_n(t) \tag{7.11}$$

$$\tilde{p}_n(t) = \mathbf{\Phi}_n^{T}\,\mathbf{P}(t),\ \tilde{m}_n = \mathbf{\Phi}_n^{T}\,\mathbf{M}\,\mathbf{\Phi}_n,\ \tilde{k}_n = \mathbf{\Phi}_n^{T}\,\mathbf{K}\,\mathbf{\Phi}_n \tag{7.12}$$

$$\mathbf{u} = \sum_{j=1}^{\text{nmod}} \mathbf{\Phi}_j\,\eta_j \tag{7.13}$$

$\tilde{m}_n$, $\tilde{c}_n$, and $\tilde{k}_n$ are the modal mass, damping, and stiffness matrices of an arbitrary mode, respectively. Sub-index *n* denotes the mode number and $\mathbf{\Phi}$ is the eigenvector.

As the equations are decoupled in modal space, as a result of the *orthogonality of modes*, just the modes, which have the largest participation factors, are considered [Clough and Penzien, 1993] and [Chopra, 2001]. This leads to a drastic decrease of the numerical cost of the simulation.

7.1.3 Time domain analysis

Through *Duhamel's integral,* it is possible to simulate the response of a linear elastic system to an impulse. An arbitrary loading can be modelled as successive impulses over a range of time, each producing its own response over the time domain (Figure 7.2). Summing all these responses over the time domain the overall response of the set is [Clough and Penzien, 1993]:

$$h(t) = \frac{1}{m\omega}\int_0^t p(\tau)\,\sin\omega(t-\tau)\,d\tau \qquad t \geq 0 \tag{7.14}$$

where m and ω are the equivalent mass and frequency of an SDOF, respectively. p is the load function in the time domain. With a slight modification the same process may be applied to damped systems.

Normally it is not possible to compute equation 7.14 analytically. However, there are several efficient numerical algorithms to compute it, as for instance *simple summation*, *trapezoidal rule*, and *the Simpson's rule*.

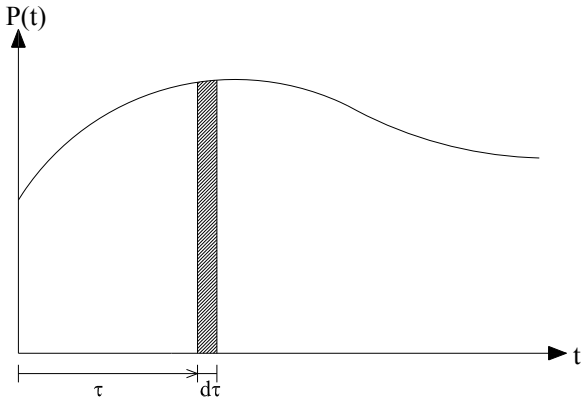

Figure 7.2 Decomposition of an arbitrary loading into several impulses.

7.1.4 Frequency domain analysis

For systems with frequency dependent parameters, as stiffness and damping of large bridges under wind load, it is more convenient to perform the analysis in the frequency domain instead of in the time domain. To this end the variables are first transformed into the frequency domain through *Fourier* (Equations 7.15) or *Laplace transformation* (Equation 7.16). After the analysis being done the results are transformed back again into the time domain. As there is normally no analytical solution for these transformations, several numerical methods have been developed to compute them, as *Discrete Fourier Transformation* (DFT) and *Fast Fourier Transformation* (FFT) methods. Because of a very high numerical cost of the frequency domain analysis, it is not normally applied for the earthquake analysis.

$$F(\omega)=\frac{1}{\sqrt{2\pi}}\int_{-\infty}^{+\infty} f(t)e^{-j\omega t}\,dt \tag{7.15}$$

$$F(s)=\int_{0}^{\infty} f(t)e^{-st}\,dt \tag{7.16}$$

7.1.5 Response spectrum analysis

Regarding time domain analysis with Duhamel's integral, the displacement produced in a system can be computed (Equation 5.6). For systems with low damping ratio, less than 10% of the critical damping, and neglecting the minus sign in the equation, as just the maximum response is desired not its direction, one may write:

$$u(t)=\frac{1}{\omega}\int_{0}^{t} -\ddot{u}_g(\tau)e^{-\xi\omega(t-\tau)}\sin\left[\omega(t-\tau)\right]d\tau \tag{7.17}$$

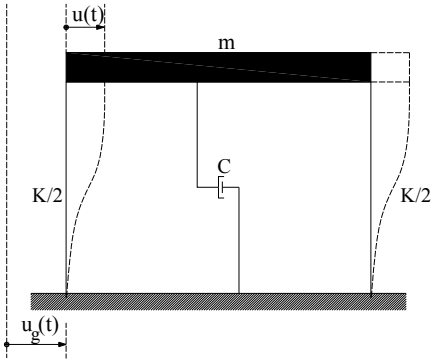

Figure 7.3 An arbitrary SDOF system under ground excitations.

By differentiating equation 7.17 the velocity and acceleration of the-degree-of-freedom can be computed. Maximum values of the response given by equation 7.17 and its derivatives are called *spectral relative displacement* (S_d), *velocity* (S_v), and *acceleration* (S_a). Taking only terms of higher order, the so-called *pseudo-velocity spectral response* and acceleration response are then formulated in term of spectral displacement response as:

$$S_{pv}(\xi,\omega) \approx [\int_0^t \ddot{u}_g(\tau)\, e^{-\xi\omega(t-\tau)} \cos\left[\omega(t-\tau)\right] d\tau]_{\max} \approx \omega S_d \tag{7.18}$$

$$S_{pa}(\xi,\omega) \approx \omega S_{pv} \approx \omega^2 S_d \tag{7.19}$$

The spectral relative acceleration is particularly significant in the structural analysis, as it is a measure for the maximum base shear:

$$F_{\max} = K S_d = \omega^2 m S_d = m S_a \tag{7.20}$$

where m is the total mass of the structure.

Spectral values can be computed in this way for a specific earthquake loading, discrete values of damping ratio, and structural natural frequency (Figure 5.1). Such plots of spectral values are called *response spectrum*, which are used by engineers to design structures.

It is much more convenient to plot all these four spectrums in a logarithmic scale, as in this way they can be demonstrated all in a four-way log plot, in which the natural frequency (or period) is taken as the abscissa and pseudo-velocity spectral values (S_{pv}) as the ordinate. There are two extra axes: the spectral displacement and the spectral pseudo-acceleration, which make angles of $\pm 45^\circ$ to the original axes (Figure 7.4):

$$\log S_d = \log S_{pv} - \log \omega \tag{7.21}$$

$$\log S_{pa} = \log S_{pv} + \log \omega \tag{7.22}$$

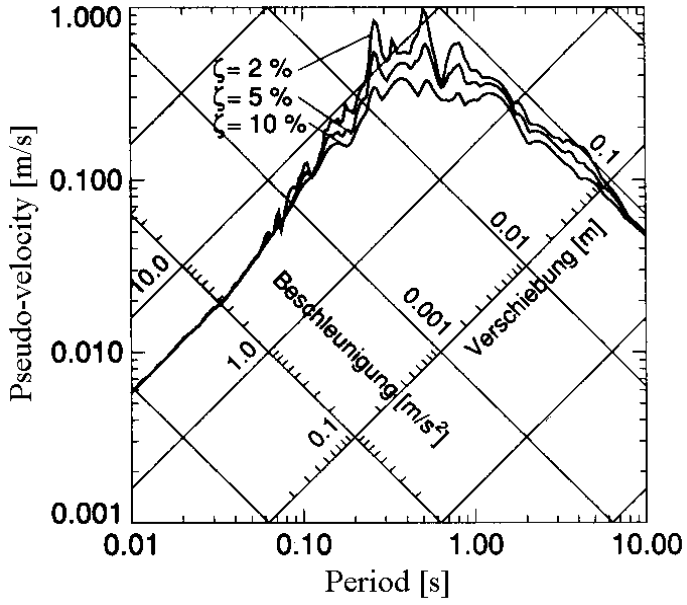

Figure 7.4 Four-way log response spectrum for the N-S component of Tolmezzo earthquake [Wenk, 1992].

Structures are simulated with several degrees of freedom. To use the same process the system must be decomposed first to several SDOF systems. A response spectrum analysis will then be done for the number of modes, which are considered. Finally, the results are combined to get the whole response of the original system. *Complete Quadratic Combination* (*CQC*) and *Square Root of Sum of Square* (*SRSS*) methods are main techniques used to get the results.

As just the maximum value of the response during an analysis for a specific system is considered in the response spectrum analysis, this method does not deliver any information about details of the response during excitations. The second drawback of this method, the same as the modal analysis, is that because of the application of the superposition method it can be only applied to linear systems. There are some experimental corrections for the response spectrum method, so that it can be used for nonlinear systems as well.

7.2 Finite element analysis of FPS

The differential equation governing an FPS isolated structure is [Almazan and Llera, 2002 and 2003]:

$$\mathbf{M}\ddot{\mathbf{q}} + \mathbf{C}\dot{\mathbf{q}} + \mathbf{K}\mathbf{q} + \mathbf{Q} = -\mathbf{M}\mathbf{L}_W\mathbf{W} \tag{7.23}$$

where $\mathbf{q}$ is the vector of the system degrees of freedom. $\boldsymbol{M}$, $\boldsymbol{C}$, and $\boldsymbol{K}$ are mass, damping, and stiffness matrices, respectively. $\boldsymbol{W}$ is the 3-D excitation input vector, $\boldsymbol{L}_W$ the input influence matrix, and $\boldsymbol{Q}$ the vector of non-linear restoring force generated by isolators with respect to the degree-of-freedom $\boldsymbol{q}$ of the structure. To keep track of the axial force in bearings a gap element has been incorporated in the set (Figure 7.5). The sliding displacement of the isolator is:

$$\boldsymbol{\delta}_k = \overline{O_k S_k} = \left[\delta_{xk}\ \delta_{yk}\ \delta_{zk}\right]^T \tag{7.24}$$

By imposing the kinetic constraint, i.e. spherical surface of the isolator, the three components of the deformation $\boldsymbol{\delta}_k$ and its velocity $\dot{\boldsymbol{\delta}}_k$ are implicitly expressed in terms of each other as:

$$\delta_{xk}^{\ 2} + \delta_{yk}^{\ 2} + (\delta_{zk} - R_k)^2 = R_k^{\ 2} \tag{7.25}$$

$$\delta_{xk}\dot{\delta}_{xk} + \delta_{yk}\dot{\delta}_{yk} + \dot{\delta}_{zk}(\delta_{zk} - R_k) = 0 \tag{7.26}$$

where R_k is the radius of curvature of the spherical surface of the k^{th} isolator.

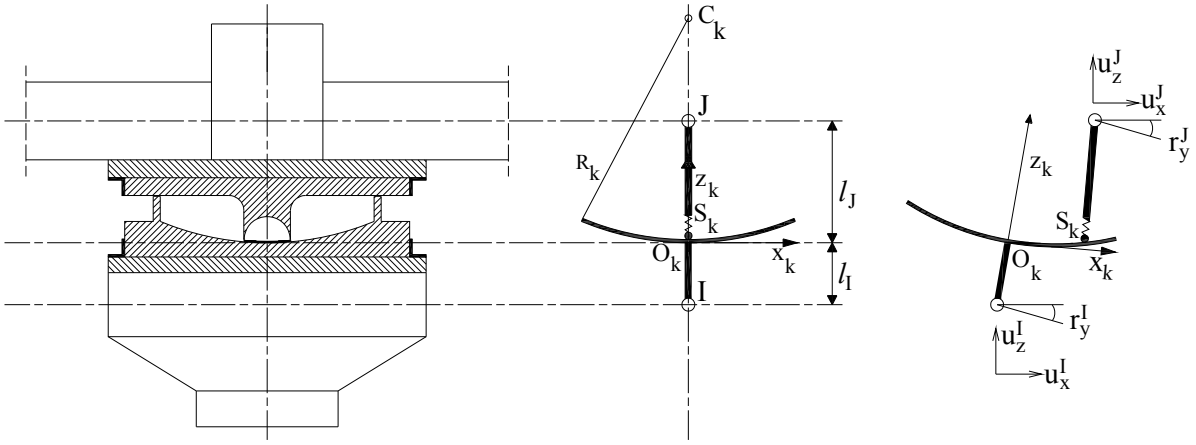

Figure 7.5 Friction pendulum element in downward position [Almazan and Llera, 2003].

The element demonstrated in figure 7.5 has 2 nodes, *I* and *J*, and 12 degrees of freedom, which are linearly related to the global degrees-of-freedom (***q***):

$$\mathbf{u}_k = \left[\mathbf{u}_k^J \ ; \mathbf{u}_k^I\right] = \mathbf{P}_k\,\mathbf{q} \tag{7.27}$$

where $\boldsymbol{P}_k$ is the nodal kinetic transformation matrix of the k^{th} isolator. $\mathbf{u}_k^J$ and $\mathbf{u}_k^I$ are nodal deformation vectors of the lower and upper element nodes.

Assuming small node rotations, it is possible to relate deformation and velocity in the isolator, $\boldsymbol{\delta}_k$ and $\dot{\boldsymbol{\delta}}_k$, with nodal deformations, $\mathbf{u}_k$ as:

$$\boldsymbol{\delta}_k = \overline{\mathbf{S}}(\mathbf{u}_k)\,\mathbf{u}_k \tag{7.28}$$

$$\dot{\boldsymbol{\delta}}_k = \hat{\mathbf{S}}(\mathbf{u}_k)\,\dot{\mathbf{u}}_k \tag{7.29}$$

in which

$$\overline{\mathbf{S}}(\mathbf{u}_k) = \begin{bmatrix} 1 & 0 & 0 & 0 & -l_j & 0 & -1 & 0 & 0 & 0 & \Delta u_z + l_I & \Delta u_y \\ 0 & 1 & 0 & -l_j & 0 & 0 & 0 & -1 & 0 & \Delta u_z + l_I & 0 & -\Delta u_x \\ 0 & 0 & 1 & 0 & 0 & 0 & 0 & 0 & -1 & \Delta u_y & \Delta u_x & 0 \end{bmatrix} \tag{7.30}$$

$$\hat{\mathbf{S}}(\mathbf{u}_k) = \begin{bmatrix} 1 & r_z^I & -r_y^I & 0 & -l_j & 0 & -1 & -r_z^I & r_y^I & 0 & -(\Delta u_z + l_I) & \Delta u_y \\ -r_z^I & 1 & r_x^I & l_j & 0 & 0 & r_z^I & -1 & -r_x^I & \Delta u_z + l_I & 0 & -\Delta u_x \\ r_y^I & -r_x^I & 1 & 0 & 0 & 0 & -r_y^I & r_x^I & -1 & -\Delta u_y & \Delta u_x & 0 \end{bmatrix} \tag{7.31}$$

where $\Delta u_i = u_i^J - u_i^I$ for $i = x, y, z,$ and l_J and l_I are vertical distances between nodes *J* and *I* and the origin O_k in the original configuration of the FPS, correspondingly (Figure 7.5).

In the next step the non-linear restoring force vector $\boldsymbol{Q}$ must be determined. The restoring force in an isolator of this type is composed of the two main terms of the pendular effect, f_p, and the frictional part, f_μ:

$$\begin{aligned}\mathbf{f}_k &= N_k\hat{\mathbf{n}}_k + \overline{\eta}_k\mu_k N_k\hat{\mathbf{s}}_k \\ &= N_k(\hat{\mathbf{n}}_k + \overline{\eta}_k\mu_k\hat{\mathbf{s}}_k) = N_k\mathbf{r}_k\end{aligned} \tag{7.32}$$

where N_k is the magnitude of the normal force. $\hat{\mathbf{n}}_k$ and $\hat{\mathbf{s}}_k$ are unit vectors in the outward normal direction and tangential to the trajectory of the isolator, respectively. μ_k is the friction coefficient. $\overline{\eta}_k$ is a positive non-dimensional variable with value one during sliding phases and less than one during sticking phases [Wen, 1976] and [Park, 1986].

In sticking phases, it is not possible to determine the magnitude and direction of the friction force, as regarding equation 7.32, the sliding velocity vanishes. To overcome this problem, instead of the Coulomb friction law an equivalent hysteretic model is applied (Section 4.4).

To compute the restoring force in the global coordinate system, the restoring force computed in equation 7.32 is transformed as (Figure7.6):

$$\mathbf{Q}_k = \mathbf{L}_k{}^T\mathbf{f}_k \tag{7.33}$$

$$\mathbf{L}_k = \hat{\mathbf{S}}_k\,\mathbf{P}_k \tag{7.34}$$

Finally adding restoring forces of all isolators in the system:

$$\mathbf{Q} = \sum_k \mathbf{Q}_k = \sum_k \mathbf{L}_k{}^T\mathbf{f}_k = \mathbf{L}^T\mathbf{F} \tag{7.35}$$

The integration of the equation of motion is performed in the state-space [Almazan and Llera, 2003]. The numerical integration is performed using *MATLAB*© function *ode15s*, an implicit multi-step integration algorithm, which is applied mainly for *stiff* differential equations [*MATLAB*], [Shampione, 1994], and [Shabana, 2001].

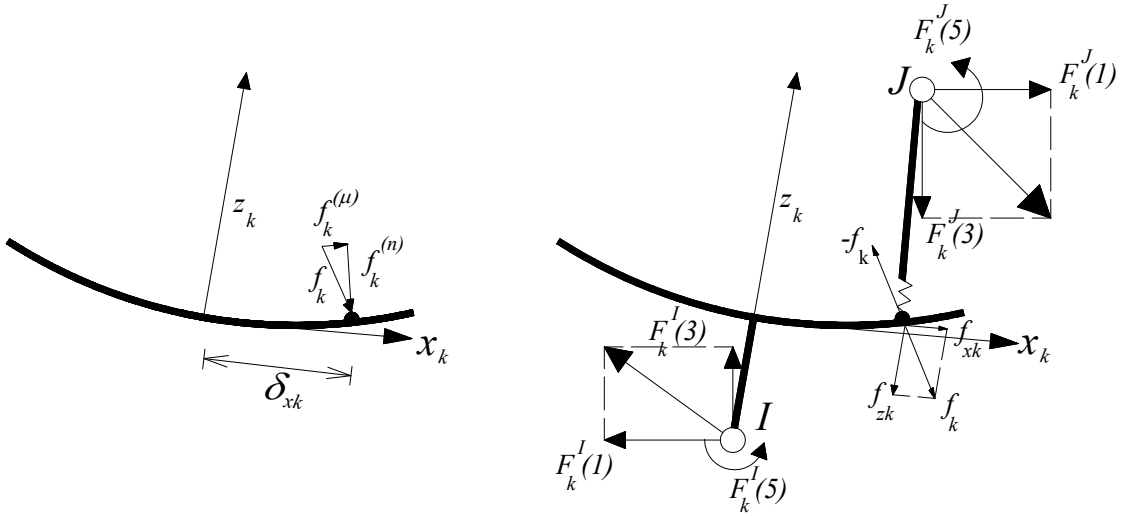

Figure 7.6 Forces acting on an FPS bearing (left) in local coordinates, (right) in global coordinates system [Almazan and Llera, 2003].

7.3 Piecewise exact solution for 1-DOF systems

One of the simplest time stepping methods for the analysis of 1-DOF systems is the piecewise exact method, which is based on the exact solution of the equation of motion for the response of a linear system to a loading, which varies linearly during a discrete time step [Clough and Penzien, 1993].

1-DOF models can nearly approximate the response of an isolated system (Section 5.2). This implies a rigid response of the structure.

Assuming that the ground acceleration varies linearly during each time step (Figure 7.7), the differential equation governing such a set is:

$$m\ddot{u} + c\dot{u} + ku \;=\; -F_f - m\ddot{u}_g^{i-1} - \frac{m\ddot{u}_g^{i} - m\ddot{u}_g^{i-1}}{\Delta t}\tau \tag{7.36}$$

where m, c, and k are mass, damping, and stiffness of the degree-of-freedom, respectively. F_f is the friction force, which can be considered constant or velocity- (pressure-) dependent. For the sake of simplicity the Coulomb friction law has been used. It does not restrict the generality of the discussion. u, $\dot{u}$, and $\ddot{u}$ are relative displacement, velocity, and acceleration of the mass with respect to the ground, correspondingly. $\ddot{u}_g^{i-1}$ and $\ddot{u}_g^{i}$ are the ground acceleration at the beginning and the end of the time step, respectively. Δt is the size of the time step.

The transient and particular solutions of the aforementioned differential equation are [Tsai et al., 2005]:

$$u_c(\tau) = (A\cos\omega_d\tau + B\sin\omega_d\tau)e^{-\xi\omega_n\tau} \tag{7.37}$$

$$u_p(\tau) = \frac{1}{\omega_n^2}\left[-\mu g\,\mathrm{sign}(\dot{u}) - \ddot{u}_g^{i-1} + \frac{2\xi}{\omega_n\Delta t}(\ddot{u}_g^{i} - \ddot{u}_g^{i-1})\right] - \frac{(\ddot{u}_g^{i} - \ddot{u}_g^{i-1})}{\omega_n^2\Delta t}\tau \tag{7.38}$$

where ω_n and ω_d are the natural and damped frequencies of vibration, respectively. ξ is the viscous damping ratio. A and B are calculated from initial conditions of the current time step as:

$$u^i(\tau=0) = u^{i-1} \quad\Rightarrow\quad A = u^{i-1} - \frac{1}{\omega_n^2}\left[-\mu g\,\mathrm{sign}(\dot{u}) - \ddot{u}_g^{i-1} + \frac{2\xi}{\omega_n\Delta t}(\ddot{u}_g^{i} - \ddot{u}_g^{i-1})\right] \tag{7.39}$$

$$\dot{u}^i(\tau=0) = \dot{u}^{i-1} \quad\Rightarrow\quad B = \frac{1}{\omega_d}(\dot{u}^{i-1} + \xi\omega_n A + \frac{\ddot{u}_g^{i} - \ddot{u}_g^{i-1}}{\omega_n^2\Delta t}) \tag{7.40}$$

Differentiating equations 7.37 and 7.38, the relative velocity and acceleration are calculated as:

$$\dot{u}(\tau) = (-\omega_d A\cos\omega_d\tau + \omega_d B\sin\omega_d\tau)e^{-\xi\omega_n\tau} - \xi\omega_n(A\sin\omega_d\tau + B\cos\omega_d\tau)e^{-\xi\omega_n\tau} - \frac{\ddot{u}_g^{i} - \ddot{u}_g^{i-1}}{\omega_n^2\Delta t} \tag{7.41}$$

$$\begin{aligned}\ddot{u}(\tau) = {} & (-\omega_d^2 A\cos\omega_d\tau - \omega_d^2 B\sin\omega_d\tau)e^{-\xi\omega_n\tau} \\ & - 2\xi\omega_n(-\omega_d A\sin\omega_d\tau + \omega_d B\cos\omega_d\tau)e^{-\xi\omega_n\tau} \\ & + \xi^2 w_n^2(A\cos\omega_d\tau + B\sin\omega_d\tau)e^{-\xi\omega_n\tau}\end{aligned} \tag{7.42}$$

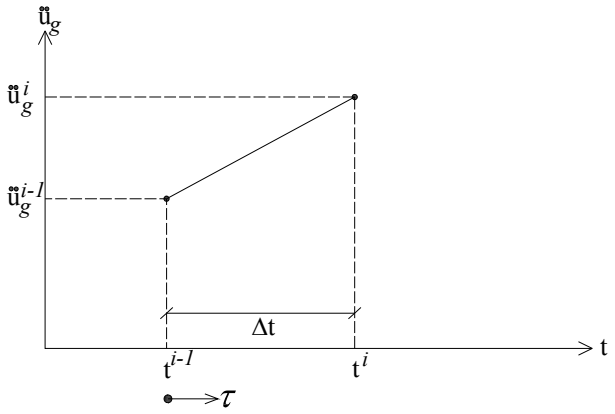

Figure 7.7 The ground acceleration in a discrete time step.

Regarding equation 7.42, the relative sliding acceleration of a degree-of-freedom in a system with no extra damping source rather than friction, at the beginning of a time step is:

$$\ddot{u}(\tau = 0) = \ddot{u}_0 = -\omega_n^2 A \tag{7.43}$$

Assuming no initial displacement in the system and applying equation 7.39, the relative acceleration can be rewritten as:

$$\ddot{u}_0 = -\mu g \,\mathrm{sign}(\dot{u}) - \ddot{u}_g^{i-1} \tag{7.44}$$

The inertial force due to ground motions is then computed as:

$$\begin{aligned} F &= m\ddot{u}_{tot} = m(\ddot{u} + \ddot{u}_g^{i-1}) \\ &= -\mu mg \,\mathrm{sign}(\dot{u}) = -F_f \end{aligned} \tag{7.45}$$

This can be compared with the inertial force due to the ground excitations in a fixed-base system, i.e. $mg\ddot{u}_g$. The lower the friction coefficient the lower is the force applied to the system. A very small friction coefficient, however, results in unacceptably large sliding displacements. Besides, the efficiency of the isolation method depends also on the maximum ground acceleration. The larger the maximum earthquake acceleration, is the more efficient an isolated system responds.

An important factor controlling the response of an isolated system is the friction force. Forces acting on such a set and their possible combinations have already been discussed (Section 6.3). As long as the resultant force acting on the mass is smaller than the static friction force, the mass remains sticking (Equation 6.7). In this case, the relative velocity and acceleration are both set to zero. As soon as the static friction force is overcome, this constraint is deactivated and the stick-slip criterion is not checked any more (Section 6.4 and Figure 7.8) [Jamali and Zahlten, 2006].

7.4 Time step refining process

The response of a sliding-based isolated system is composed of two distinct parts: sliding and sticking phases. The set responds completely different in these phases (Chapter 6). Therefore, it is very important to find precisely *zero crossing points* of the sliding velocity. There is no

analytical solution to find these points exactly, as the response of these systems is highly non-linear, because of the nature of the friction force. To get good results, time steps must be in the order of 10^{-5}-10^{-6} seconds. On the other hand, it is very time-consuming to perform the whole analysis with time steps in this order. To overcome this problem, a time step refining process has been developed, in which extremely short time steps are used only when a phase change, i.e. sticking or sliding initiation or a change in the direction of sliding, is close to happen. At the end of each time step it is checked first whether sticking or sliding has been initiated or not (through the stick-slip criterion). Secondly, it is controlled whether the direction of sliding has been changed or not. If one of them occurred, the time step is halved and the same process is repeated until the zero crossing point is found with the desired precision (Figure 7.9). This process has a fast rate, as for example for a time step in the order of 10^{-3} seconds in less then 10 iterations the desired point can be found with an accuracy of 10^{-6} seconds. Afterwards, the previous time step is applied again [Jamali and Zahlten, 2006].

```
input parameters (m, c, k, μ , ü_g)
while time(i) ≤ max(time)
   if phase_state == 'stick'
      computation of friction_force (Equation of equilibrium)
   else
      computation of friction_force (Sections 4.2 – 4.4)
   end
   assignment of initial conditions (Equations 7.39 and 7.40)
   solution of the differential equation (Equations 7.36-38 and 7.41-
42)
   if phase_state == 'stick'
      if resultant_force ≥ friction_force
         phase_state = 'slide';
      else
         velocity_rel = 0;
         acceleration_rel = 0;
      end
   end
   if (phase_state == 'slide')  &  (sign(velocity_rel(t_i) * velocity_rel(t_i-
1)) < 0)
      velocity_rel(t_i) = 0;
      acceleration_rel(t_i) = 0;
      phase_state = 'stick';
   end
   i = i + 1;
   end
end
```

Figure 7.8 Pseudo-algorithm for piecewise exact solution of 1-DOF systems.

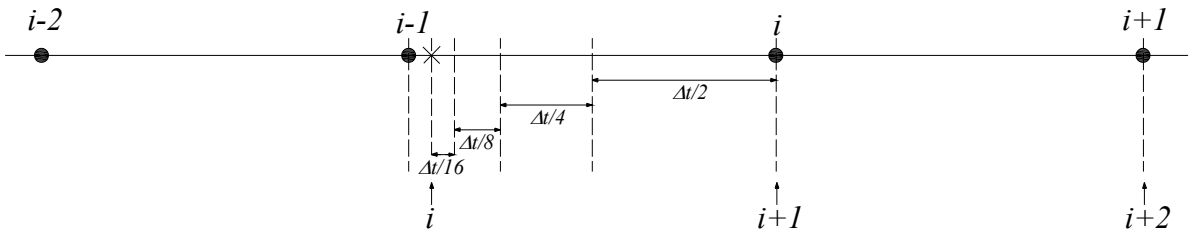

Figure 7.9 A schematic view of the time step refining process.

7.5 Numerical Simulation of 2-DOF isolated systems

SDOF systems are appropriate to get the general features of the response of isolated sets. Especially for initial design phases, in which there is no detailed information of the structural system, they give a rough estimate of the structural response. It helps the designer to decide about other design aspects, as for example an additional damping mechanism; features of the isolation system, as maximum sliding displacement capacity, maximum permanent displacement after excitations, etc.

For the next phases, a more detailed model is required. At least the isolation mechanism and the structure must be modelled separately to get some insight of their interaction effect.

The simplest model fulfilling this goal is a 2-DOF model, in which the first degree of freedom resembles the isolation mechanism, here the friction pendulum bearing, and the second one stands for the structure. The response of such a system is governed by the following set of differential equations [Jamali et al., 2007]:

$$m\ddot{s} + c\dot{s} + ks = -(\ddot{u} + \ddot{u}_g)\, m \tag{7.46}$$

$$(M+m)\ddot{u} + C\dot{u} + Ku = -(M+m)\ddot{u}_g - F_f - m\ddot{s} \tag{7.47}$$

where

s : relative structural displacement (to the base)

$\dot{s}$: relative structural velocity (to the base)

$\ddot{s}$: relative structural acceleration (to the base)

u : relative base displacement (to the ground)

$\dot{u}$: relative base velocity (to the ground)

$\ddot{u}$: relative base acceleration (to the ground)

F_f : friction force

K: base stiffness

k: structural stiffness

C: base damping

c: structural damping

M: base mass

m: structural masses

α : mass ratio [m/(M+m)]

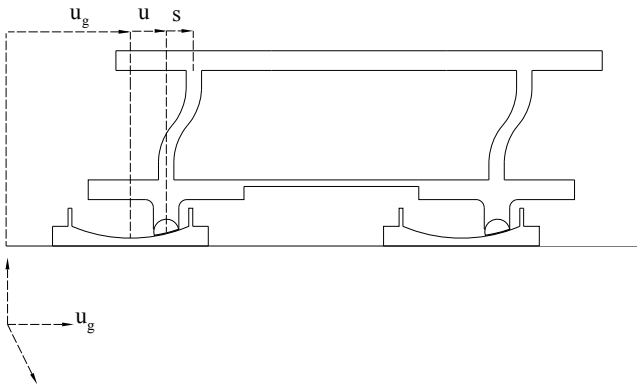

Figure 7.10 2-DOF system configuration [Jamali et al., 2007].

The base stiffness is calculated according to the geometrical stiffness of the FPS bearing (Section 6.2). Base and structural displacement, velocity, and acceleration are all defined in a relative coordinate system (Figure 7.10).

Defining Ω and ζ, the natural frequency and damping ratio of the FPS bearing, respectively, as:

$$\Omega = \sqrt{\frac{K}{M+m}} \tag{7.48}$$

$$2\zeta\Omega = \frac{C}{M+m} \tag{7.49}$$

Equation 7.47 can be written as:

$$\ddot{u} + 2\zeta\Omega\dot{u} + \Omega^2 u = -F_f/(M+m) - \ddot{u}_g - \alpha\ddot{s} \tag{7.50}$$

The structural natural frequency and damping ratio are defined as:

$$\omega = \sqrt{\frac{k}{m}} \tag{7.51}$$

$$2\xi\omega = \frac{c}{m} \tag{7.52}$$

Regarding equations 7.51 and 7.52 the differential equation governing the structural response is rewritten as (Equation 7.46):

$$\ddot{s} + 2\xi\omega\dot{s} + \omega^2 s = -(\ddot{u} + \ddot{u}_g) \tag{7.53}$$

Equations 7.50 and 7.53 govern the response of a 2-DOF system isolated with FPS bearings in a sliding phase (Figure 7.10). In sticking phases, equation 7.50 vanishes and the system turns into a 1-DOF set.

It has been assumed that the ground acceleration is changing linearly during every time step. This is a logical assumption, as time steps are very short, in the order of 10^{-2}-10^{-3} seconds during analysis and 10^{-5}-10^{-6} when a phase change is to happen. The ground acceleration during a time increment is (Figure 7.7):

$$\begin{aligned}\ddot{u}_g(t_i+\tau) &= \ddot{u}_g(t_i) + \Delta\ddot{u}_g(t_{i+1})\frac{\tau}{\Delta t} \\ &= \ddot{u}_g^b + \frac{\ddot{u}_g^e - \ddot{u}_g^b}{\Delta t}\tau\end{aligned} \tag{7.54}$$

where indices *b* and *e* stand for the beginning and end of a time step, respectively. The same assumption are used for the relative structural acceleration:

$$\ddot{s}(t_i+\tau) = \ddot{s}(t_i) + \Delta\ddot{s}(t_{i+1})\frac{\tau}{\Delta t} \tag{7.55}$$

$$\Delta\ddot{s}(t_{i+1}) = \ddot{s}(t_{i+1}) - \ddot{s}(t_i) \tag{7.56}$$

Equations 7.54-56 are substituted in equation 7.50:

$$\ddot{u} + 2\zeta\Omega\dot{u} + \Omega^2 u = P_i + Q_{i+1}\frac{\tau}{\Delta t} \tag{7.57}$$

in which P_i contains parameters of the right hand side of the differential equation at the current known time step t_i.

The remaining terms are defined in Q_{i+1} *as*:

$$P_i = -\left[F_f /(M+m) + \ddot{u}_g^b + \alpha \ddot{s}(t_i) \right] \tag{7.58}$$

$$Q_{i+1} = -\left[\Delta \ddot{u}_g(t_{i+1}) + \alpha \Delta \ddot{s}(t_{i+1}) \right] \tag{7.59}$$

The solution of the equation 7.57 is:

$$u(t_{i+1}) = u_i^e = \frac{1}{\Omega^2}\left[P_i + (1 - \frac{2\zeta}{\Omega \Delta t}) Q_{i+1} \right] + z(t_{i+1}) \tag{7.60}$$

$$\dot{u}(t_{i+1}) = \dot{u}_i^e = \frac{1}{\Omega^2 \Delta t} Q_{i+1} + \dot{z}(t_{i+1}) \tag{7.61}$$

$$\ddot{u}(t_{i+1}) = \ddot{u}_i^e = \ddot{z}(t_{i+1}) \tag{7.62}$$

in which z(t) is the complementary solution [Mostaghel and Khodaverdian, 1988]:

$$z(t_{i+1}) = A + R_1 Q_{i+1} \tag{7.63}$$

$$\dot{z}(t_{i+1}) = (B - \zeta \Omega A) + (R_2 - \zeta \Omega R_1) Q_{i+1} \tag{7.64}$$

$$\ddot{z}(t_{i+1}) = -C - R_3 Q_{i+1} \tag{7.65}$$

where

$$A = \frac{1}{\Omega_d} e^{-\zeta \Omega \Delta t} (D \sin \Omega_d \Delta t + E \cos \Omega_d \Delta t) \tag{7.66}$$

$$B = e^{-\zeta \Omega \Delta t} (D \cos \Omega_d \Delta t - E \sin \Omega_d \Delta t) \tag{7.67}$$

$$R_1 = e^{-\zeta \Omega \Delta t} (-\frac{1 - 2\zeta^2}{\Omega^2 \Omega_d \Delta t} \sin \Omega_d \Delta t + \frac{2\zeta}{\Omega^3 \Delta t} \cos \Omega_d \Delta t) \tag{7.68}$$

$$R_2 = \Omega_d \, e^{-\zeta \Omega \Delta t} (-\frac{1 - 2\zeta^2}{\Omega^2 \Omega_d \Delta t} \cos \Omega_d \Delta t - \frac{2\zeta}{\Omega^3 \Delta t} \sin \Omega_d \Delta t) \tag{7.69}$$

$$R_3 = 2\zeta \Omega R_2 + \Omega^2 (1 - 2\zeta^2) R_1 \tag{7.70}$$

$$C = 2\zeta \Omega B + \Omega^2 (1 - 2\zeta^2) A \tag{7.71}$$

$$D = \dot{u}(t_i) + \zeta \Omega u(t_i) - \frac{\zeta}{\Omega} P_i \tag{7.72}$$

$$E = \Omega_d (u(t_i) - \frac{1}{\Omega^2} P_i) \tag{7.73}$$

$$\Omega_d = \Omega \sqrt{1 - \zeta^2} \tag{7.74}$$

Regarding equations 7.54-56:

$$\ddot{s}(t_{i+1}) = \ddot{s}(t_i) + \Delta \ddot{s}(t_{i+1}) \tag{7.75}$$

and integrating equation 7.75 yields the following expressions:

$$\begin{aligned}\dot{s}(t_{i+1}) &= \dot{s}(t_i)+\int_0^{\Delta t}(\ddot{s}(t_i)+\frac{\ddot{s}(t_{i+1})-\ddot{s}(t_i)}{\Delta t}\tau)d\tau \\ &= \dot{s}(t_i)+\ddot{s}(t_i)\tau\Big|_0^{\Delta t}+\frac{1}{2}\tau^2\,\frac{\ddot{s}(t_{i+1})-\ddot{s}(t_i)}{\Delta t}\Big|_0^{\Delta t} \\ &= \dot{s}(t_i)+\ddot{s}(t_i)\Delta t+\Delta\ddot{s}(t_{i+1})\frac{\Delta t}{2}\end{aligned} \tag{7.76}$$

$$\begin{aligned}s(t_{i+1}) &= s(t_i)+\int_0^{\Delta t}[\dot{s}(t_i)+\ddot{s}(t_i)\tau+\frac{\ddot{s}(t_{i+1})-\ddot{s}(t_i)}{\Delta t}\frac{\tau^2}{2}]d\tau \\ &= s(t_i)+\dot{s}(t_i)\Delta t+\ddot{s}(t_i)\frac{\Delta t^2}{2}+\Delta\ddot{s}(t_{i+1})\frac{\Delta t^2}{6}\end{aligned} \tag{7.77}$$

Substituting equations 7.75-77 in equation 7.53 and rearranging the equation in term of the unknown $\Delta\ddot{s}(t_{i+1})$ gives:

$$R_4\Delta\ddot{s}(t_{i+1})+R_5\ddot{s}(t_i)+R_6\dot{s}(t_i)+\omega^2 s(t_i) = -(\ddot{u}_g(t_{i+1})-C)+R_3Q_{i+1} \tag{7.78}$$

in which

$$R_4 = 1+\xi\omega\Delta t+\omega^2\frac{\Delta t^2}{6} \tag{7.79}$$

$$R_5 = 1+2\xi\omega\Delta t+\omega^2\frac{\Delta t^2}{2} \tag{7.80}$$

$$R_6 = 2\xi\omega+\omega^2\Delta t \tag{7.81}$$

Substituting Q_{i+1} from equation 7.59 in equation 7.78, $\Delta\ddot{s}(t_{i+1})$ is computed as:

$$\Delta\ddot{s}(t_{i+1}) = \frac{-\ddot{u}_g(t_{i+1})+C-R_3\Delta\ddot{u}_g(t_{i+1})-R_5\ddot{s}(t_i)-R_6\dot{s}(t_i)-\omega_1^2 s(t_i)}{R_3+R_4} \tag{7.82}$$

Once $\Delta\ddot{s}(t_{i+1})$ is computed, the relative structural variables at the end of the time step, $s(t_{i+1})$, $\dot{s}(t_{i+1})$, and $\ddot{s}(t_{i+1})$ can also be computed (Equations 7.75-77). Base variables (u_i^e, $\dot{u}_i^e$, and $\ddot{u}_i^e$) are recalculated using $\Delta\ddot{s}(t_{i+1})$ and Q_{i+1} (Equation 7.50 and 7.59). Substituting $\ddot{u}_i^e$ in equation 7.53 the structural variables (s, $\dot{s}$, and $\ddot{s}$) are recomputed. At this stage $\Delta\ddot{s}(t_{i+1})$ is known based on the computed Q_{i+1}:

$$\Delta\ddot{s}(t_{i+1}) = \frac{-\ddot{u}_g(t_{i+1})+C+R_3Q_{i+1}-R_5\ddot{s}(t_i)-R_6\dot{s}(t_i)-\omega^2 s(t_i)}{R_4} \tag{7.83}$$

which is used to control the convergence of the iterative process. This iterative process of the computation of structural variables according to the base variables and vice versa must be repeated several times, until $\Delta\ddot{s}(t_{i+1})$ converges.

Based on the same principle stated before (Section 6.4) a stick-slip criterion is defined for such a system as:

$$\left|\ddot{u}_g + \alpha\ddot{s} + \Omega^2 u\right| \overset{?}{\geq} F_f / M_{tot.} \tag{7.84}$$

where $M_{tot.}$ is the total mass of the structure with its foundation. If the resultant force acting on the bearing, left hand side of the equation 7.84, does not overcome the static friction force, equation 7.50 vanishes and equation 7.53 is rewritten as:

$$\ddot{s}(t_{i+1}) + 2\xi\omega\dot{s}(t_{i+1}) + \omega^2 s(t_{i+1}) = -\ddot{u}_g(t_i) - \Delta\ddot{u}_g(t_{i+1})\frac{\tau}{\Delta t} \tag{7.85}$$

Its complete solution is [Mostaghel and Khodaverdian, 1988]:

$$s(t_{i+1}) = s_c(t_{i+1}) + s_p(t_{i+1}) \tag{7.86}$$

$$\dot{s}(t_{i+1}) = \dot{s}_c(t_{i+1}) + \dot{s}_p(t_{i+1}) \tag{7.87}$$

$$\ddot{s}(t_{i+1}) = \ddot{s}_c(t_{i+1}) \tag{7.88}$$

in which

$$s_c = e^{-\xi\omega\Delta t}(A^* \sin\omega_d\Delta t + B^* \cos\omega_d\Delta t) \tag{7.89}$$

$$\dot{s}_c = -\xi\omega s_c + \omega_d e^{-\xi\omega\Delta t}(A^* \cos\omega_d\Delta t - B^* \sin\omega_d\Delta t) \tag{7.90}$$

$$\ddot{s}_c = -(1-2\xi^2)\omega^2 s_c - 2\xi\omega_d\omega e^{-\xi\omega\Delta t}(A^* \cos\omega_d\Delta t - B^* \sin\omega_d\Delta t) \tag{7.91}$$

$$s_p(t_{i+1}) = -\frac{1}{\omega^2}\left[\ddot{u}_g(t_i) + (1 - \frac{2\xi}{\omega\Delta t})\Delta\ddot{u}_g(t_{i+1})\right] \tag{7.92}$$

$$\dot{s}_p(t_{i+1}) = -\frac{1}{\omega^2\Delta t}\Delta\ddot{u}_g(t_{i+1}) \tag{7.93}$$

$$A^* = \frac{1}{\omega_d}\left\{\dot{s}(t_i) + \xi\omega s(t_i) + \frac{\xi}{\omega}\left[\ddot{u}_g^b - \frac{2\xi}{\omega\Delta t}\Delta\ddot{u}_g(t_{i+1})\right] + \frac{1}{\omega^2\Delta t}\Delta\ddot{u}_g(t_{i+1})\right\} \tag{7.94}$$

$$B^* = s(t_i) + \frac{1}{\omega^2}\left[\ddot{u}_g^b - \frac{2\xi}{\omega\Delta t}\Delta\ddot{u}_g(t_{i+1})\right] \tag{7.95}$$

As the variables are all defined in a relative coordinate system, the total (absolute) structural displacement and acceleration are:

$$s_{tot} = u_g + u + s \tag{7.96}$$

$$\ddot{s}_{tot} = \ddot{u}_g + \ddot{u} + \ddot{s} \tag{7.97}$$

in which u_g is the ground displacement due to earthquake motions.

The process of the numerical simulation is explained in a pseudo-algorithm (Figure 7.11). Its time refining process is explained in detail in Appendix *C*.

```
input parameters
while time(i) ≤ max(time)
   computation of the friction_force (Sections 4.2-4)
   assignment of initial conditions (from the last time step)
   computation of P (Equation 7.58)
   computation of R1-R6 and A-E (Equations 7.66–81)
   computation of del_s_acc(t_i,iteration 1) (Equation 7.82)
   j = 1;
   while |del_s_acc(t_i,iteration j)- del_s_acc(t_i,iteration j-1)| > tolerance
      computation of Q (Equation 7.59)
      computation of z, z_dot, z_dot_dot (Equations 7.63-65)
      computation of base_dis, base_vel, base_acc (Equations 7.60-62)
      computation of struc_dis, struc_vel, struc_acc (Equations 7.75-77)
      j = j+1;
   end
   computation of base_shear (stick-slip criterion)
   if (phase state == 'stick')  &  (base_shear < friction_force)
      base_vel(t_i) = 0;
      base_acc(t_i) = 0;
      solution of 1-DOF system (Equations 7.85-95)
   end
   if (sign(base_vel(t_i) * base_vel(t_i-1)) < 0) or (base_shear >
 friction_force)
      time step refining process (Appendix C)
   end
   assignment of phase_state
   if (phase_state == 'slide')  &  (sign(base_vel(t_i) *base_ vel(t_i-1)) < 0)
 & ...
   (time_step has been refined)
      velocity_rel(t_i) = 0;
      acceleration_rel(t_i) = 0;
      phase_state = 'stick'
   end
   i = i + 1;
end
```

Figure 7.11 Pseudo-algorithm for the numerical simulation of a 2-DOF isolated system.

7.6 Modal analysis of MDOF isolated systems

The two degree-of-freedom model is an appropriate means to study the interaction between sliding bearings and the structure in an isolated system. It helps in initial design phases not only to choose an eligible isolation method, but also to consider specific features for the adopted system to optimize the seismic structural response. However, to consider more aspects a more detailed model is required. The challenging task is to develop a rather simple numerical model, which estimates the actual response of such structures relatively well.

As explained earlier in this chapter, modal analysis is an appropriate numerical method to simulate systems with many degrees-of-freedom. In the modal space, merely modes with higher participation factors are considered. This decreases the numerical effort of this method drastically.

[Mostaghel and Khodaverdian, 1988] applied this method to develop a numerical model to simulate the seismic response of Resilient-Friction Base Isolated (*R-FBI*) systems.

To this end, firstly the fixed-base mode shapes of the superstructure, i.e. the structure without its foundation, are computed as (assuming a linear structural response):

$$s_i(t) = \sum_{j=1}^{N} \phi_{ij} v_j \tag{7.98}$$

where ϕ is the matrix of mode shapes of the superstructure with N degrees of freedom. The differential equations governing such an MDOF system are (Figure 7.12):

$$\mathbf{m\ddot{s} + c\dot{s} + ks} = -(\ddot{u} + \ddot{u}_g)\mathbf{mr} \tag{7.99}$$

$$\ddot{u} + \frac{C}{M + \sum_{i=1}^{N} m_i}\dot{u} + \frac{K}{M + \sum_{i=1}^{N} m_i}u = -\ddot{u}_g - \frac{1}{M + \sum_{i=1}^{N} m_i}F_f - \sum_{i=1}^{N} \alpha_i \ddot{s}_i \tag{7.100}$$

with the same variables which have been already defined (Equations 7.46 and 7.47).

Regarding equation 7.98, the term $\sum_{i=1}^{N} \alpha_i \ddot{s}_i$ in equation 7.100 is replaced by its modal amplitudes as:

$$\sum_{i=1}^{N} \alpha_i \ddot{s}_i = \sum_{j=1}^{N} \beta_j \ddot{v}_j \tag{7.101}$$

in which

$$\beta_j = \sum_{i=1}^{N} \alpha_i \phi_{ij} \tag{7.102}$$

Therefore equation 7.100 can be rewritten as:

$$\ddot{u} + 2\zeta\Omega\dot{u} + \Omega^2 u = -F_f/(M + \sum_{i=1}^{N} m_i) - \ddot{u}_g - \sum_{j=1}^{N} \beta_j \ddot{v}_j \tag{7.103}$$

Substituting equation 7.101 in equation 7.99 and applying the orthogonality property, it yields:

$$\ddot{v}_n + 2\xi_n \omega_n v_n + {\omega_n}^2 v_n = -\lambda_n(\ddot{u} + \ddot{u}_g) \tag{7.104}$$

where the subscript *n* denotes the mode number. λ_n is the participation factor, which is:

$$\lambda_n = \frac{\sum_{i=1}^{N} m_i \phi_{in}}{\sum_{i=1}^{N} m_i {\phi_{in}}^2} \tag{7.105}$$

In a process similar to the one explained in the previous section for a 2-DOF isolated system, the seismic response of this system can be modelled. The main drawback of this method is the modal transformation of the superstructure regardless of its foundation into the modal space. Thereby, the interaction between the isolation block, in this case the friction pendulum bearing, and the structure itself cannot be fully simulated.

To solve this problem the whole set of differential equations (Equations 7.99 and 7.100) is transformed into the modal space. This requires the transformation of the friction force as well as the inertial force (due to the ground motions) into the modal space.

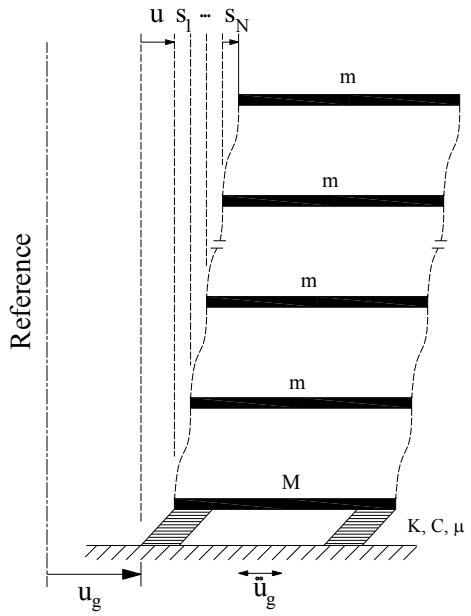

Figure 7.12 A structure supported on an R-FBI system [Mostaghel and Khodaverdian, 1988].

To this end, first of all the set of differential equations must be rewritten in a matrix form, which makes a modal transformation of the system possible. The matrix form of equations 7.99 and 7.100 is (Figure 7.13):

$$\mathbf{M}\ddot{\mathbf{U}} + \mathbf{C}\dot{\mathbf{U}} + \mathbf{K}\mathbf{U} = -F_f\,\mathbf{r}_1 - \mathbf{P}_g\mathbf{r}_2 \tag{7.106}$$

where $\mathbf{U}$, $\dot{\mathbf{U}}$, and $\ddot{\mathbf{U}}$ are the generalized displacement, velocity, and acceleration vectors, respectively. $\mathbf{r}_1$ and $\mathbf{r}_2$ are the influence matrices, which are mapping the friction and inertial forces to corresponding degrees-of-freedom. **M**, **C**, and **K** are the mass, damping, and stiffness matrices of the whole system, correspondingly. In a 2-degree-of-freedom system these matrices are (Figure 7.10):

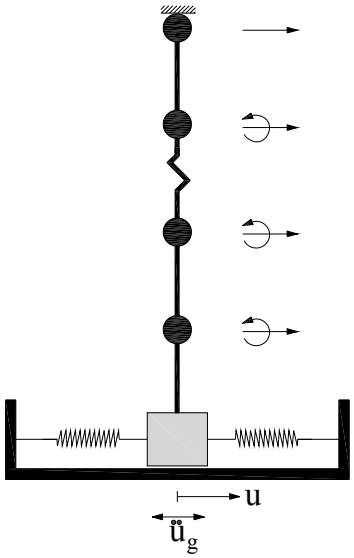

Figure 7.13 (*N+1*) degree-of-freedom isolated system with rotational and translational degrees of freedom.

$$\begin{bmatrix} M+m & m \\ m & m \end{bmatrix}\begin{bmatrix} \ddot{u} \\ \ddot{s} \end{bmatrix} + \begin{bmatrix} C & 0 \\ 0 & c \end{bmatrix}\begin{bmatrix} \dot{u} \\ \dot{s} \end{bmatrix} + \begin{bmatrix} K & 0 \\ 0 & k \end{bmatrix}\begin{bmatrix} u \\ s \end{bmatrix} = -\begin{bmatrix} 1 \\ 0 \end{bmatrix} F_f - \begin{bmatrix} M+m & m \\ m & m \end{bmatrix}\begin{bmatrix} 1 \\ 0 \end{bmatrix}\ddot{u}_g \tag{7.107}$$

Plane beam elements have been used for the discretization of the set. Local stiffness and consistent mass matrices of this type of element are defined as (Figure 7.14) [Cook, 1995]:

$$\mathbf{k} = \frac{EI}{L^3}\begin{bmatrix} 12 & -6L & -12 & -6L \\ -6L & 4L^2 & 6L & 2L^2 \\ -12 & 6L & 12 & 6L \\ -6L & 2L^2 & 6L & 4L^2 \end{bmatrix} \tag{7.108}$$

$$\mathbf{m} = \mathbf{m}_{trns.} + \mathbf{m}_{rot.} = \frac{\rho AL}{420}\begin{bmatrix} 156 & -22L & 54 & 13L \\ -22L & 4L^2 & -13L & -3L^2 \\ 54 & -13L & 156 & 22L \\ 13L & -3L^2 & 22L^2 & 4L^2 \end{bmatrix} + \frac{\rho I}{30L}\begin{bmatrix} 36 & -3L & -36 & -3L \\ -3L & 4L^2 & 3L & -L^2 \\ -36 & 3L & 36 & 3L \\ -3L & -L^2 & 3L & 4L^2 \end{bmatrix} \tag{7.109}$$

where E and I are the Young's modulus and the moment of inertia, respectively. ρ, A, and L are the density, cross sectional area, and length of the element, correspondingly.

By the initiation of sliding a new element is activated in the system, which is representing the isolation bearing. In sticking phases, however, the added element is deactivated and the rest of the system is simulated as a classical fixed-base structure. In classical finite element method a permanent element is defined, in which the element is very stiff in sticking phases; so that no sliding displacement would be produced in sticking phases. Activating a new element in comparison to a permanent element in classical finite element method has the advantage that it is not required to perform an iterative process in sticking phases to compute the resultant force in this element. This iterative process is time consuming. In this new model base shear is the deciding factor controlling whether the bearing starts sliding at the end of a time step or not (stick-slip criterion).

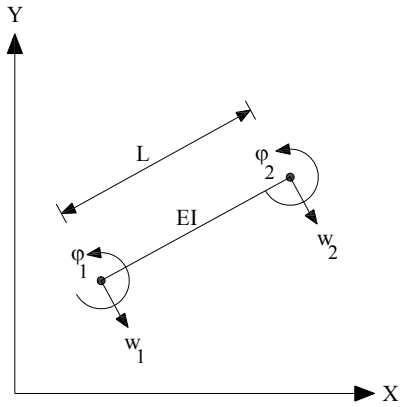

Figure 7.14 Simple plane beam in local coordinate system.

Transforming the differential equation (Equation 7.106) into the modal space by:

$$\mathbf{U} = \boldsymbol{\varphi}\,\boldsymbol{\eta} \tag{7.110}$$

where $\boldsymbol{\varphi}$ is the matrix of mode shapes of the whole set of the differential equations, equation 7.106 is rewritten in the modal space as:

$$\boldsymbol{\varphi}^T\mathbf{M}\boldsymbol{\varphi}\,\ddot{\boldsymbol{\eta}}+\boldsymbol{\varphi}^T\mathbf{C}\boldsymbol{\varphi}\,\dot{\boldsymbol{\eta}}+\boldsymbol{\varphi}^T\mathbf{K}\boldsymbol{\varphi}\,\boldsymbol{\eta} = -\boldsymbol{\varphi}^T\,\mathrm{F}_f\,\mathbf{r}_1\,-\boldsymbol{\varphi}^T\mathbf{P}_g\mathbf{r}_2 \tag{7.111}$$

$$\tilde{\mathbf{M}}\,\ddot{\boldsymbol{\eta}}+\tilde{\mathbf{C}}\,\dot{\boldsymbol{\eta}}+\tilde{\mathbf{K}}\,\boldsymbol{\eta} = -\tilde{\mathbf{F}}_f\,-\tilde{\mathbf{P}}_g \tag{7.112}$$

in which $\tilde{\mathbf{M}}$, $\tilde{\mathbf{C}}$, and $\tilde{\mathbf{K}}$ are the modal mass, damping, and stiffness matrices, respectively, and $\tilde{\mathbf{F}}_f$ and $\tilde{\mathbf{P}}_g$ are the modal friction and inertial forces.

It must be taken into consideration that these modal values, in particular the modal friction force, cannot be physically interpreted as in the original space. For instance, the modal resultant force in an arbitrary mode cannot be compared with the static friction force transformed into the modal space. In other words, the stick-slip criterion is not valid in the modal space (Equation 7.113). Hence, the variables must be transformed back into the original space for further considerations.

$$\left|\mathbf{M}\ddot{\mathbf{U}}_{abs.} + k_{base}u_{base}\right| \overset{?}{\geq} F_f \tag{7.113}$$

The first step to solve the differential equation (Equation 7.112) in the modal space is the introduction of initial conditions. For those time steps where no phase change has happened in their previous time step, i.e. stick-stick or slide-slide cases, it is straight forward. The final values of the last time step in the modal space are directly used as the initial values of the current time step. When a phase change happens, however, the initial conditions must be computed differently, as the number of degrees of freedom has been changed because of the activation (or deactivation) of the sliding element. Regarding equation 7.110:

$$\boldsymbol{\eta}_{initial} = \boldsymbol{\varphi}^{-1}\,\mathbf{U}^{i-1} \tag{7.114}$$

$$\dot{\boldsymbol{\eta}}_{initial} = \boldsymbol{\varphi}^{-1}\,\dot{\mathbf{U}}^{i-1} \tag{7.115}$$

where $\mathbf{U}^{i-1}$ and $\dot{\mathbf{U}}^{i-1}$ are displacement and velocity of the degrees of freedom at the end of the last time step, respectively. $\boldsymbol{\varphi}^{-1}$ is the inverse matrix of eigenvectors. It should be noted, that depending on the type of a phase change, i.e. sticking to sliding or sliding to sticking, the

appropriate matrix of eigenvectors must be used. This is because of the different number of degree-of-freedom in sticking and sliding phases.

The great advantage of the modal analysis method is the independence of the modes of vibration from each other. This makes it possible to consider only modes that play an important role in the general structural response (Figure 7.15). They are normally the first few modes of vibration. This causes a drastic reduction of the numerical costs of the simulation. As discussed before (Chapter 5), the global response of an isolated system is governed mainly by its first modes. This makes modal analysis an appropriate method to simulate such systems.

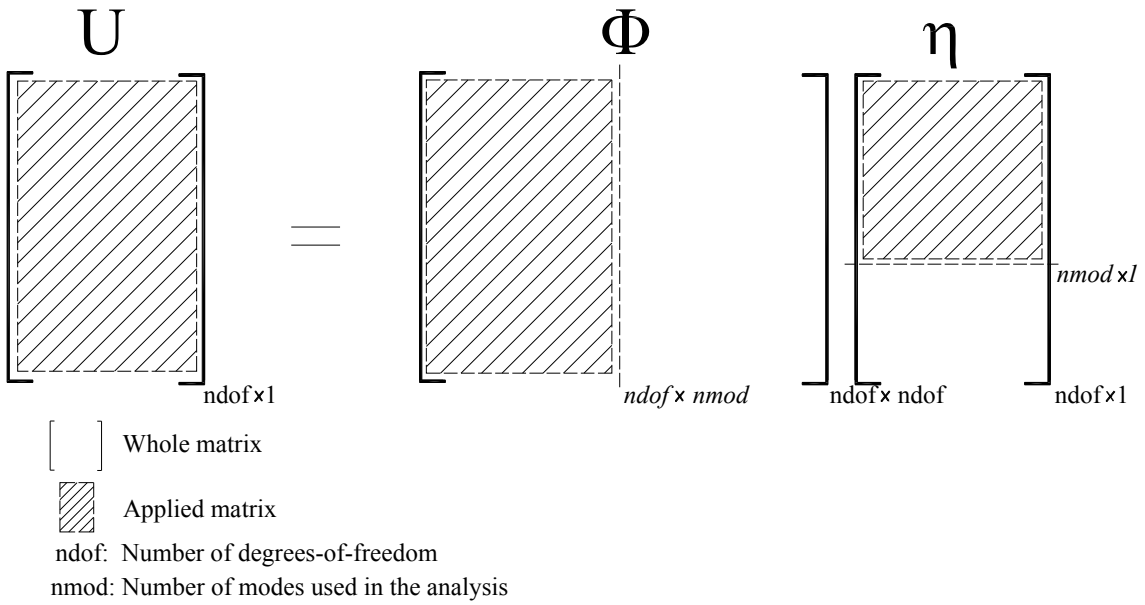

Figure 7.15 Partial consideration of the eigenvector in modal analysis.

In case of partial consideration of mode shapes, the initial conditions are calculated as [Petersen, 1996]:

$$\boldsymbol{\eta}_{initial} = \left[(\boldsymbol{\varphi}^T M \, \mathbf{U}^{i-1})^T \tilde{M}^{-1} \right]^T \tag{7.116}$$

$$\dot{\boldsymbol{\eta}}_{initial} = \left[(\boldsymbol{\varphi}^T M \, \dot{\mathbf{U}}^{i-1})^T \tilde{M}^{-1} \right]^T \tag{7.117}$$

Now the differential equation can be solved. The constant average acceleration method (Section 7.1.1) has been used. The load **P**(t) is (Equation 7.8):

$$\tilde{\mathbf{P}}(t) = -\tilde{\mathbf{F}}_f(t) - \tilde{\mathbf{P}}_g(t) \tag{7.118}$$

The process of the numerical simulation is explained in a pseudo-algorithm (Figure 7.16 and Appendix *D*).

7.7 Damping considerations

The dynamic response of a structure to ground motions depends on its mechanical characteristics and the nature of earthquake-induced forces. Mechanical properties that are efficient to mitigate the structural response to some excitations might have undesirable effects during other inputs. Base isolation is an efficient method to reduce forces and interstory drift during severe shakings (Sections 8.2-4). However, under seismic excitations with relatively

long periods of vibration or impulse-shape loads, numerical simulations and large-scale experiments have shown that they do not respond properly. Integrating an additional damping mechanism to the isolated structure located near active faults or in regions over thick sedimentary soil layers improve to some extent the structural response [Makris and Chang, 1998]. On the other hand, it must be taken into consideration that a very high damping ratio may have negative effects on the efficiency of isolation [Kelly, 1999]. In highly damped isolated structures, the maximum sliding displacement is decreased at the cost of higher base shear and larger interstory drift that are both counterproductive.

In most cases it is assumed that damping is small enough that the effect of the off-diagonal components of the damping matrix are negligible; so the required solution can be obtained from the uncoupled modal equations of motion [Kelly, 1999].

```
input parameters
assembling mass, damping, and stiffness matrices of the superstructure
    (for sticking phases an M-DOF system)
solution of the eigenvalue problem
computation of parameters of the CAA method (Equations 7.7-10)
assembling mass, damping, and stiffness matrices of the whole system (for
    sliding phases an (M+1)-DOF)
solution of the eigenvalue problem
computation of parameters of the CAA method (Equations 7.7-10)
while time(i) ≤ max(time)
   if the time refining process has been activated (Appendix D)
      recalculation of parameters of the CAA method (Equations 7.7-10)
   end
   if phase_state(t_{i-1}) == 'stick'
      computation of the modal inertial force (Equation 7.111)
      assignment of the initial conditions (Equations 7.114-117)
      solution of the differential equations for the considered modes
    (Equation
      7.112)
      transformation of the results into the original space (Equation
    7.110)
      control of the stick-slip criterion (Equation 7.113)
      assignment of the phase_state parameter
   else
      computation of modal friction and inertial forces (Equation 7.111)
      assignment of initial conditions (Equations 7.114-117)
      solution of the differential equations for the considered modes
    (Equation
      7.112)
      transformation of the results into the original space (Equation
    7.110)
      if (sign(base_vel(t_i) * base_vel(t_{i-1})) < 0)
         time step refining process
         if delta_t_new  < tolerance
            phase_state = 'stick'
            base_vel(t_i) = 0;
         end
      end
   i = i + 1;
end
```

Figure 7.16 Pseudo-algorithm for the numerical simulation of multi degree-of-freedom isolated systems.

In Rayleigh damping, the damping matrix is defined as a linear combination of mass and stiffness matrices:

$$\mathbf{C} = \alpha_0 \mathbf{M} + \alpha_1 \mathbf{K} \tag{7.119}$$

where

$$\alpha_0 = \xi \frac{2\omega_i \omega_j}{\omega_i + \omega_j} \tag{7.120}$$

$$\alpha_1 = \xi \frac{2}{\omega_i + \omega_j} \tag{7.121}$$

in which ξ is the damping ratio at natural frequencies of ω_i and ω_j. Throughout this study, the damping ratio is taken in a range that the *off diagonal* damping components can be ignored.

The response of isolated structures in sticking and sliding phases are completely different. As long as sliding bearings are not activated, the structure responds the same as a fixed-base structure. After initiation of sliding, the interstory drift (main reason of the structural damages) decreases. Hence, the damping ratio in isolated structures is taken usually smaller than the one in fixed-base structures.

For the sake of numerical stability, a minimum damping ratio of 0.5% of the critical damping is assigned for the first and second modes of vibration in both sticking and sliding phases in this study.

Chapter 8

Case Studies

In this chapter, several case studies are simulated with the numerical models developed in the previous chapter. They are classified into three main groups of one, two, and many degree-of-freedom systems. Main features of friction-based isolated systems, e.g. efficiency of the isolation method and its relation to the level of input excitation, frequency dependency of the structural response, restoring mechanism, the effect of concavity of the sliding surface, etc. are discussed. In the last section, an experimental test done on a shaking table is simulated. Results computed with the developed model are then compared with those reported elsewhere.

8.1 1-DOF model under harmonic excitation

The very large participation factor of the first mode of vibration of FPS isolated systems in comparison with the participation factor of the other modes motivates the idea to simulate such systems with 1-DOF models. First the response of such a system to a harmonic ground acceleration $a_g(t)$ is studied (Section 7.3), in which:

$$a_g(t) = \hat{a}_g \sin(\Omega t) \tag{8.1}$$

System properties are as follows (Figures 6.6 and 8.1):

m= 10000 kg, k = 10^6 N/m, c = 0 Ns/m, μ = 0.075, F_f = 7500 N, $\hat{a}_g$ = 0.981 m/s^2, ω = 10 s^{-1}, and Ω = 6.284 s^{-1}.

The constant Coulomb friction law has been used. The time step is taken as 10^{-2} seconds.

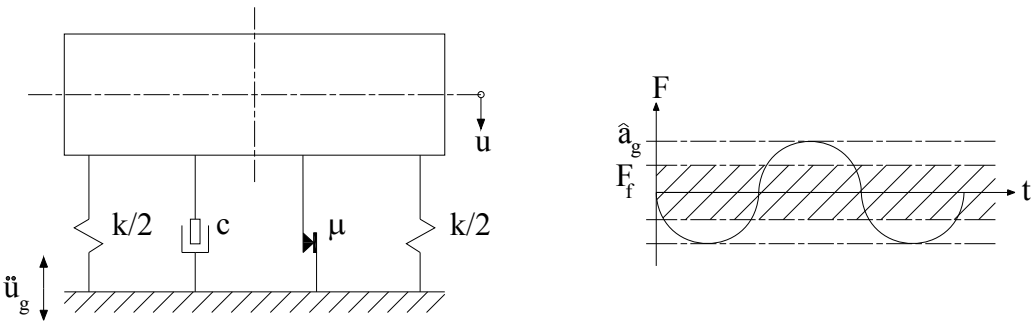

Figure 8.1 Physical model of an isolated system under a harmonic load.

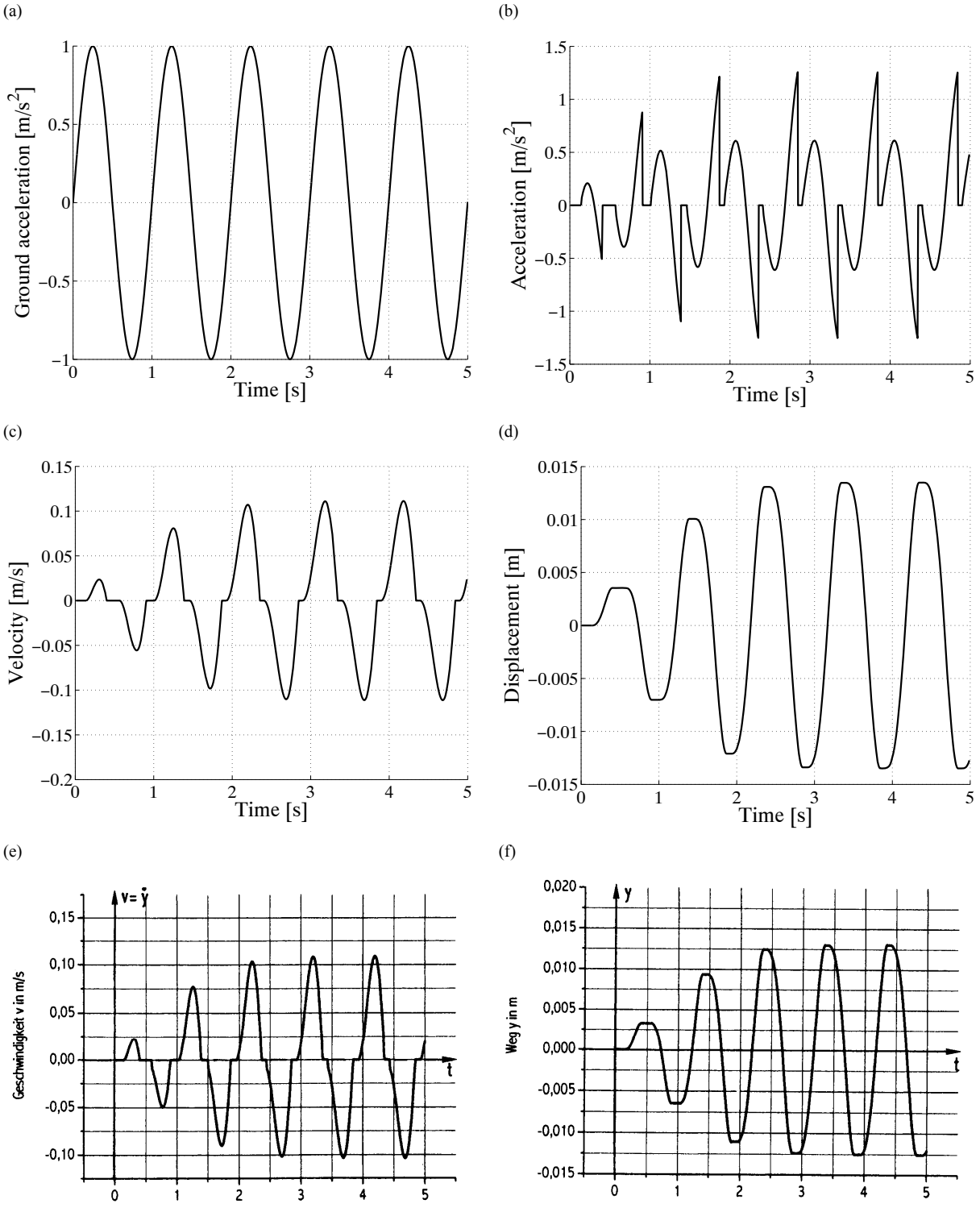

Figure 8.2 The response of a friction isolated system to a harmonic excitation: (a) the harmonic ground acceleration, (b) relative acceleration, (c) relative velocity, (d) relative displacement, (e) relative velocity according to [Petersen, 2005], and (f) relative displacement according to [Petersen, 2005].

As long as the load is smaller than the static friction force, no sliding has been initiated (Figures 8.2 and 3). Because of the Coulomb friction model, the friction force remains constant during sliding phases. In sticking phases (constant sliding displacement) the friction force is calculated regarding the equation of equilibrium that is not constant, but its maximum value is bounded. The restoring force is composed of the spring force (geometrical stiffness)

and the friction force. Because the friction force is always in the opposite direction of the sliding velocity, as soon as the direction has changed, a jump occurred in the diagram, which is two times of the friction force (Figure 8.3.c).

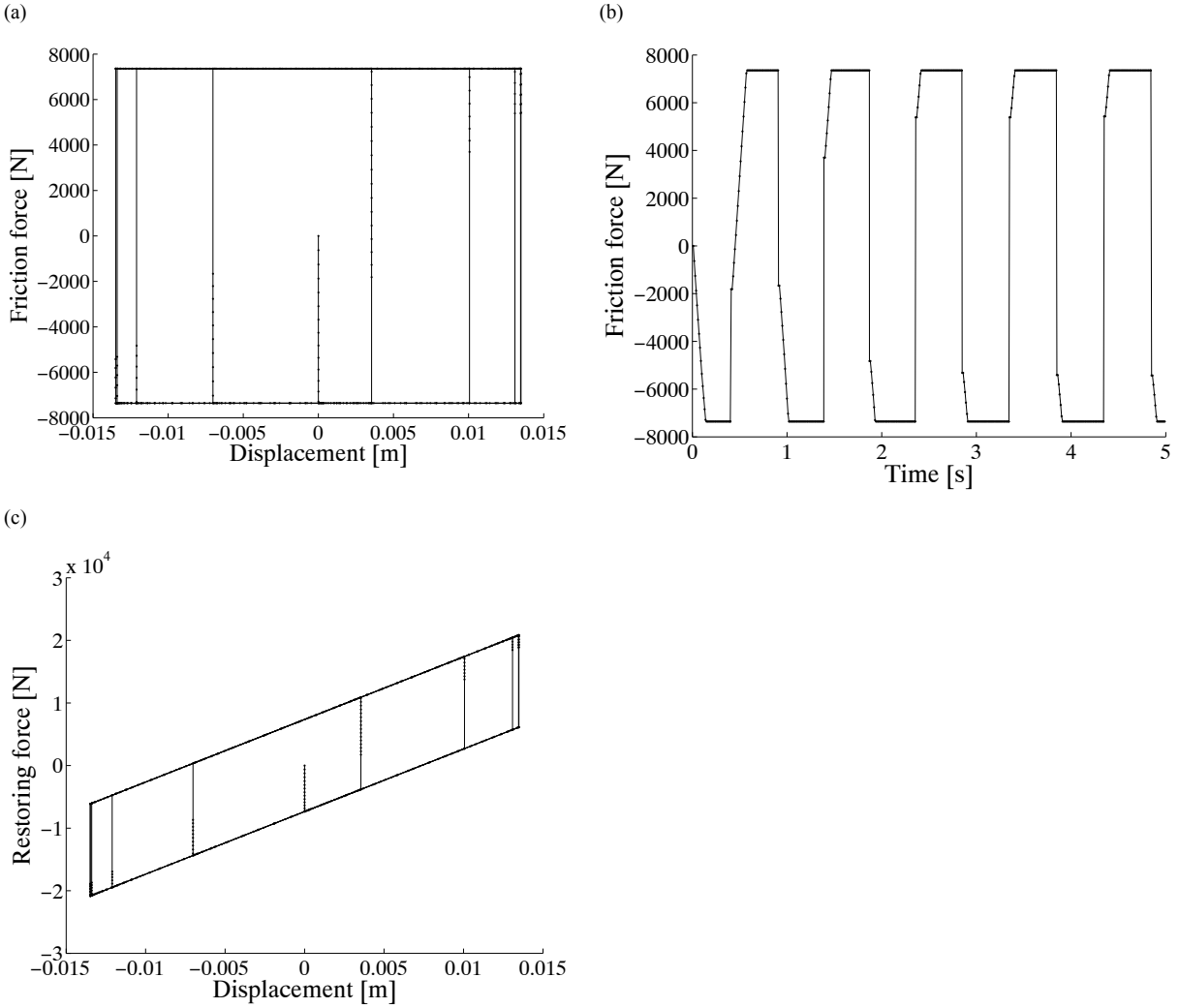

Figure 8.3 The response of a friction isolated system to a harmonic loading: (a) Friction force versus displacement, (b) Friction force versus time, and (c) the restoring force versus displacement.

Adding a viscous damping source to the system (c = 5000 Ns/m) decreases the sliding displacement in comparison to the former case (Figure 8.4).

The efficiency of the isolation method under different circumstances is an important issue in base isolated systems. The stick-slip criterion is the key factor distinguishing the two possible phases of sticking and sliding (Equation 6.7). As long as base shear force does not overcome the static friction force, the isolated system remains sticking and responds the same as a fixed-base system (sticking phase). Therefore, apart from the system properties the efficiency of an isolated system is depending mainly on the level of input excitations. The lower this level is the later the isolator begins to slide. Only after the initiation of sliding, a relative sliding acceleration is initiated in the opposite direction of the input acceleration (excitation). This reduces the inertial force applied to the mass, as the inertial force is a function of the *total* (absolute) acceleration of the degree-of-freedom, not the *relative* acceleration.

To examine this issue a similar system is excited with two levels of harmonic ground acceleration. The response of the set and the efficiency of the isolation method are then compared in both cases (Figure 8.5). System properties are as follows:

m = 10000 kg, k = 10^6 N/m, c = 0 Ns/m, $\mu = 0.075$, $\ddot{u}_g = 0.9$ (1.2) m/s^2, $\omega = 10$ s^{-1}, and $\Omega = 6.284$ s^{-1}.

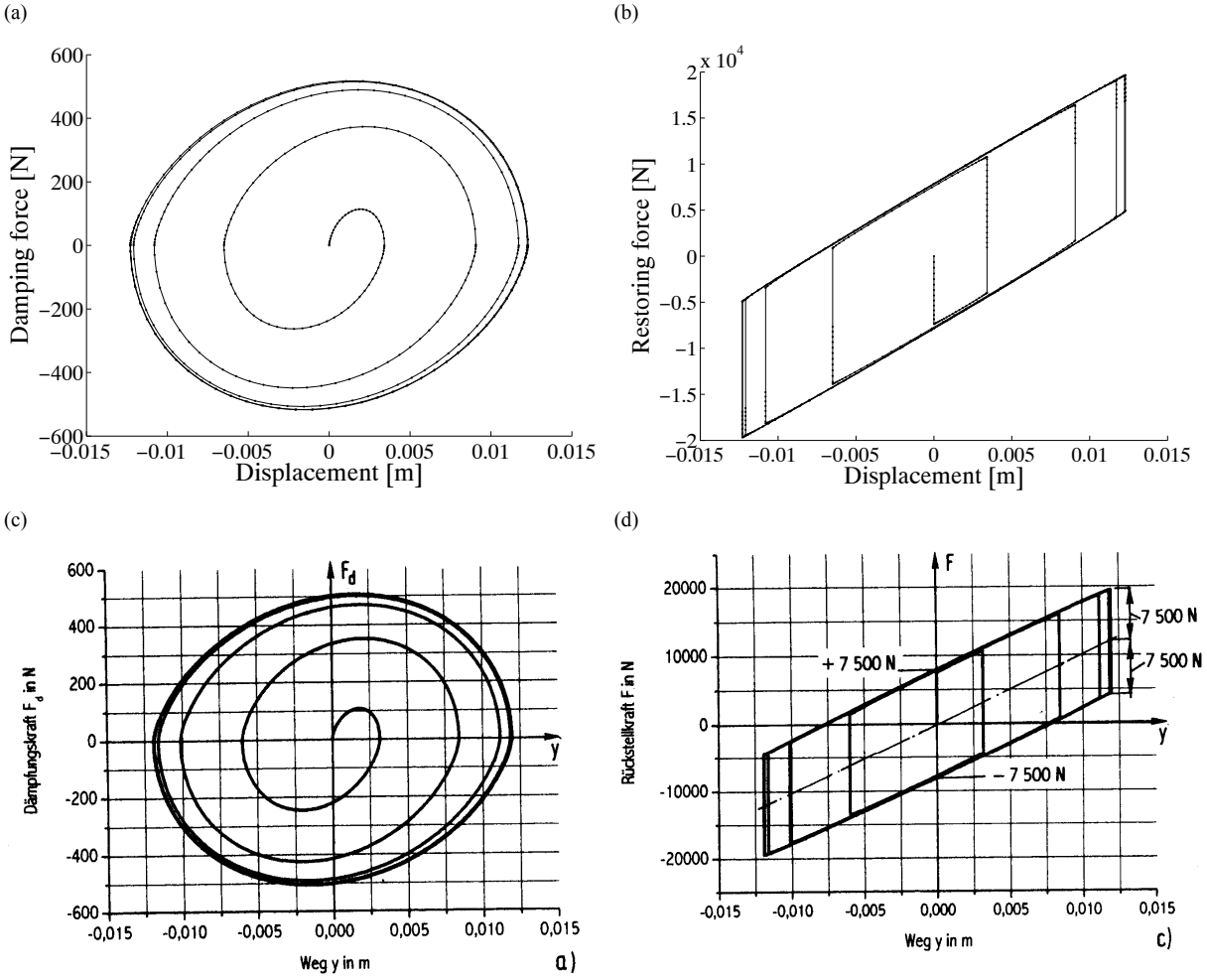

Figure 8.4 The response of a friction isolated system with viscous damping to a harmonic loading: (a) Damping force versus displacement, (b) Restoring force versus displacement, (c) Damping force versus displacement according to [Petersen, 2005], and (d) restoring force versus displacement according to [Petersen, 2005].

For lower levels of excitations the isolated system is activated later in comparison with a system excited with a higher level of loading. This implies that sticking phases, in which isolators are not active, last for longer periods of time (Figure 8.5).

Not only the maximum amplitude of loading (excitation) affects the response of an isolated system, but also the frequency content of the excitation plays an important role in the response of such systems. A period of vibration close to the natural period of isolation causes resonance and instability in form of a very large sliding displacement. The closer the period of vibration to the natural period of isolation, the larger are relative displacement and velocity of the sliding bearing (Figures 8.6 and 8.7). The same system discussed before is excited with two harmonic excitations with circular frequencies of vibration of 2 and 8 s^{-1}.

Another important issue in friction pendulum isolated systems is the restoring mechanism. Because of the concavity of the sliding surface a restoring force is produced, which restrains

the permanent displacement of the isolator, i.e. the displacement remains in the system after cessation of excitations. The restoring mechanism restricts to some extent the maximum displacement during excitations as well. However, it does not guarantee that after cessation of the excitation the bearing would be located exactly in its initial position. A sliding bearing would stick somewhere in between, as soon as the restoring force cannot overcome the friction force anymore. The response of an FPS system is compared with a bearing sliding simply on a flat surface (Figure 8.8). The same system properties and loading used before are applied.

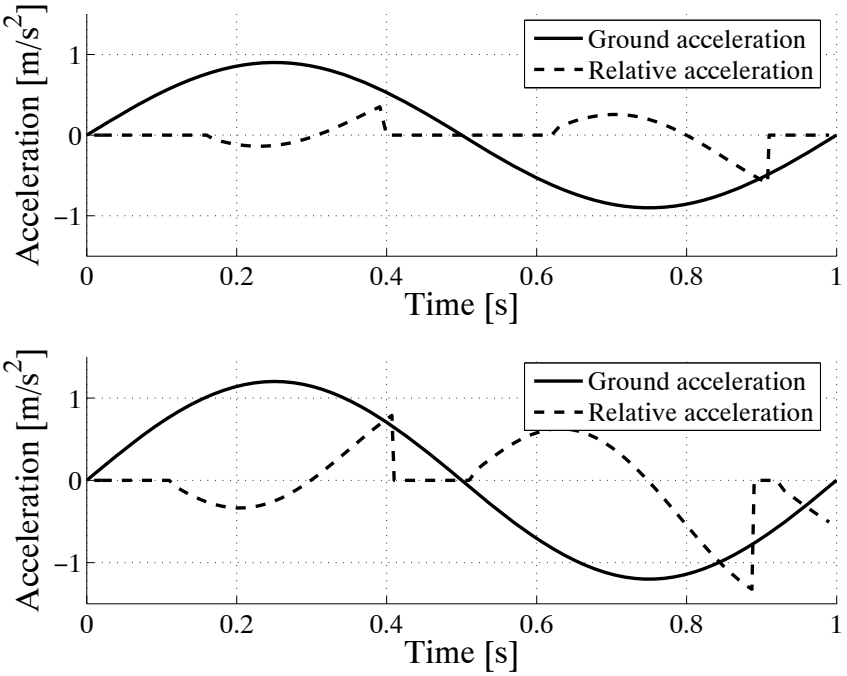

Figure 8.5 Comparison of the response of an isolated system to two different levels of harmonic ground excitations: $\ddot{u}_g$ = 0.9 and 1.2 m/s^2.

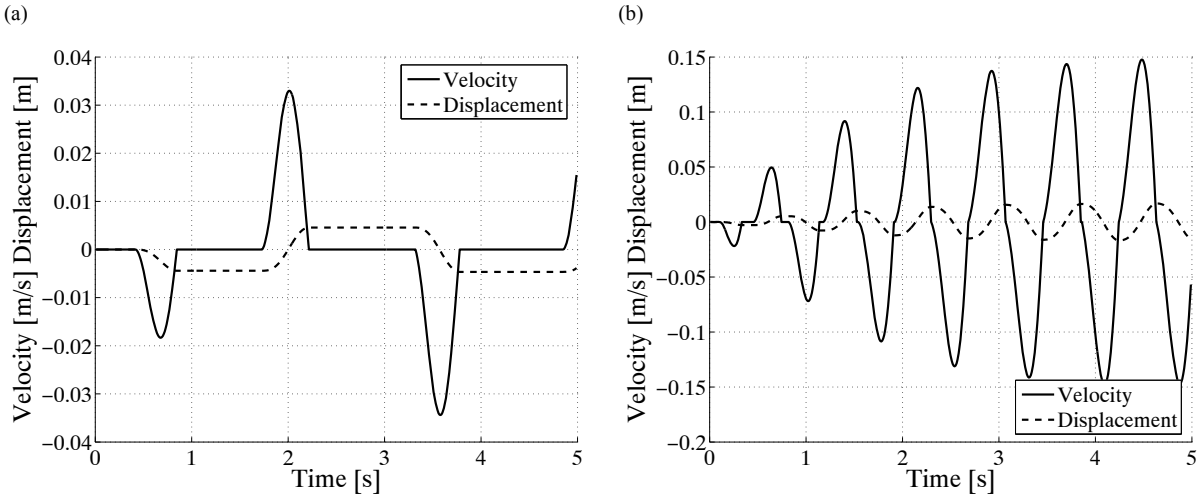

Figure 8.6 The response of an isolated 1-DOF system to harmonic excitations with circular frequencies of vibration (a) 2 s^{-1}, (b) 8 s^{-1}.

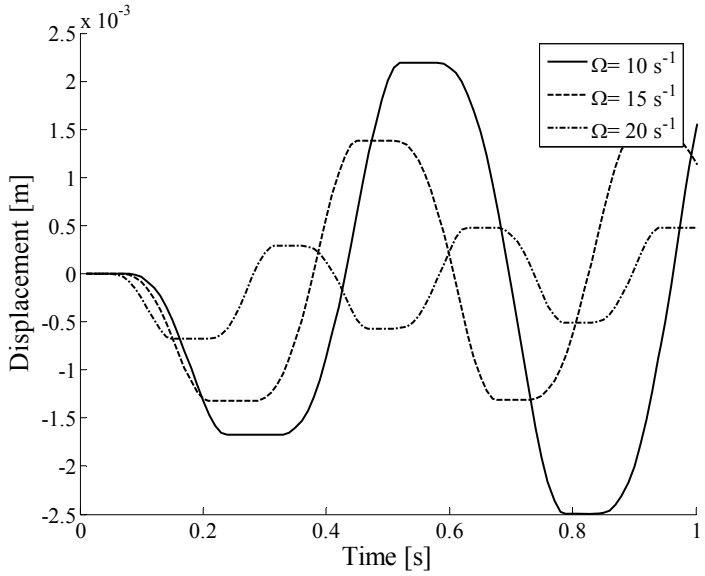

Figure 8.7 The response (relative displacement) of an isolated 1-DOF system to harmonic excitations with different circular frequencies of vibration.

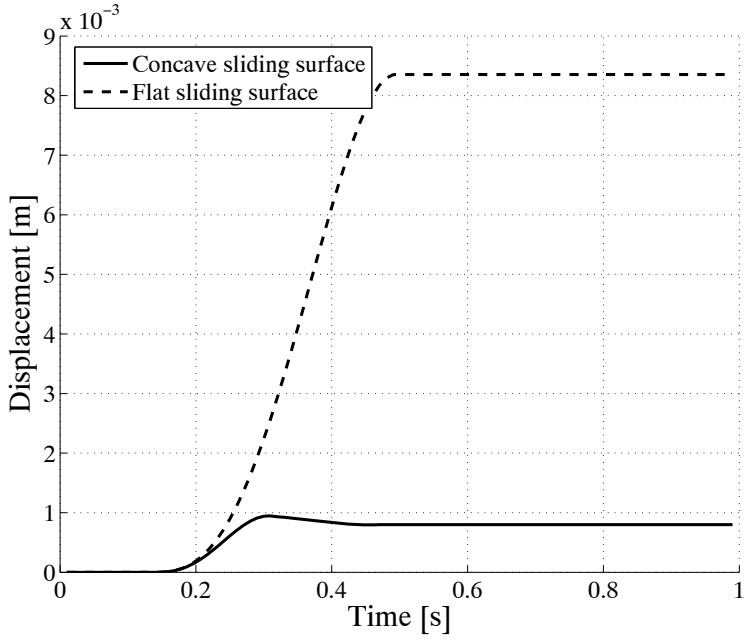

Figure 8.8 Comparison of the response (relative displacement) of an isolated 1-DOF system sliding on a concave surface (R = 0.2 m) with the one sliding on a flat surface.

8.2 1-DOF model under non-harmonic loading

The same numerical model as in section 8.1 has been used to simulate an isolated 1-DOF set under non-harmonic excitation. The El Centro earthquake accelerogram (USA, 1940 with a magnitude of 7.1) is used as the input ground acceleration (Figure 8.9). System properties are as follows:

m = 250 ton, k = 1000 kN/m, c = 0 Ns/m, $\mu = 0.07$, $F_f = 175$ KN, $\omega = 2$ s^{-1}, and $R = 2.5$ m.

Time steps are considered to be 0.02 seconds. If a phase change happens, time steps are refined to 0.002 seconds. The maximum sliding displacement is about 4 centimeters. The permanent displacement at the end of the analysis is less than 4 millimeters, as a result of the concavity of the sliding surface. The friction force is considered to be of the Coulomb type (Figure 8.10). The same as before, in sticking phases it has been computed with regard to the equation of equilibrium.

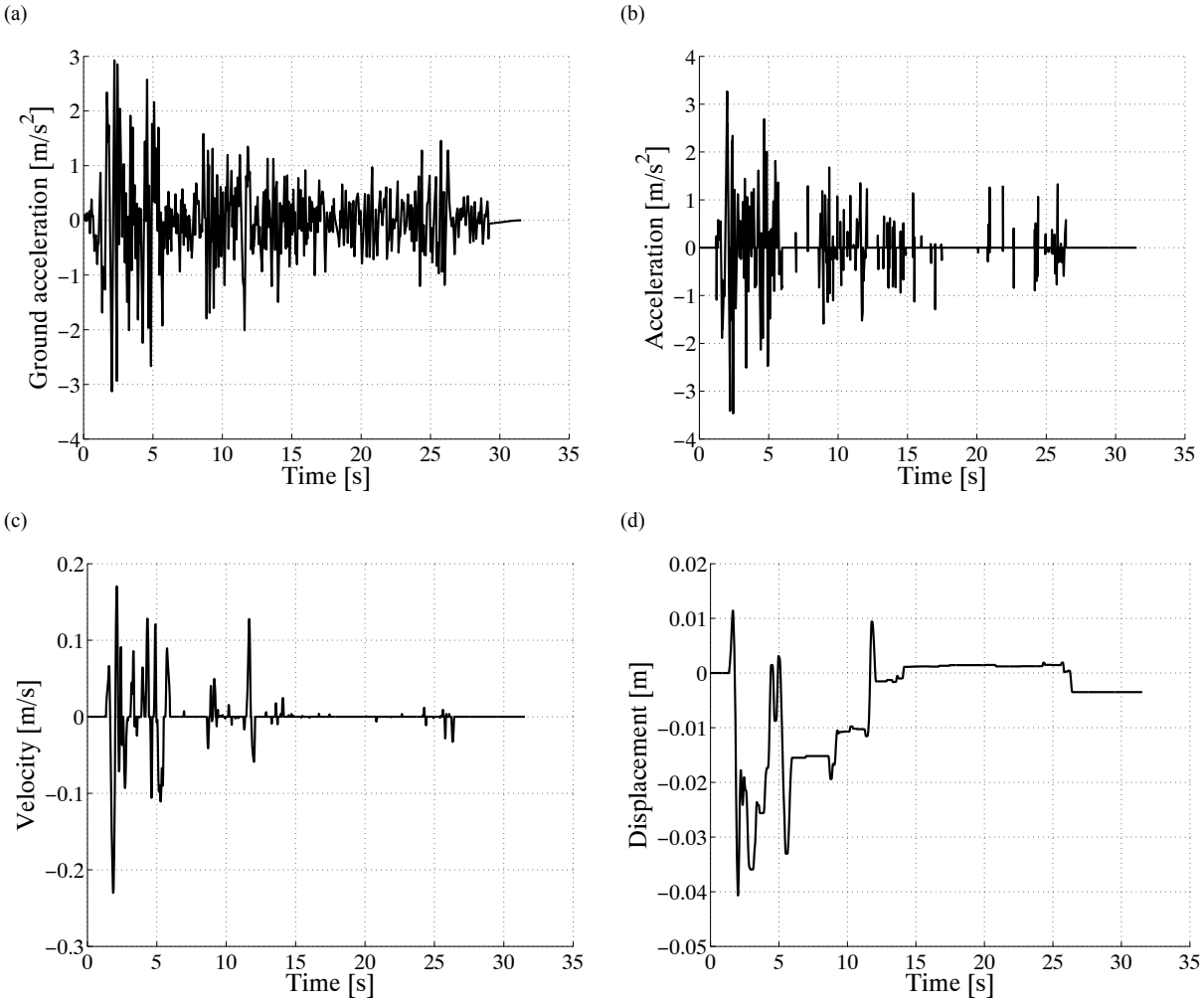

Figure 8.9 Response of an isolated 1-DOF set to El Centro earthquake: (a) the ground excitation, (b) relative acceleration, (c) relative velocity, and (d) relative displacement of the degree-of-freedom.

The initiation of sliding is directly controlled by the static friction force. The larger the friction coefficient the later the isolation mechanism is activated. In an extreme case, during the entire period of loading the base shear force does not overcome the friction force. In such a case, an isolated system responds the same as a classical fixed-base system (*blocking*). The response of the aforementioned system to the same excitation (El Centro earthquake) with different levels of friction force is studied (Figure 8.11). For friction coefficients larger than 0.32 the set is blocked (Table 8.1).

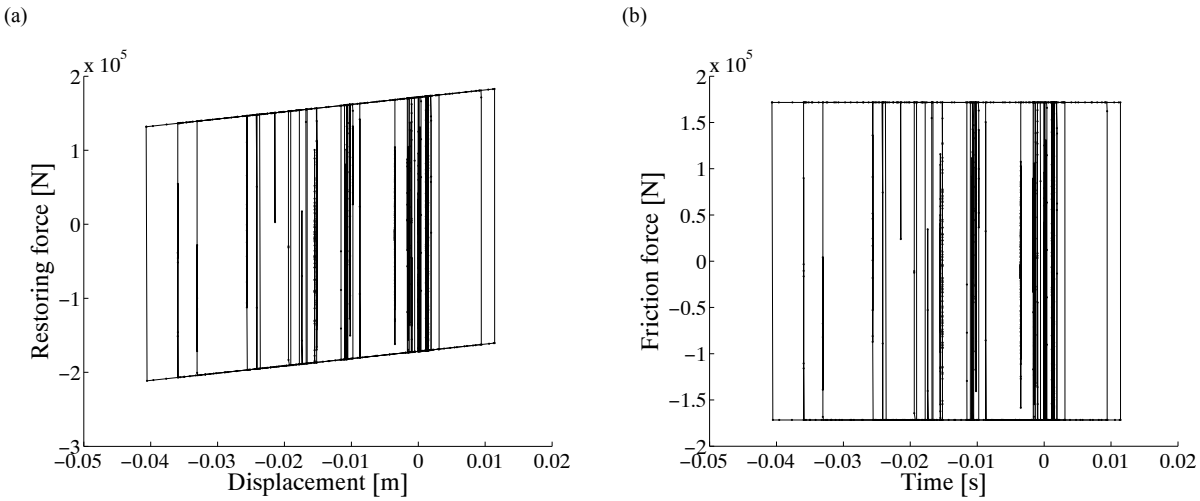

Figure 8.10 Restoring and friction forces versus relative displacement in an isolated 1-DOF set.

Table 8.1 Maximum and minimum values of relative acceleration and sliding displacement of an FPS isolated set for different levels of the friction force.

μ	$\ddot{u}\ [m/s^2]$		$u\ [m]$	
	max	*min*	*max*	*min*
0.02	3.35	-3.15	0.102	-0.121
0.08	3.12	-3.59	0.013	-0.034
0.15	2.69	-3.45	0.002	-0.014
0.25	3.89	-5.24	0.001	0.000

The concavity of the sliding surface in friction pendulum systems produces a recentering mechanism, which decreases the permanent deviation of the set from its original configuration at the end of excitations. To study this effect, the same model as before with a friction coefficient of 0.08 is analysed for four different radii of curvature (Figure 8.12). As expected, a smaller radius of curvature, i.e. a more concaved sliding surface with accordingly larger geometrical stiffness, reduces the permanent displacement of the bearing. For different radii of curvature a similar trend in the response is observed. A higher geometrical stiffness has not caused the bearing to slide later than a bearing sliding on a flat surface. Therefore, it does not impair the isolation efficiency of sliding bearings (Figure 8.13). Jumps in the diagram are because of the dependency of the friction force on the direction of the sliding velocity. They are equal to $2F_f$.

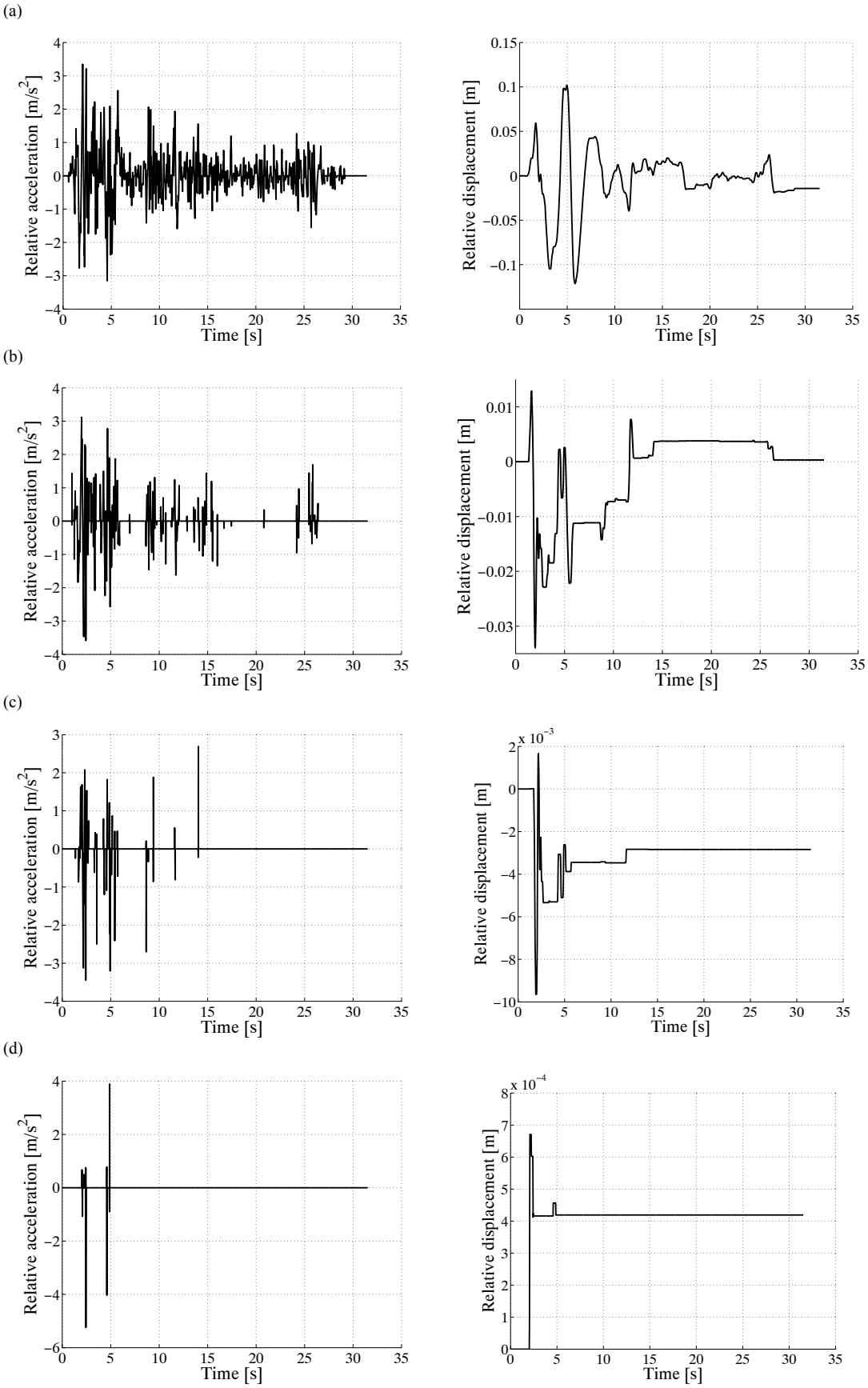

Figure 8.11 Response of an isolated 1-DOF set (relative acceleration and sliding displacement) to El Centro earthquake with bearings sliding on a surface with friction coefficients of:
(a) 0.02, (b) 0.08, (c) 0.15, and (d) 0.25.

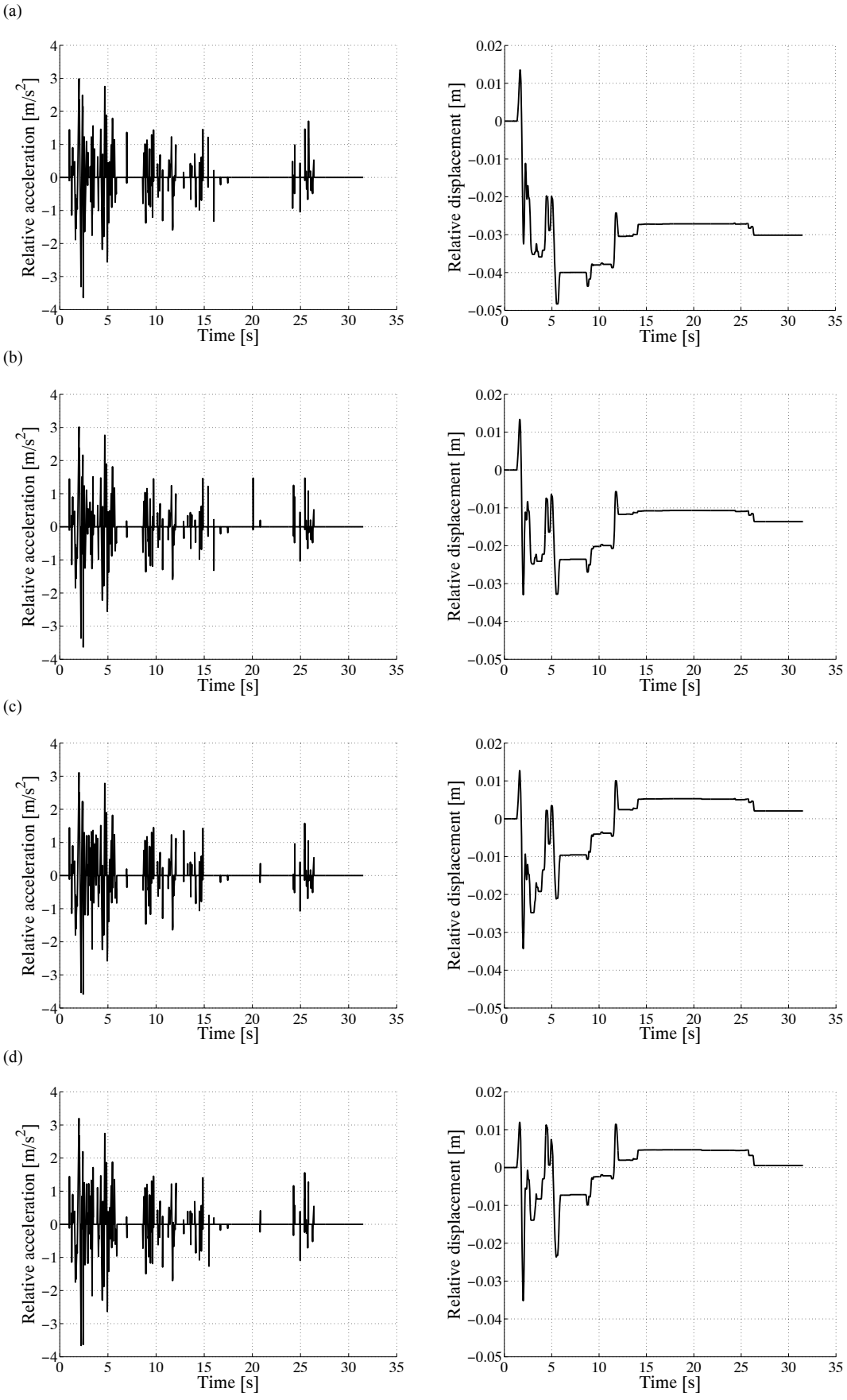

Figure 8.12 Response of an isolated 1-DOF set (relative acceleration and sliding displacement) to El Centro earthquake with bearings sliding (a) on a flat surface, or over a concave surface with radii of curvature of: (b) 10 m, (c) 2 m, and (d) 1 m.

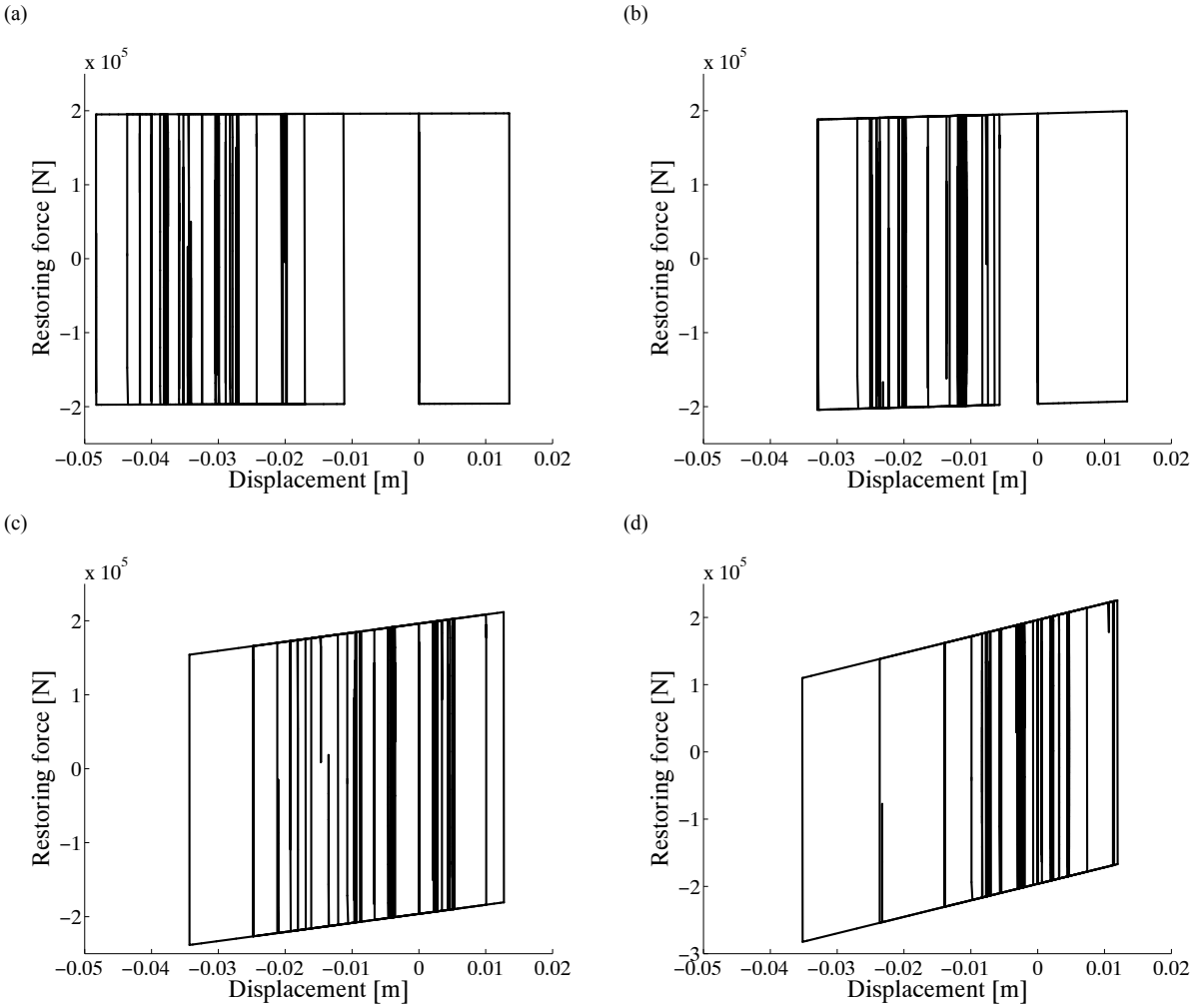

Figure 8.13 Restoring force in an isolated 1-DOF set with bearings sliding (a) on a flat surface, or over a concave surface with radii of curvature of: (b) 10 m, (c) 2 m, and (d) 1 m.

8.3 2-DOF model

In the initial phases of the design process one-degree-of-freedom models are appropriate to simulate roughly the response of an FPS isolated set. In subsequent phases, however, more detailed models are required to study the interaction effect between the structure and the isolation block. The simplest model of this type is a 2-DOF system, in which the first degree-of-freedom stands for the isolation module and the second one for the structure. The ground excitation is applied to the isolation block and through FPS bearings it is transmitted to the structure.

The response of this system to a triangular loading in form of forced ground acceleration is studied (Figure 8.14). System properties are as follows (Figure 7.10 and Appendix *C*):

m = 350 kg, M = 700 kg, k = 86400 N/m, K = 10300 N/m, c = 220 Ns/m, C = 0 Ns/m, $\mu = 0.08$, $F_f = 824$ N, $\omega = 15.7$ s^{-1}, $\Omega = 3.13$ s^{-1}, $\alpha = 0.33$, $R = 1$ m, $\Delta t = 0.001$ s.

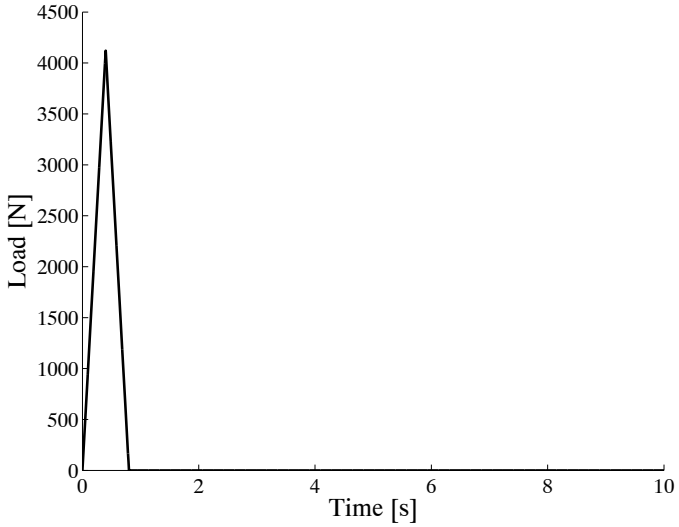

Figure 8.14 Triangular forced ground acceleration.

It takes 0.104 seconds until the bearing starts sliding. The load lasts 0.8 seconds. The bearing, however, slides much longer until 2.91 s (Figure 8.15). Structural relative and absolute accelerations are then compared (Figure 8.16). The structural damping ratio is taken to be 2% (rather than the classical 5%) of the critical damping, as structural damages, e.g. plastic deformations and cracks in columns and walls, in isolated systems are less than those in fixed-base structures.

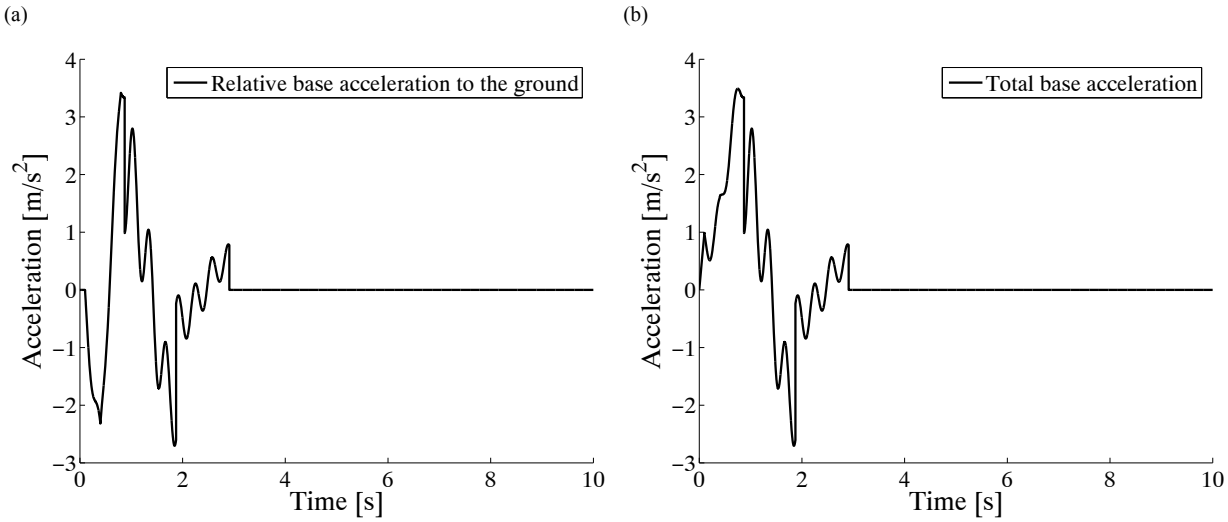

Figure 8.15 Response of an isolated 2-DOF system to a triangular load: (a) relative base acceleration to the ground, (b) total base acceleration.

The main source of damage in a structure under earthquake excitations is the relative deformation in floors (*drift*). Through sliding isolation it can be drastically decreased (Figures 8.19 and 8.20). The main part of the generated displacement is concentrated in the isolation layer. Thereby, a large deformation in the second degree-of-freedom (the structure) is prevented.

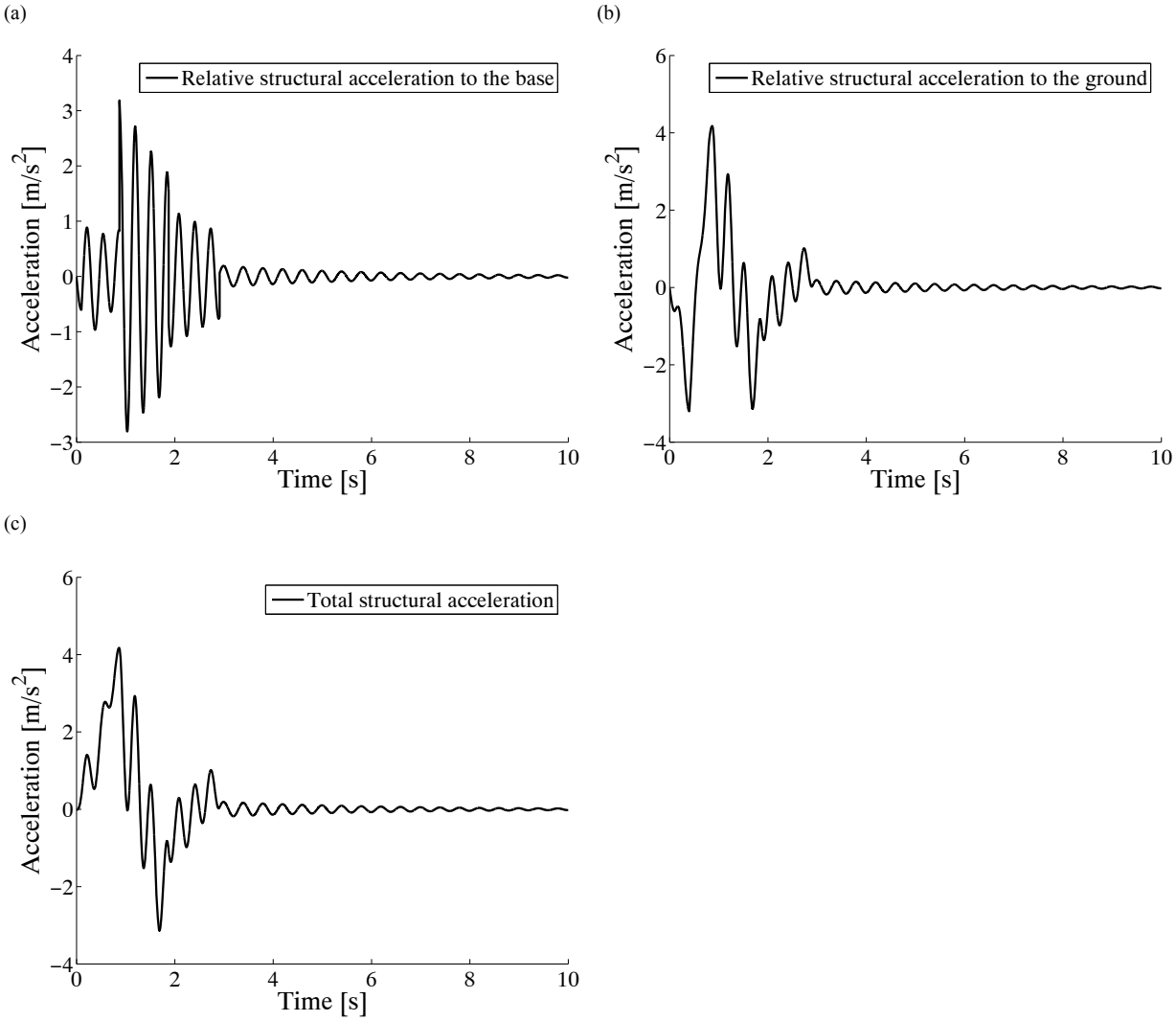

Figure 8.16 Response of an isolated 2-DOF system to a triangular load: (a) relative structural acceleration to the base, (b) relative structural acceleration to the ground , and (c) total structural acceleration.

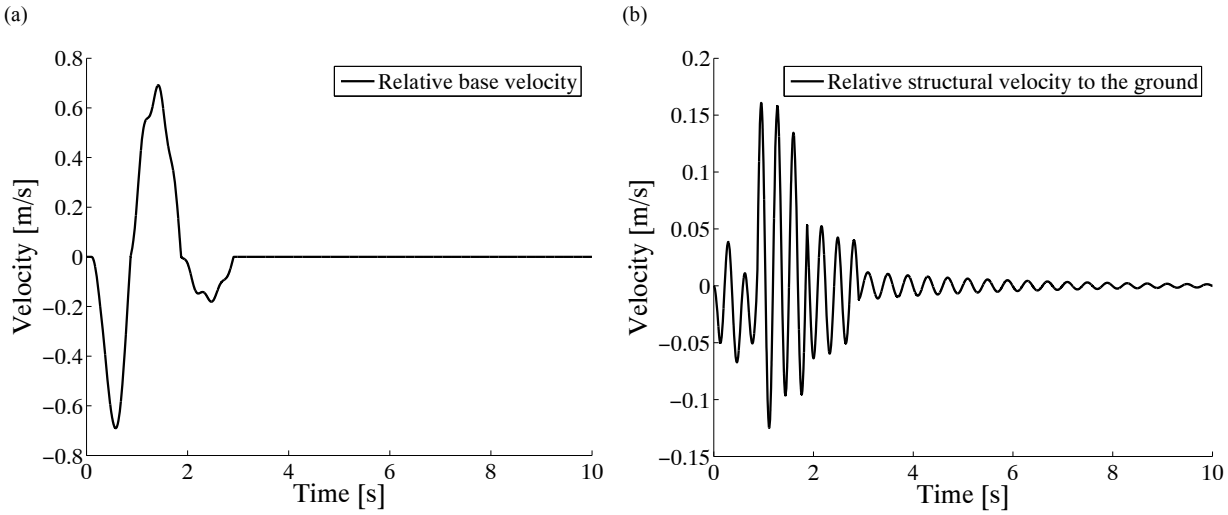

Figure 8.17 Response of an isolated 2-DOF system to a triangular load: (a) base relative velocity and (b) structural relative velocity to the base.

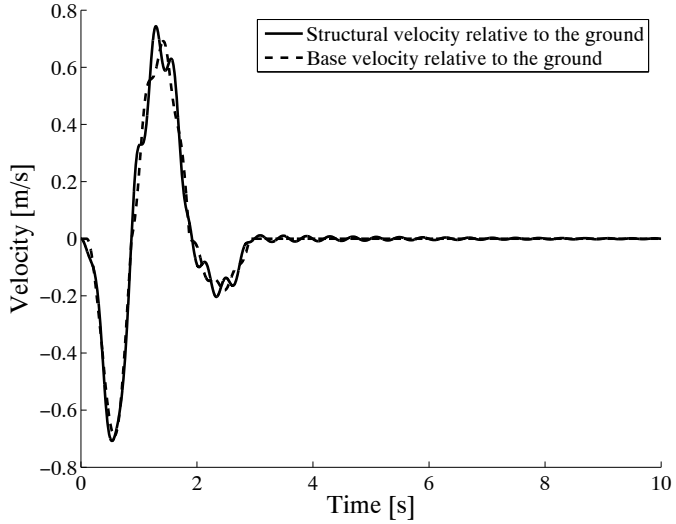

Figure 8.18 Comparison of the total velocity of the first and second degrees-of-freedom relative to the ground.

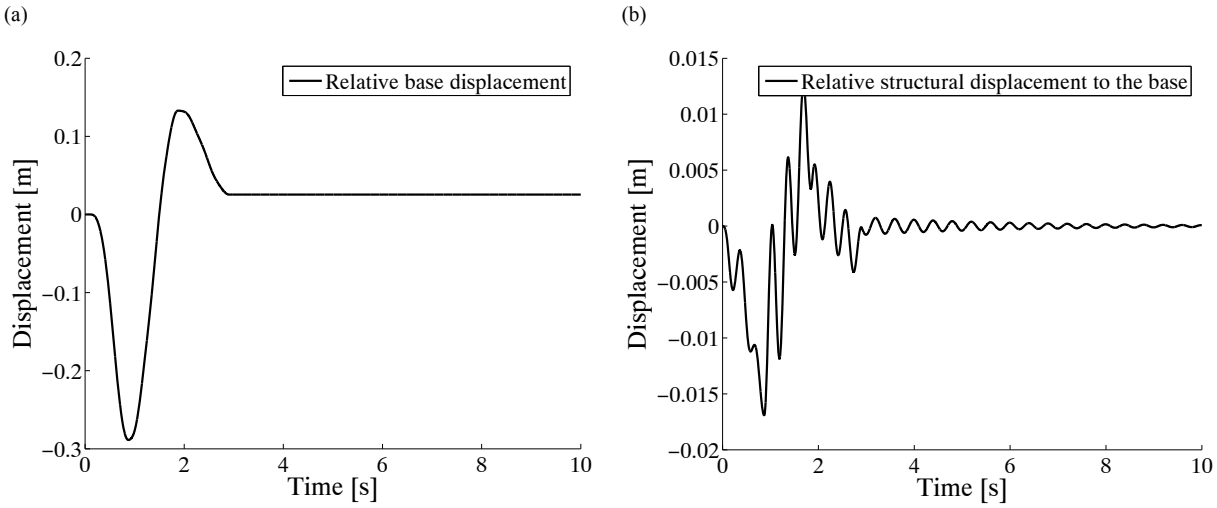

Figure 8.19 Comparison of the relative displacement of the first and second degrees-of-freedom.

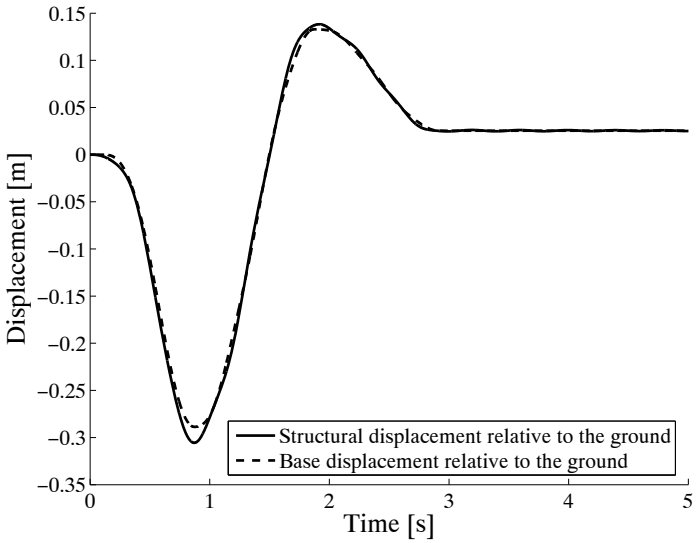

Figure 8.20 Comparison of the total displacement of the first and second degrees-of-freedom relative to the ground.

The response of the same system studied before to the El Centro earthquake excitations is computed (Figure 8.21). The maximum ground acceleration is scaled to *one g* (9.81 m/s^2). The Relative base acceleration is almost in the same order of the ground acceleration, but in the opposite direction. Because of the isolation, there is a delay between the maximum amplitude of the ground acceleration and the structural response to it.

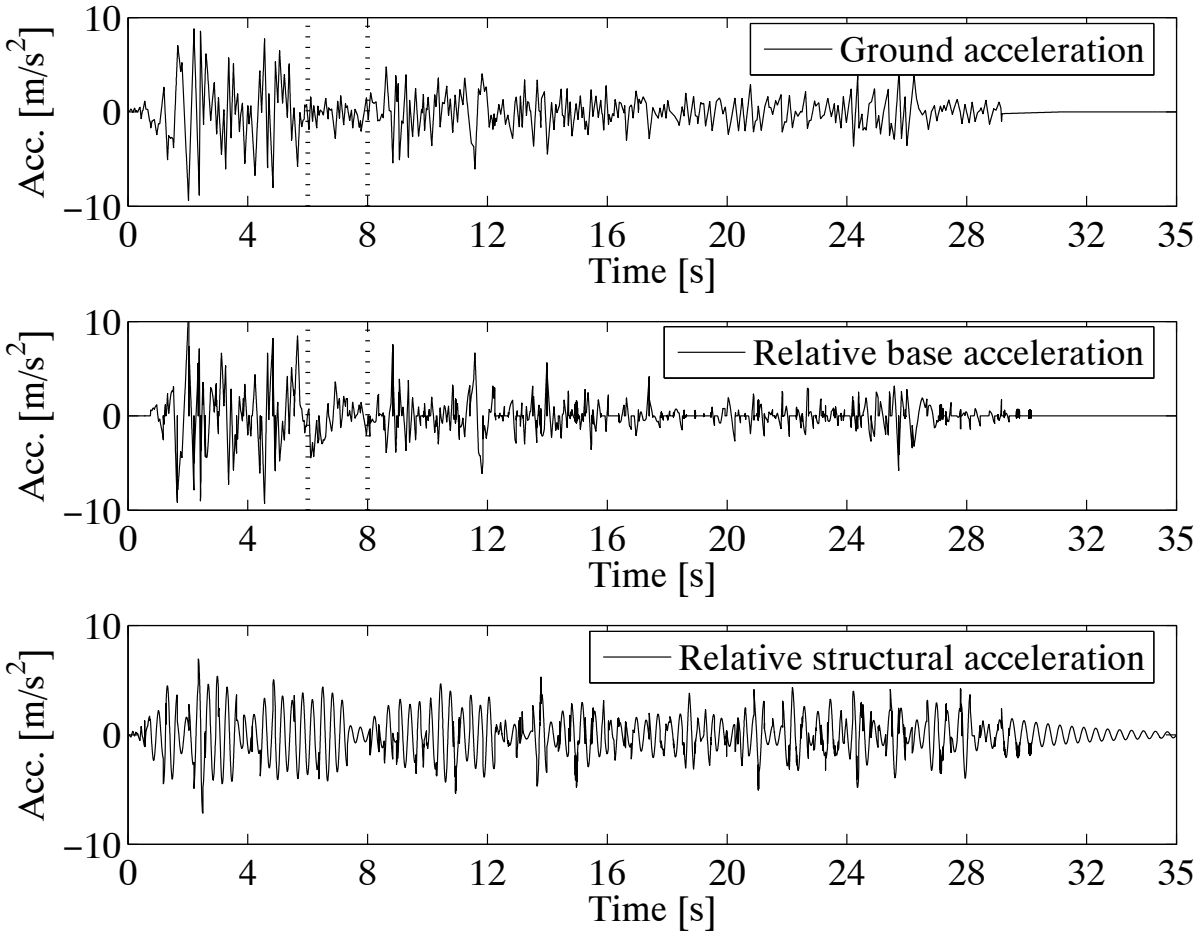

Figure 8.21 Structural response of an isolated 2-DOF set to El Centro earthquake.

Even in intervals with a ground acceleration smaller than the friction coefficient, e.g. between the 6th and 8th seconds of the analysis, the bearing has not stopped sliding because of the inertial force of the second degree of freedom (Equation 7.84 and Figure 8.21).

It takes such an isolated system a longer time to come to rest, as a result of a smaller damping ratio considered in the system in comparison with a fixed-base system (Figure 8.22).

The relative displacement of the second degree of freedom as a measure of the structural damage is one order smaller than the sliding displacement of the bearing (Figure 8.23). Besides, the concavity of the sliding surface has restricted the permanent displacement to less than 2 centimeters.

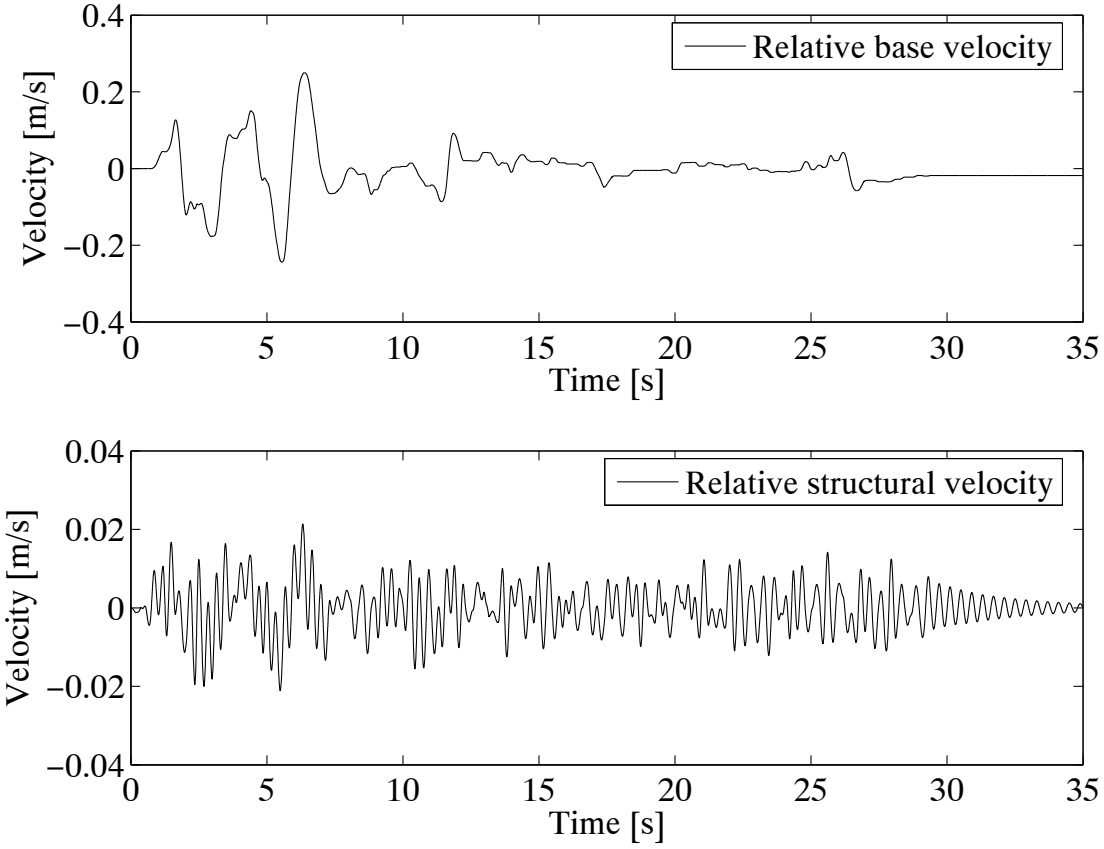

Figure 8.22 Relative velocities of the first and second degrees-of-freedom in an isolated 2-DOF system

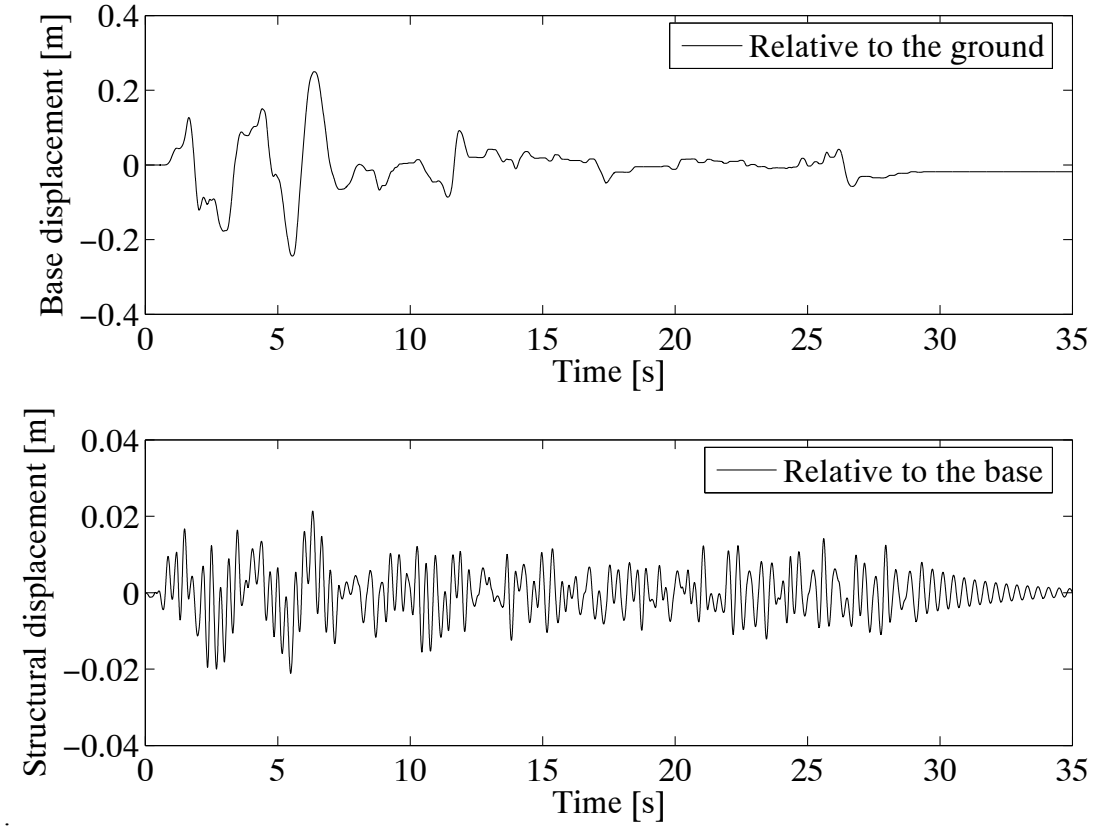

Figure 8.23 Relative displacements of the first and second degrees-of-freedom in an isolated 2-DOF system.

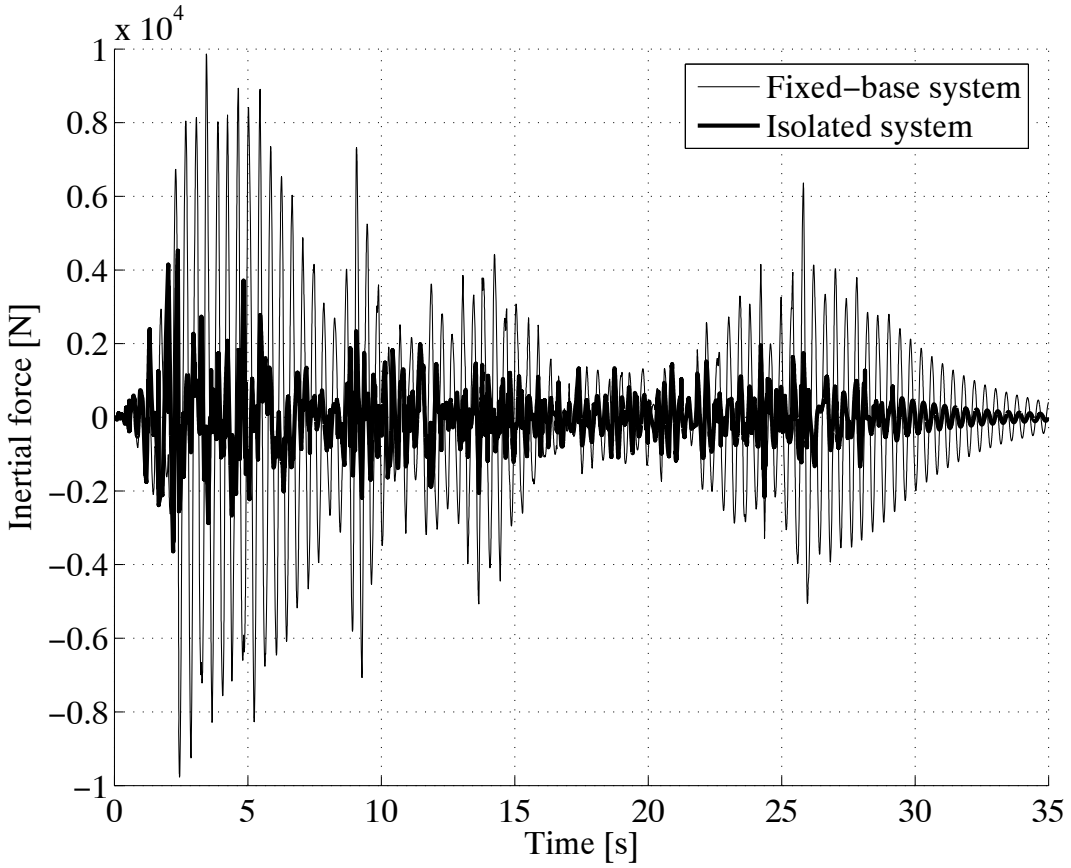

Figure 8.24 Comparison of the base shear in an isolated system with the one in a fixed-base structure.

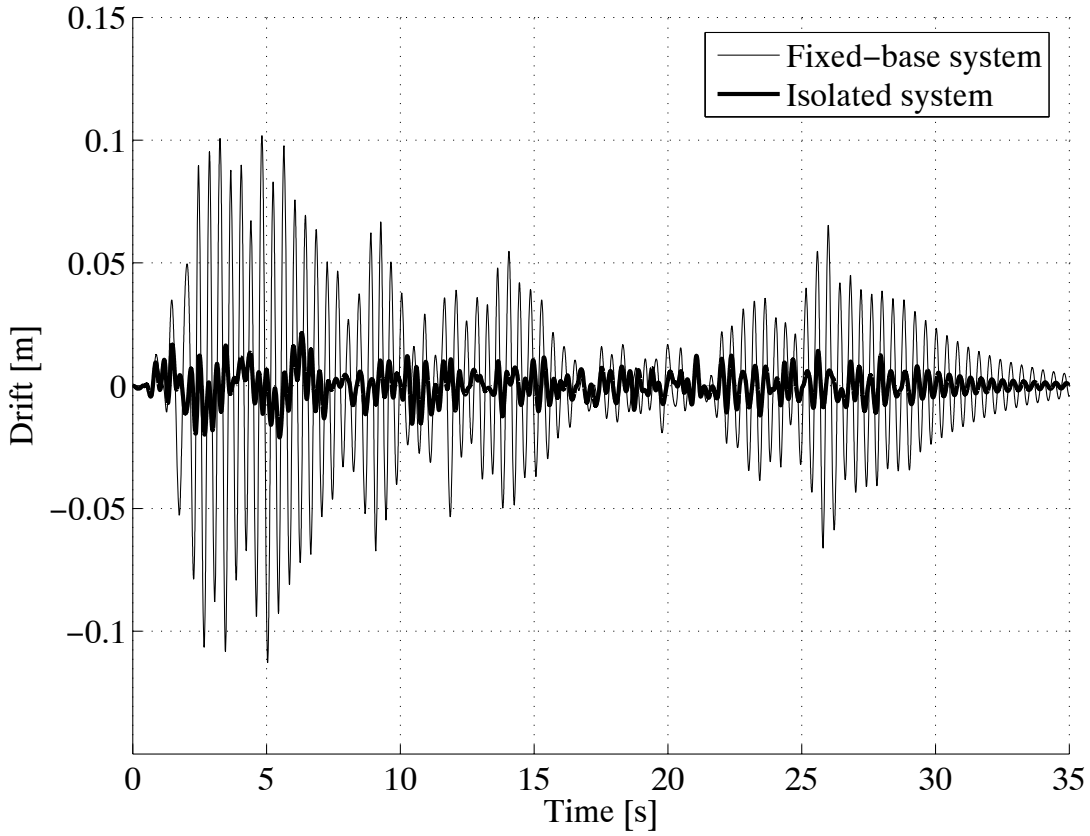

Figure 8.25 Comparison of the drift in an isolated system with the one in a fixed-base structure.

In comparison to a fixed-base system base shear in an isolated structure is reduced about 55% (Figure 8.24). The drift in such a system is strongly decreased as well (Figure 8.25).

A coarser time stepping decreases numerical costs. However, the moment, in which the sliding has been initiated, cannot be found as exactly as before. Maximum values of response are also to some extent different in comparison with a very fine time digitization (Figure 8.26). The results of the base displacement are more sensitive in this issue (Table 8.2).

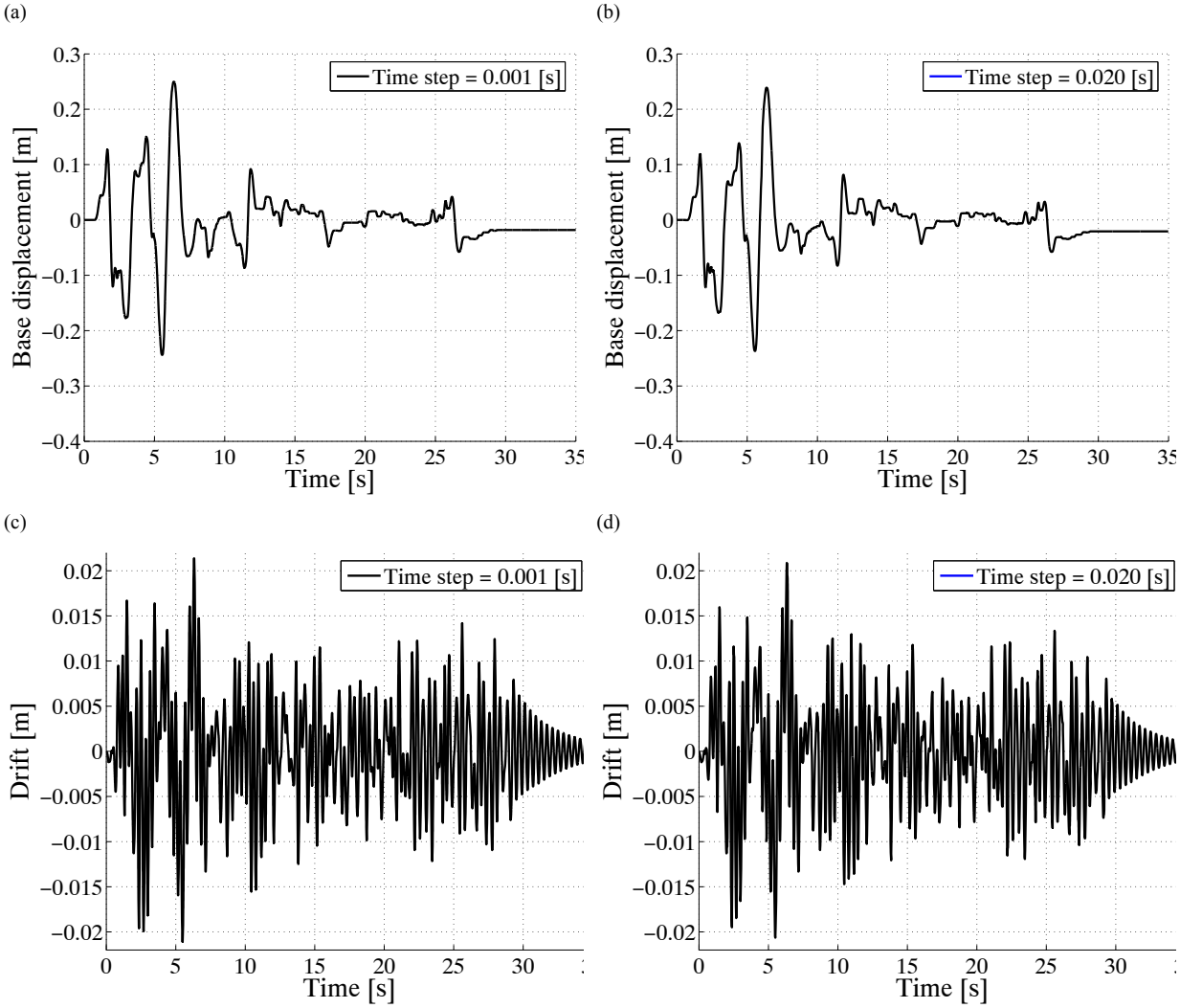

Figure 8.26 Two degree-of-freedom model analyzed with coarse and fine time steps: (a) and (b) base relative displacement with time steps of 0.001 and 0.02 s, (c) and (d) drift with time steps of 0.001 and 0.02 s, respectively.

Table 8.2 Comparison of the base relative displacement and drift with different time stepping.

Time step [s]	**Base displacement [m]**		**Drift [m]**		**Permanent base displacement [m]**
	max	***min***	***max***	***min***	
0.02	0.239	-0.237	0.021	-0.021	-0.021
0.001	0.250	-0.244	0.021	-0.021	-0.018

8.4 General MDOF model

Modal analysis facilitates the numerical simulation of FPS isolated systems. By considering several degrees of freedom the interaction effect between the isolation block and the structure can be studied more precisely. To this end the numerical model developed in the previous chapter has been applied to model a multi degree-of-freedom system (Figure 8.27).

A consistent mass matrix has been used. The system is discretized with 12 beam elements. The first element is allocated to the isolation bearing. As soon as the bearing starts sliding it is activated. The rotation degrees-of-freedom of the first and last nodes are blocked. The discretization and the first five modes of vibration in the sticking phase are given in figure 8.27.

To guarantee the condition of orthogonality of modes, Rayleigh damping has been used. Half a percent of the critical damping has been considered for the first and second modes of vibration in both sticking and sliding phases.

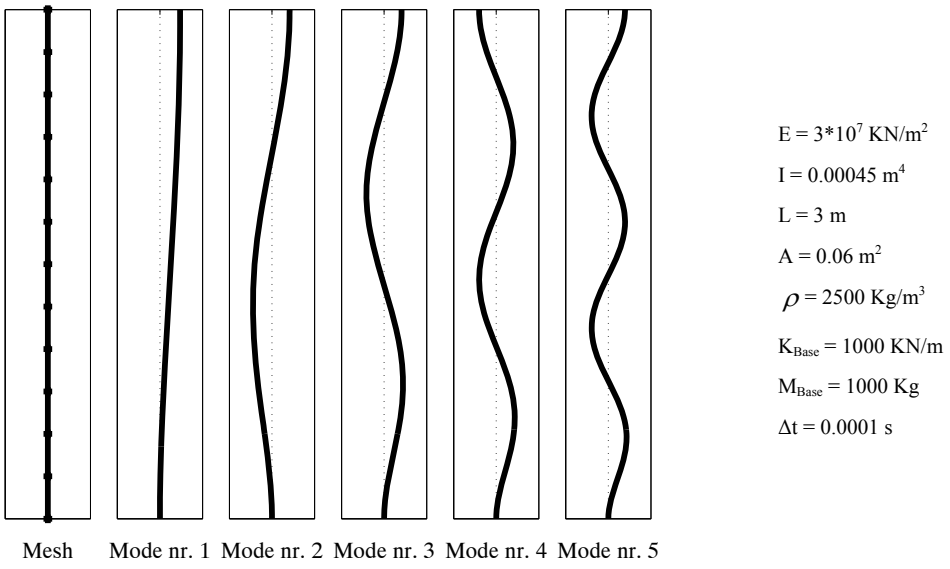

Figure 8.27 First five modes of vibration in the sticking phase.

Δt is taken to be 10^{-4} seconds, which is fine enough to capture the response of all modes of vibration that have been taken into consideration. To decrease computational costs, time steps have been refined to 10^{-6} seconds in case of a phase change. In addition, instead of considering all modes of vibration, only the first five modes out of 24 ones, which have larger participation factors, are considered. The response of such a system to forced triangular ground excitations is simulated (Figures 8.14 and 8.28-30).

Sticking of the sliding bearing produces a shock in the structure (Figure 8.28.a at 0.45 and 0.8 seconds). For sensitive structures and equipments, this can be damaging. The shock can be reduced by adding a damping source to the isolator.

To examine the efficiency of the refining process, results of the previous analysis are compared with those computed with a coarser time digitization and without any refining process (Figure 8.31). The refining process decreases computational costs of the simulation drastically (about 100 times) and saves the accuracy of simulation even in comparison with an analysis with much smaller time steps (Figure 8.32).

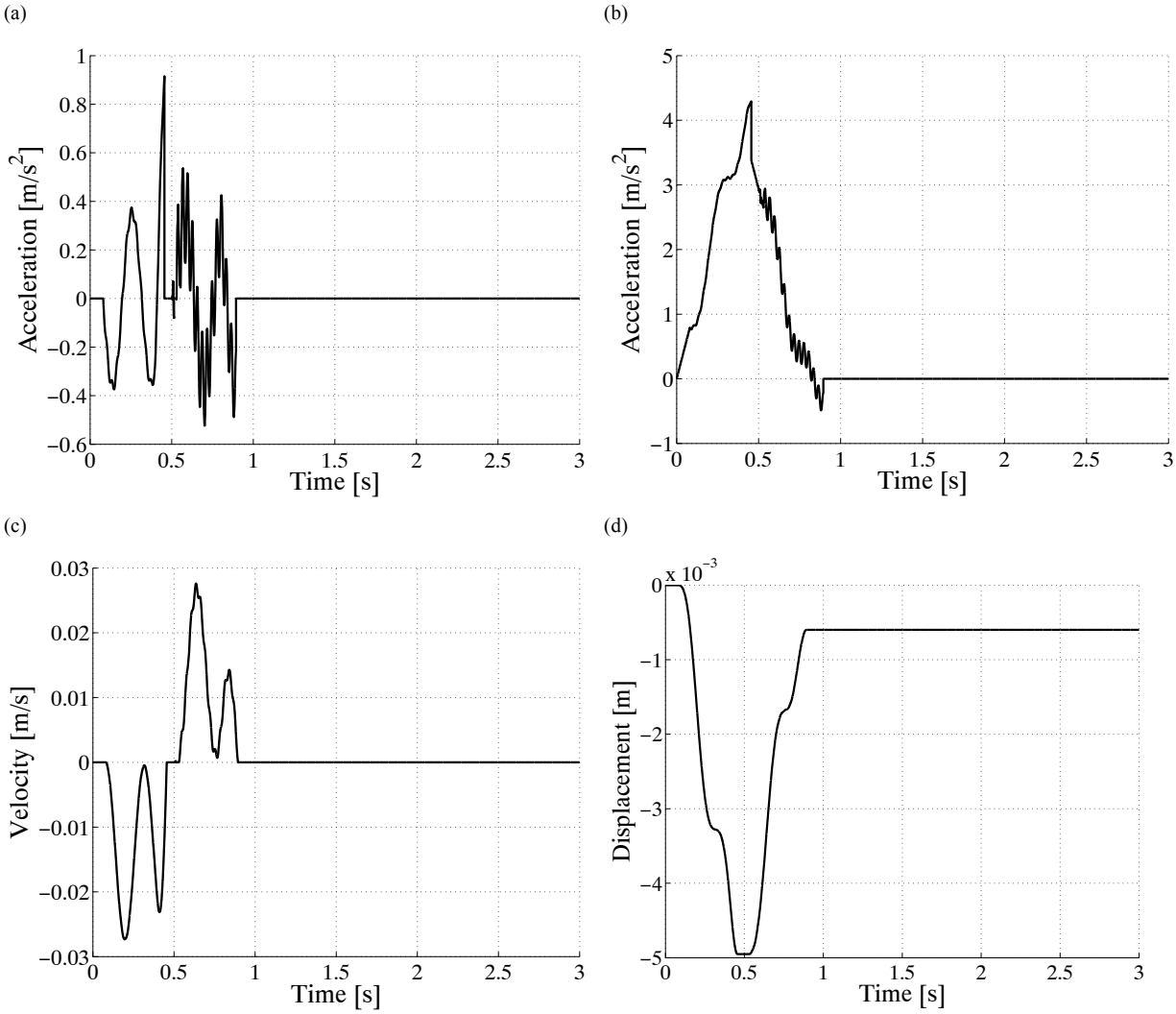

Figure 8.28 Response of the sliding bearing to a triangular loading: (a) relative acceleration, (b) absolute acceleration, (c) relative velocity, and (d) displacement.

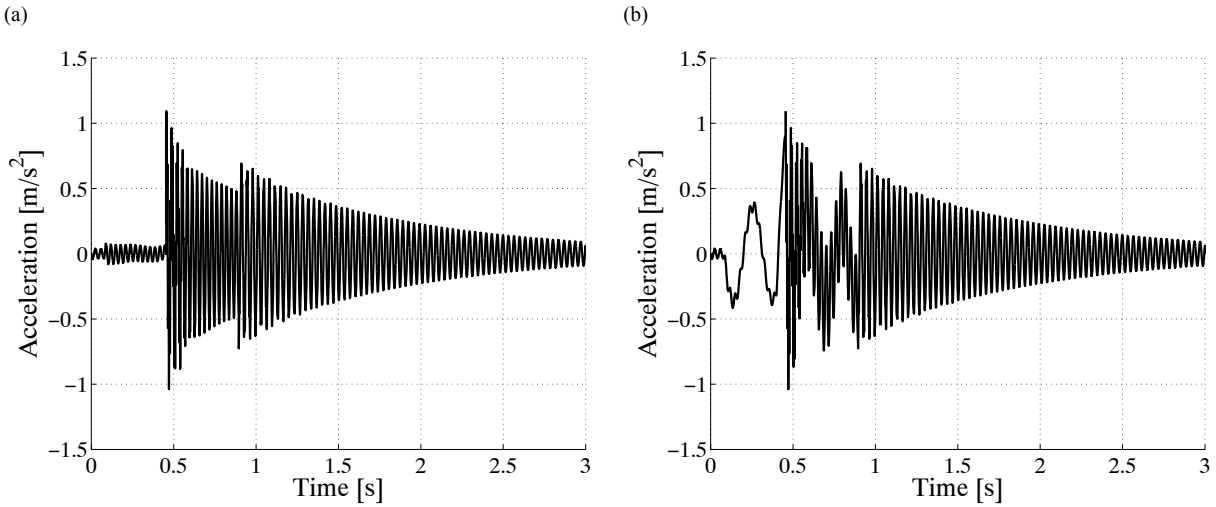

Figure 8.29 Response of an isolated M-DOF system at its mid height: (a) relative acceleration, (b) absolute acceleration, (c) displacement, and (d) rotation.

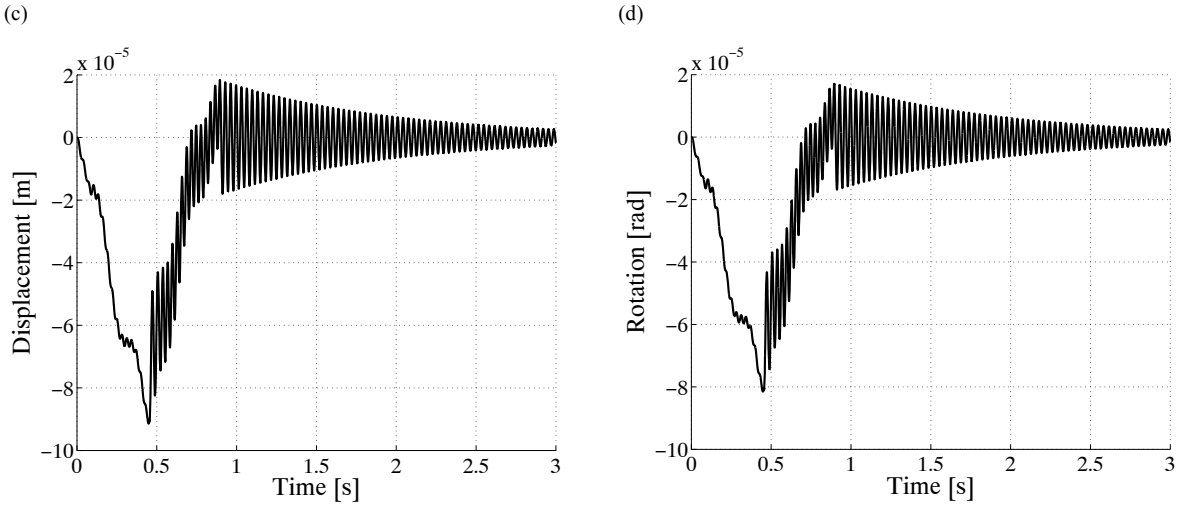

Figure 8.29 Response of an isolated M-DOF system at its mid height: (a) relative acceleration, (b) absolute acceleration, (c) displacement, and (d) rotation.

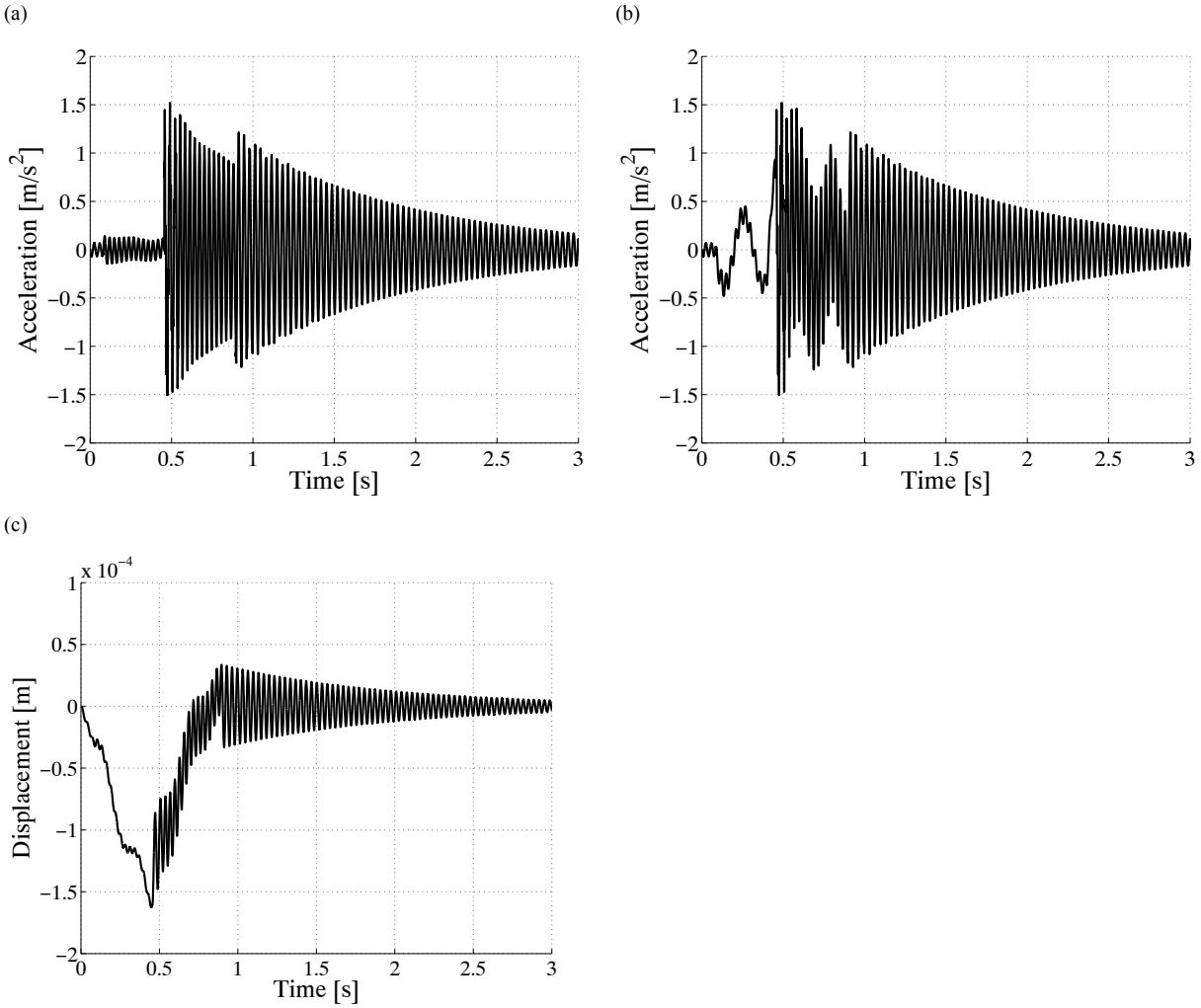

Figure 8.30 Response of the system at its top: (a) relative acceleration, (b) absolute acceleration, (c) displacement.

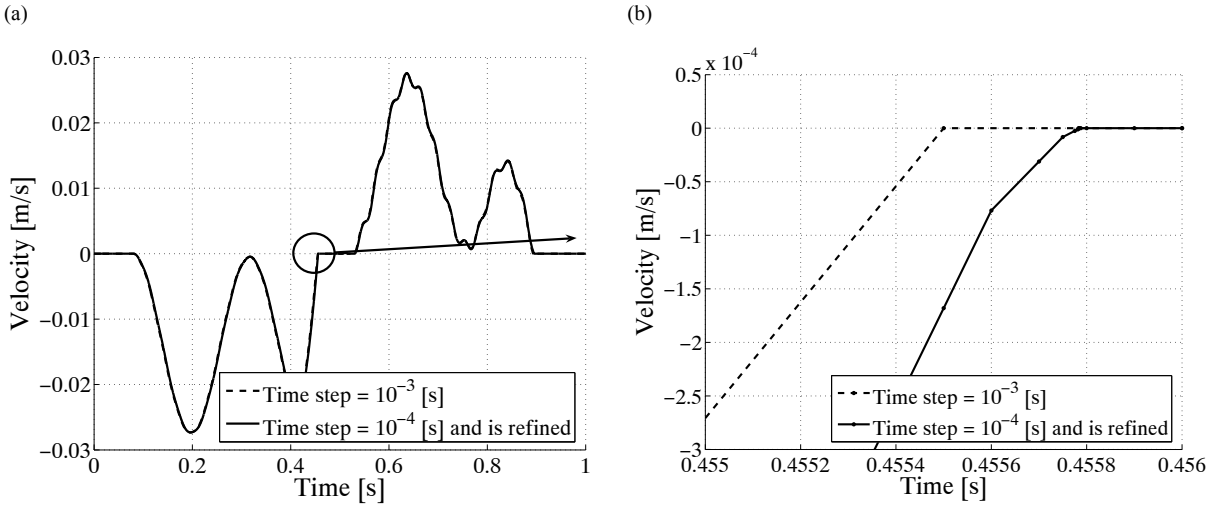

Figure 8.31 Sliding displacement of the FPS bearing computed with coarse time steps in comparison with the one computed with the time refining process: (a) the whole response, and (b) the response near a phase change.

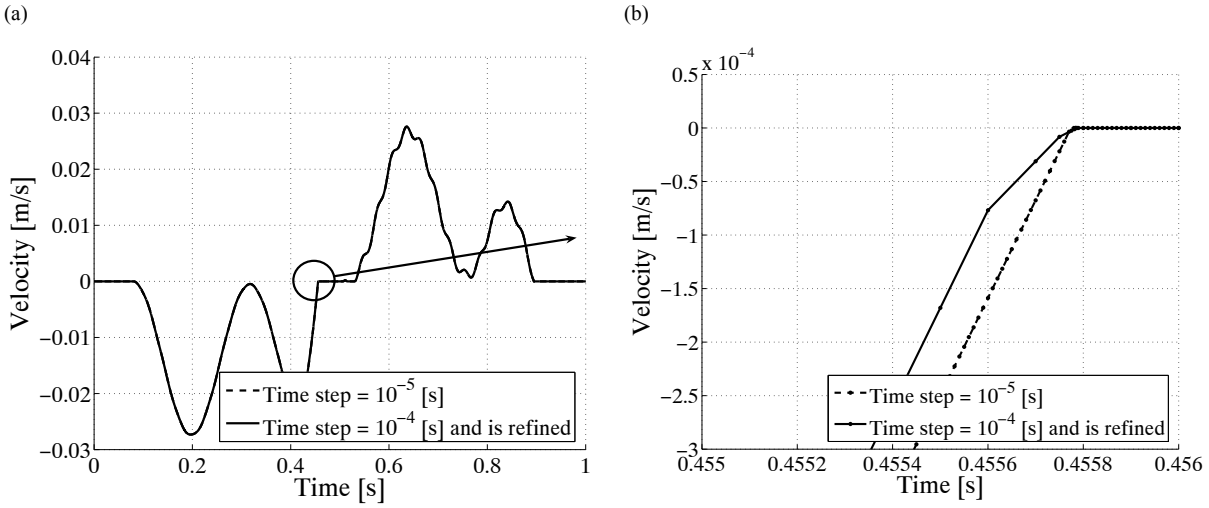

Figure 8.32 Sliding displacement of the FPS bearing computed with very fine time steps in comparison with those computed with larger time steps with a time refining process (a) the whole response, and (b) the response near a phase change.

By performing modal analysis it is possible to consider only a few of the modes of vibration without risking the accuracy of the entire simulation. Because of the physical nature of isolated systems the first few modes of vibration construct the main part of the response (Chapter 5). The same system presented before is simulated considering all of its eigenmodes. The result is compared with the case, in which only the first three modes of vibration are considered. With a good precision relative displacements and base shear force match the results of the analysis done considering all modes of vibration. Structural accelerations, in contrary to them, are in some small details different (Figure 8.33). The difference is negligible.

Simulating such an isolated system with more eigenshapes with a constant time step (Δt) does not necessarily yield a more accurate response, as higher modes of vibration have smaller periods. To catch their response, the time step must be at least one order shorter than the period of vibration of the highest mode that is taken into consideration. In this way the numerical cost of the simulation increases exponentially, as not only the transformation into the modal space and back to the original space become much more time-consuming, but also

the number of time steps increases rapidly. Hence, it is logical to take only modes with large participation factors and to perform the analysis with a reasonably small time step.

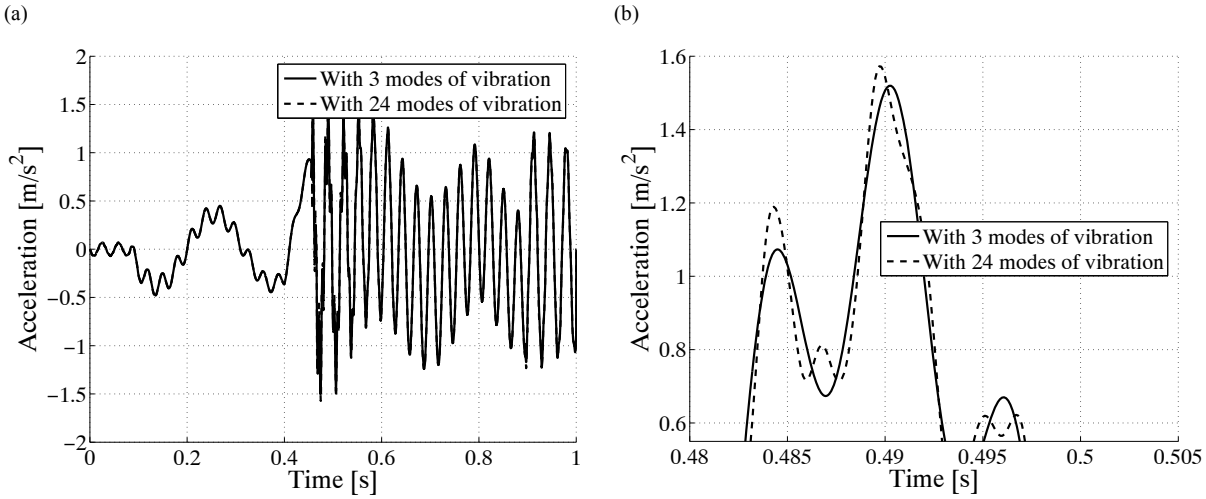

Figure 8.33 Top structural acceleration computed with modal analysis considering all degrees of freedom in comparison with an analysis taking just the first 3 modes of vibration: (a) the whole response, and (b) the response around a peak.

Many experimental studies on the friction coefficient of sliding surfaces coated with a Teflon layer over stainless steel plates have shown a big difference with the prediction of the Coulomb friction model. [Mocha et al. and Constantinou et al., 1990]. It has been observed that the friction coefficient rises as the sliding velocity increases. To take this issue into consideration the modified Coulomb friction model has been used instead of the classical Coulomb friction model (Section 4.3):

$$\mu_s = f_{\max} - (f_{\max} - f_{\min})\, e^{-\beta \dot{u}} \tag{8.2}$$

in which maximum and minimum friction coefficients are taken to be 0.095 and 0.06, respectively. β is reported to be 43.3 [s/m] for bearings coated with *Techmet-B* material sliding on stainless steel plates (Figure 8.34) [Mokha et al., 1990].

The same system introduced before is simulated considering the modified Coulomb friction model and the results are compared with the previous results. In case of a constant friction force μ is considered to be 0.06 (Figure 8.35). The case simulated with the modified Coulomb friction model has resulted in less sliding velocity and displacement. It is because of larger friction and restoring forces in comparison to the case of constant friction force (Figures 8.35.c and d). It shows how susceptible a sliding-isolated structure is to changes of the friction force.

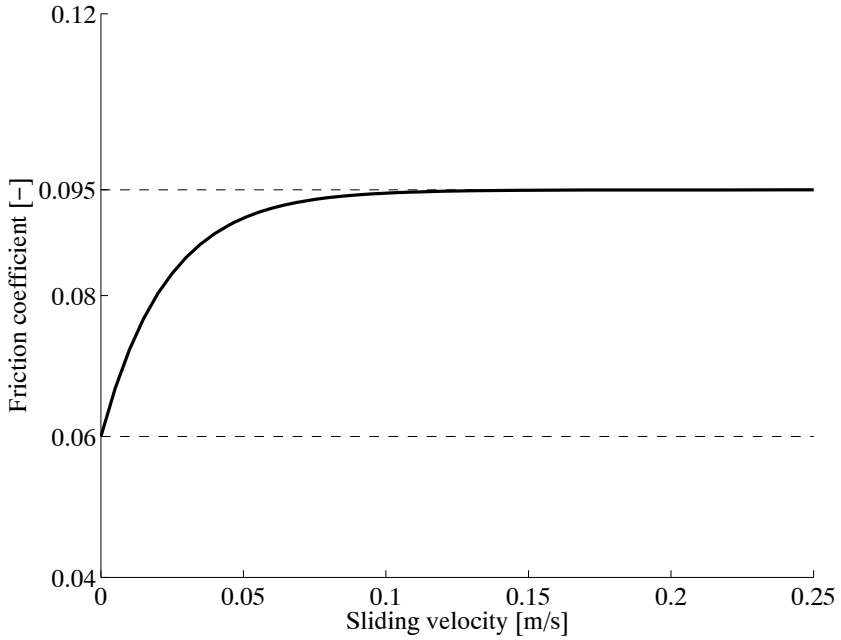

Figure 8.34 Friction coefficient based on the modified Coulomb model.

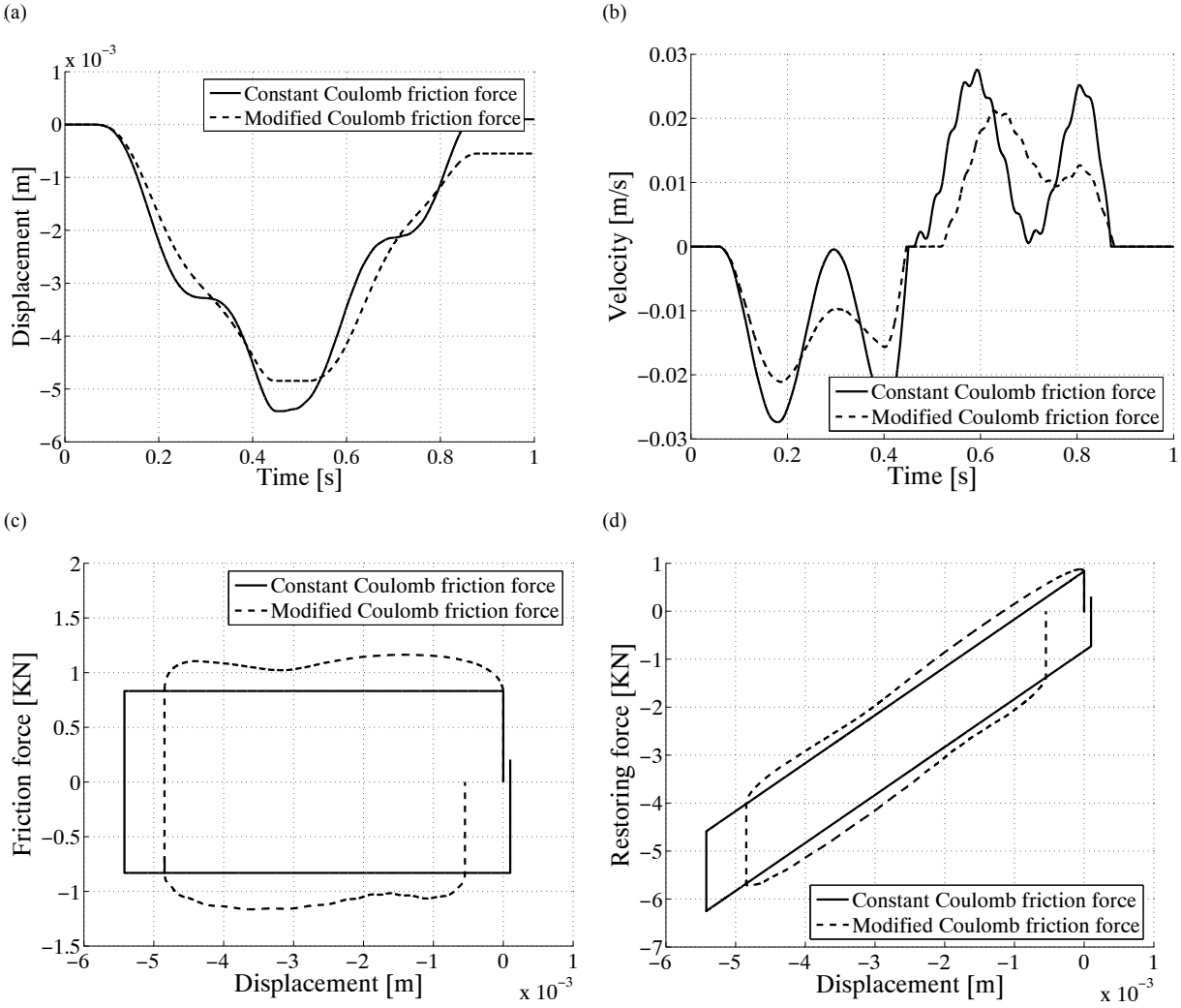

Figure 8.35 Comparison of the response of the set simulated with constant and modified Coulomb models: (a) relative displacement of the bearing, (b) relative sliding velocity, (c) friction force, and (d) restoring force.

8.5 Simulation of a shaking table test with general MDOF model

To evaluate the numerical model an experiment done on a shaking table is simulated with this model [Mokha et al., 1990]. The experiment was carried out with a model representing a section in the weak direction of a typical steel moment-resisting frame at a quarter scale (Figure 8.36). The model is a six-story structure with three bays. The weight distribution is approximately as follows: 34.1 KN at the sixth floor, 34.9 KN at the fifth to first floors, and 20.3 KN at the base. Columns are bolted to two heavy W14 x 90 sections (rotation degrees of freedom are blocked in this simulation). Bearings are placed between these beams and the shaking table.

A planar numerical model has been used to simulate the response of model building. The set has been simulated with beam elements. There are 13 degrees of freedom. The first seven mode shapes has been considered. Time step is taken to be one millisecond and in case of possibility of a phase change, it is refined to 10^{-6} seconds.

Natural frequencies of vibration under fixed-base condition are compared with those computed in the simulation (Table 8.3). They are in good agreement with each other. For higher modes of vibration some discrepancies can be seen. They are mainly because of the simple discretization applied here.

Half a percent damping ratio as before has been taken for the first and second modes of vibration for both sticking and sliding phases.

The structure is isolated through four FPS bearings. Each bearing consists of an articulated slider on a polished concave surface with a radius of curvature equal to 248 mm (Figure 8.37). The period of vibration is one second (Equation 6.2). The period of vibration of the prototype is 2 seconds because of four to one length scaling. The slider is coated with a material, Techmet-B, with a low friction coefficient similar to Teflon (Figure 8.34).

The response of the aforementioned system to six strong earthquakes is studied (Table 8.4 and Figure 8.38). The bearing displacement, the drift at the top of the structure (sixth floor), base shear, and structural shear (measured at its first floor) are four main outputs of the analysis. Base and structural shear forces are normalized by the total weight of the structure including its base weight (229.2 KN).

Results of the simulations are then compared with those reported elsewhere (Tables 8.5 and 8.6) [Mokha et al., 1990].

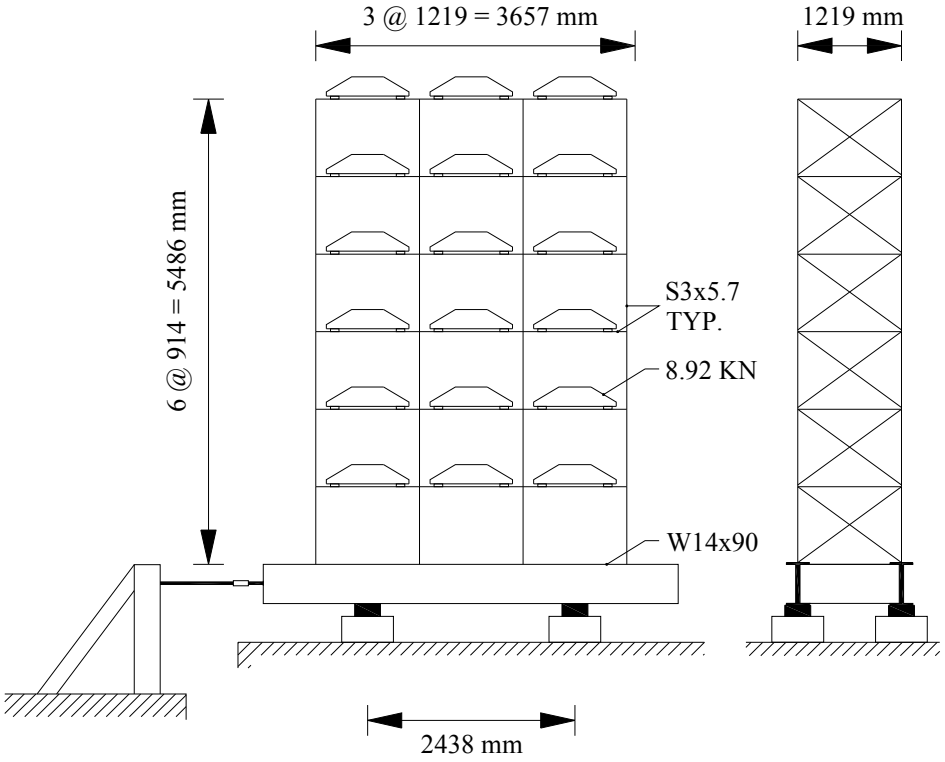

Figure 8.36 Six-story steel test structure [Mokha et al., 1990].

Table 8.3 Eigenfrequencies of modes of vibration.

Frequency [Hz]		**Mode 1**	**Mode 2**	**Mode 3**	**Mode 4**	**Mode 5**	**Mode 6**
Experiment (fixed)		2.34	7.76	13.28	19.04	24.80	28.92
Simulation	**Fixed**	2.37	7.47	13.47	20.70	28.58	32.55
	isolated	1.03	5.31	9.87	14.57	21.17	28.78

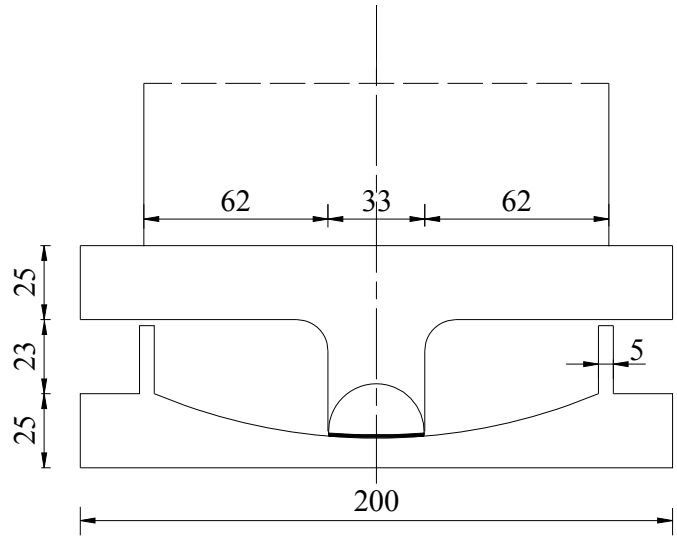

Figure 8.37 FPS bearing design (all dimensions are in mm) for the model structure [Mokha et al., 1990].

Table 8.4 Earthquake motions used in the analysis.

Excitation	Record	Peak ground accel. [*g*]	Duration [s]	Magnitude
El Centro	USA, Imperial Valley, May 18, 1940 S00E	0.36	60	6.7
Pacoima	USA, San Fernando, Feb., 9, 1971 S74W	0.92	60	6.4
Pacoima	USA, San Fernando, Feb., 9, 1971 S16E	1.17	30	6.4
Manjil	Iran, Manjil, June, 20, 1990	0.94	60	7.7
Kobe	Japan, Kobe, Jan., 17, 1995	0.34	50	7.3
Bam	Iran, Bam Dec., 26, 2003	0.79	60	6.5

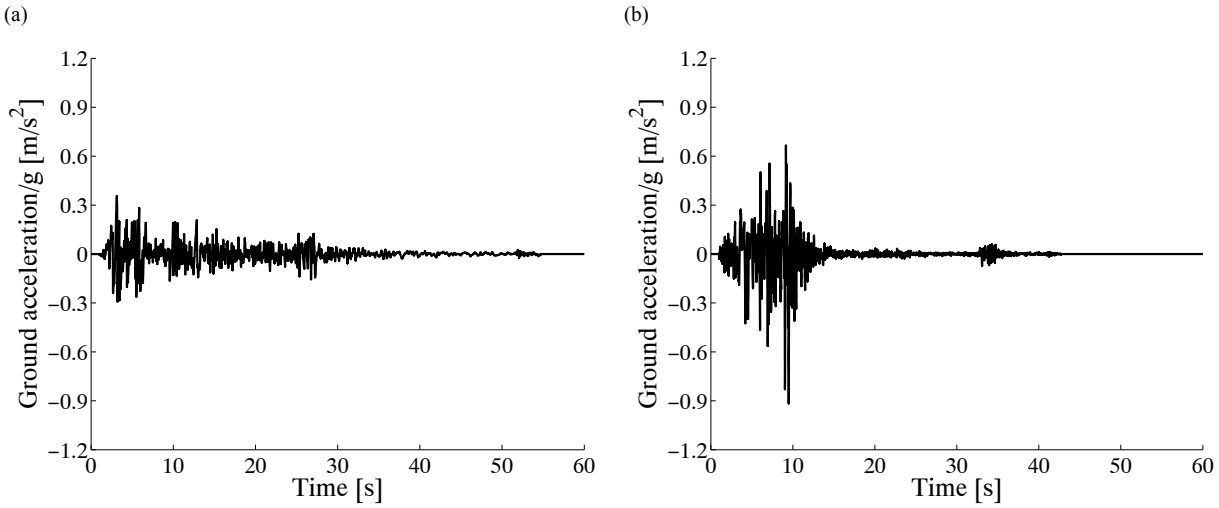

Figure 8.38 Time histories of the ground acceleration of: (a) El Centro, (b) Pacoima S74W component, (c) Pacoima S16E component, (d) Manjil, (e) Kobe, and (f) Bam earthquakes.

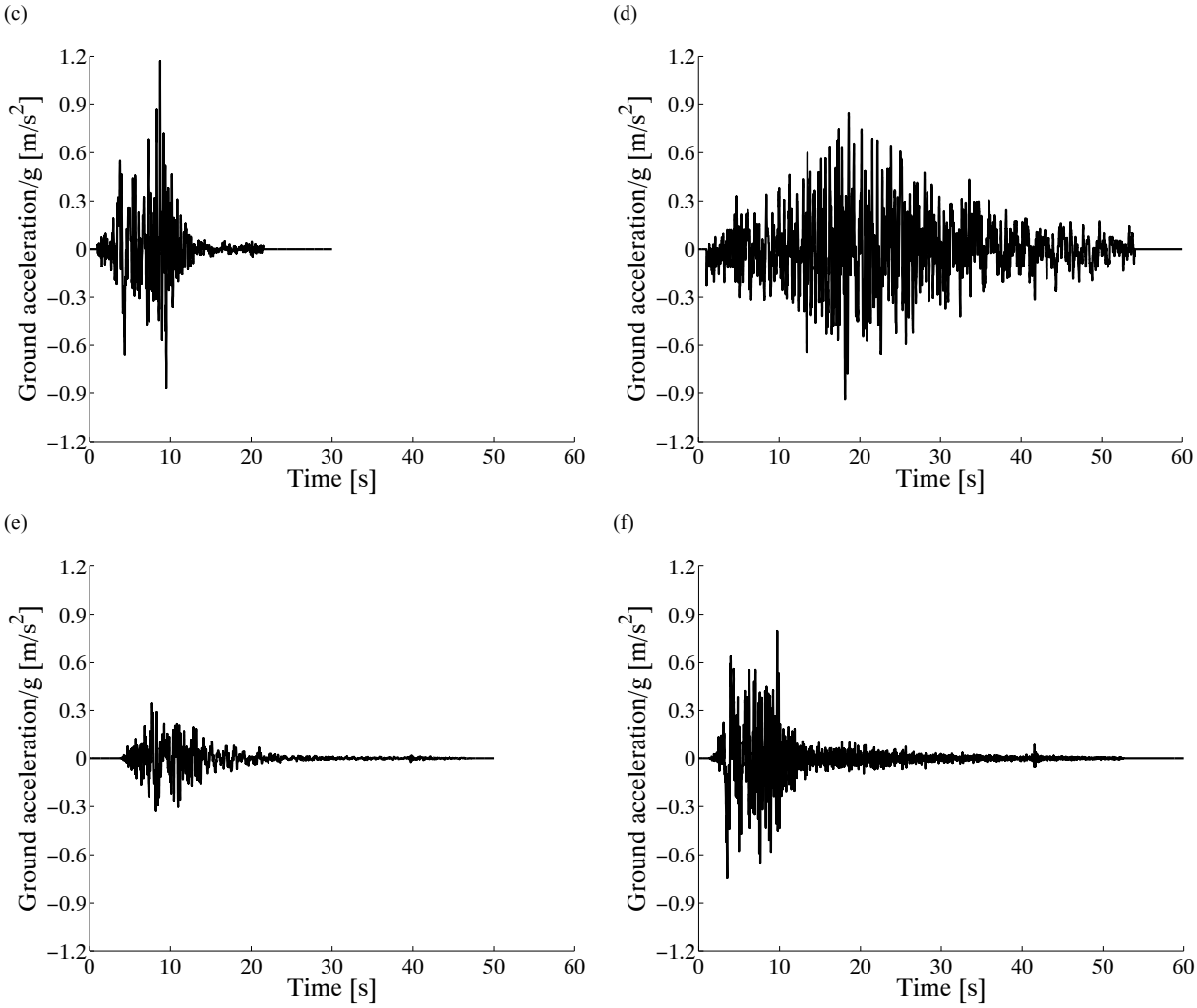

Figure 8.38 Time histories of the ground acceleration of: (a) El Centro, (b) Pacoima S74W component, (c) Pacoima S16E component, (d) Manjil, (e) Kobe, and (f) Bam earthquakes.

The first analysis is done with the El Centro earthquake with a maximum ground acceleration of 3.5 m/s^2 (0.357 *g*). To be consistent with the four to one length scaling, time axis is scaled by a factor of two (Figures 8.38 and 8.39). Drift at the top of the structure in the isolated system is three times smaller than the one in the fixed-base structure (Figure 8.39 and 8.40). Maximum base and structural shear are both less than 15% of the total structural weight. In the fixed-base structure, however, structural shear is more than 65% of the total weight. Results of the sliding displacement, base shear, and permanent sliding displacement are in good agreement with the results reported by [Mokha et al., 1990]. Unlike them, the drift in the structural system has not been anticipated exactly. It can be explained by the fact of lack of information about properties of the structural system.

Second and third analyses are done with Pacoima earthquake S74W and S16E (50% of the original magnitude) components with a maximum ground acceleration of 9.03 and 5.74 m/s^2 (0.92 and 0.58 *g*), respectively (Figures 8.38 and 8.41-44). As a result of stronger ground excitations in comparison to El Centro earthquake the maximum sliding displacements are in these analyses larger. In spite of that, base and structural shear remain almost in the same range as before.

Table 8.5 Summary of the results based on the developed numerical model.

Excitation	Isolation condition	Sliding displ. [mm]	Base (struct.*) shear over weight [-]	Drift** [mm]	Permanent displ. [mm]
El Centro S00E (100%)	Isolated	9.4	0.12	2.8	0.2
	Fixed-base	-	0.67	14.5	-
Pacoima S74W (100%)	Isolated	25.6	0.19	4.3	0.5
	Fixed-base	-	0.76	16.0	-
Pacoima S16E (50%)	Isolated	29.1	0.20	4.6	1.6
	Fixed-base	-	0.54	11.6	-
Manjil (100%)	Isolated	9.1	0.46	8.4	0.7
	Fixed-base	-	2.15	45.9	-
Kobe (100%)	Isolated	16.0	0.15	2.8	0.0
	Fixed-base	-	0.61	13.1	-
Bam (100%)	Isolated	9.9	0.50	9.3	0.1
	Fixed-base	-	0.97	20.8	-

* Base shear if the structure is isolated, otherwise structural shear.

** The maximum interstory drift in the structure

Table 8.6 Summary of the experimental results [Mokha et al., 1990].

Excitation	Isolation condition	Sliding displ. [mm]	Base shear over weight [-]	Drift [mm]	Permanent displ. [mm]
El Centro S00E (100%)	Isolated	10.0	0.13	3.0	0.3
Pacoima S74W (100%)	Isolated	35.6	0.20	4.2	0.5
Pacoima S16E (50%)	Isolated	28.2	0.20	4.4	0.9

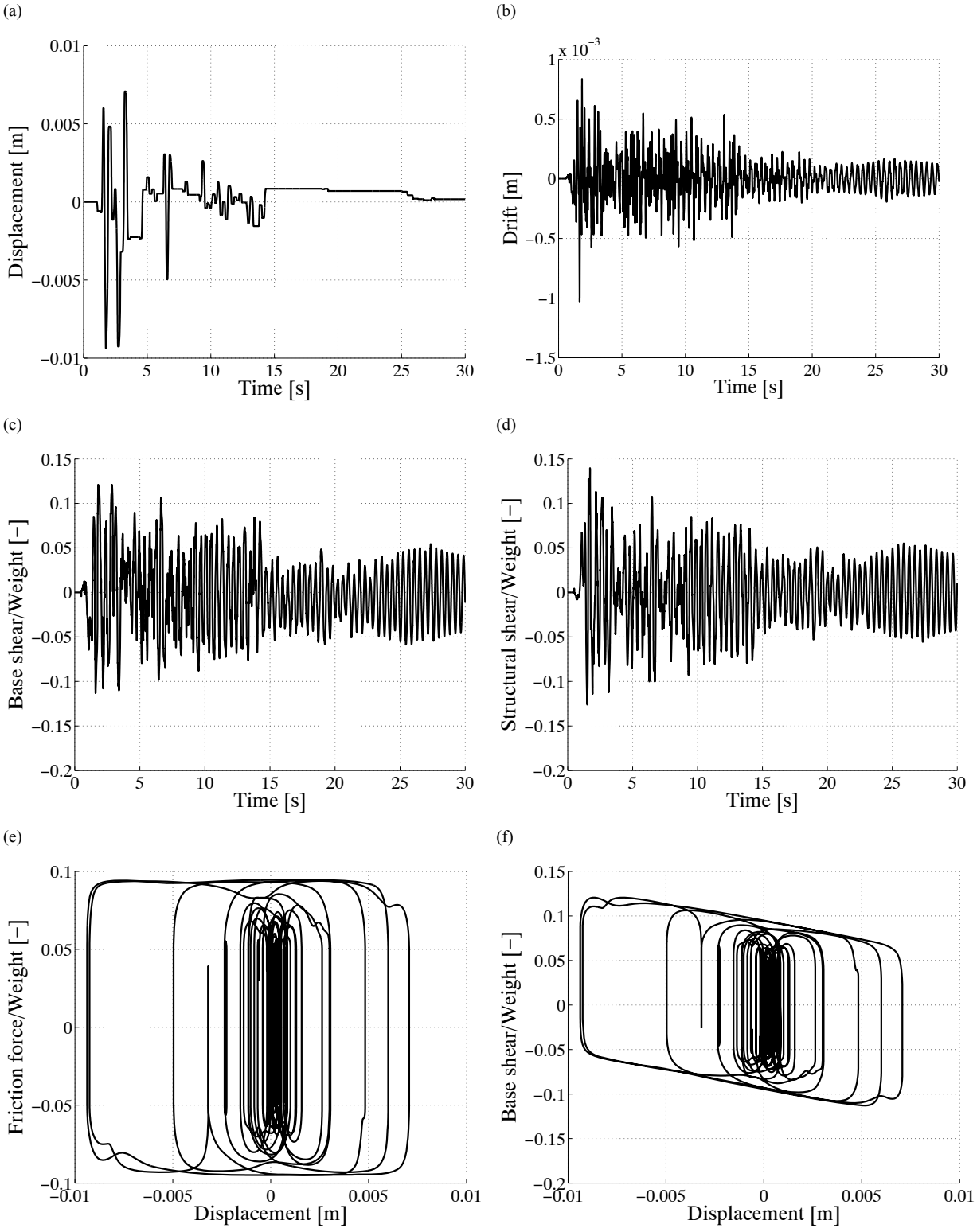

Figure 8.39 Structural response to El Centro earthquake: (a) base (bearing) displacement, (b) drift at the top of the structure (sixth floor), (c) base shear, (d) structural shear (measured at its first floor), (e) Friction force, and (f) restoring force versus sliding displacement.

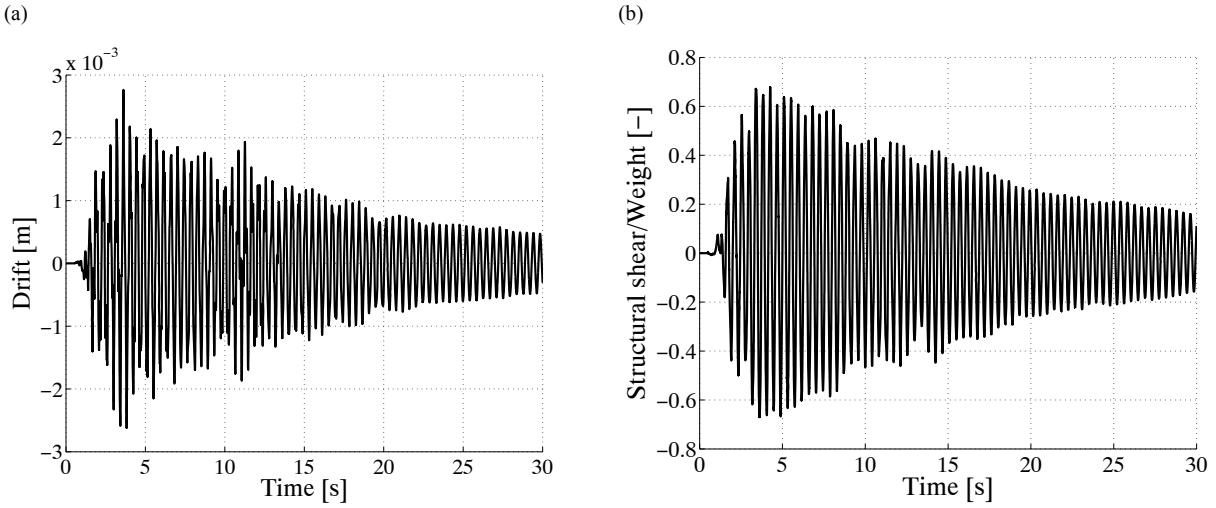

Figure 8.40 Structural response of the fixed-base structure to El Centro earthquake: (a) drift at the top of the structure (sixth floor), and (b) structural shear (measured at its first floor).

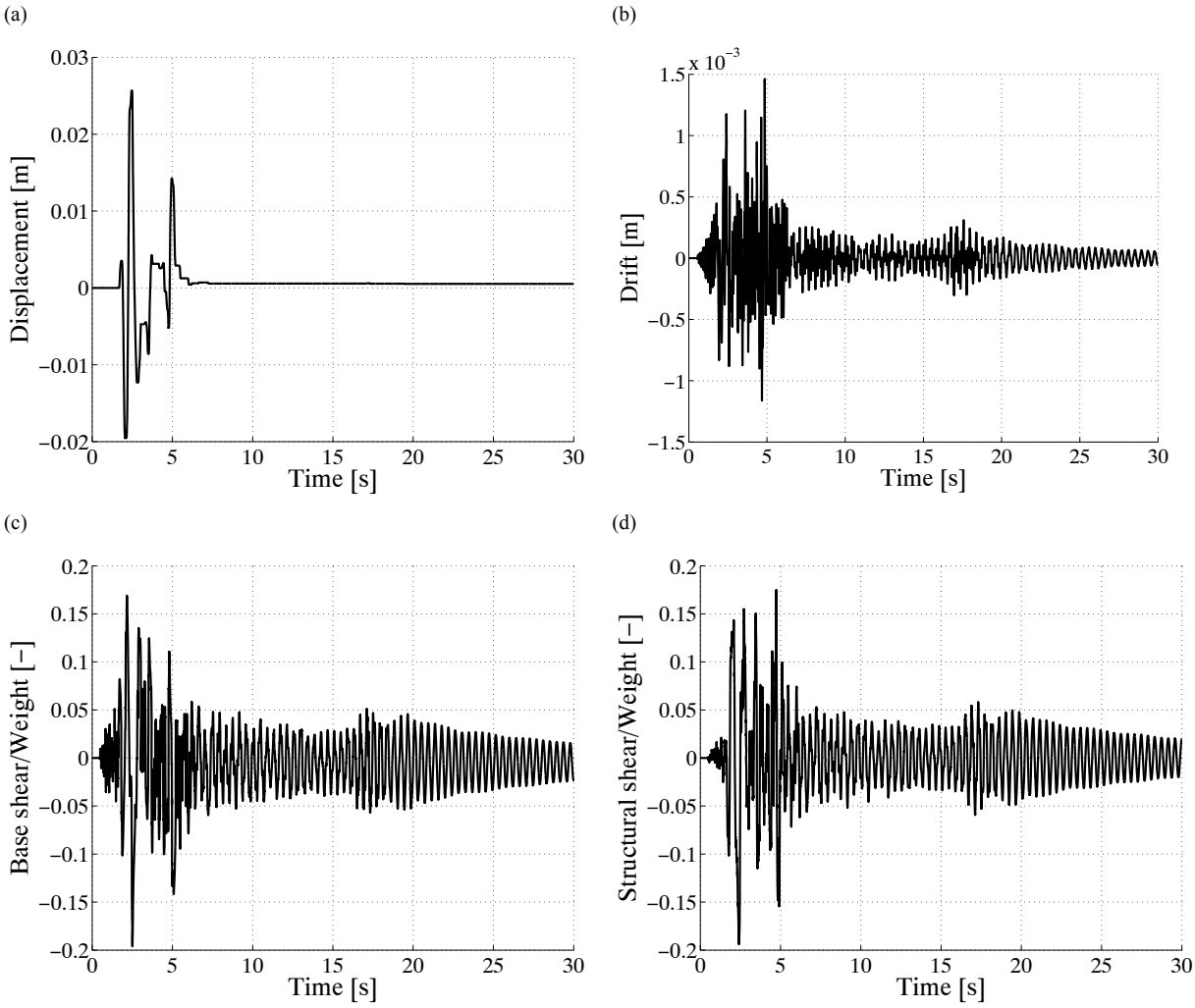

Figure 8.41 Structural response to Pacoima earthquake S74W component (a) base (bearing) displacement, (b) drift at the top of the structure (sixth floor), (c) base shear, (d) structural shear (measured at its first floor), (e) Friction force, and (f) restoring force versus sliding displacement.

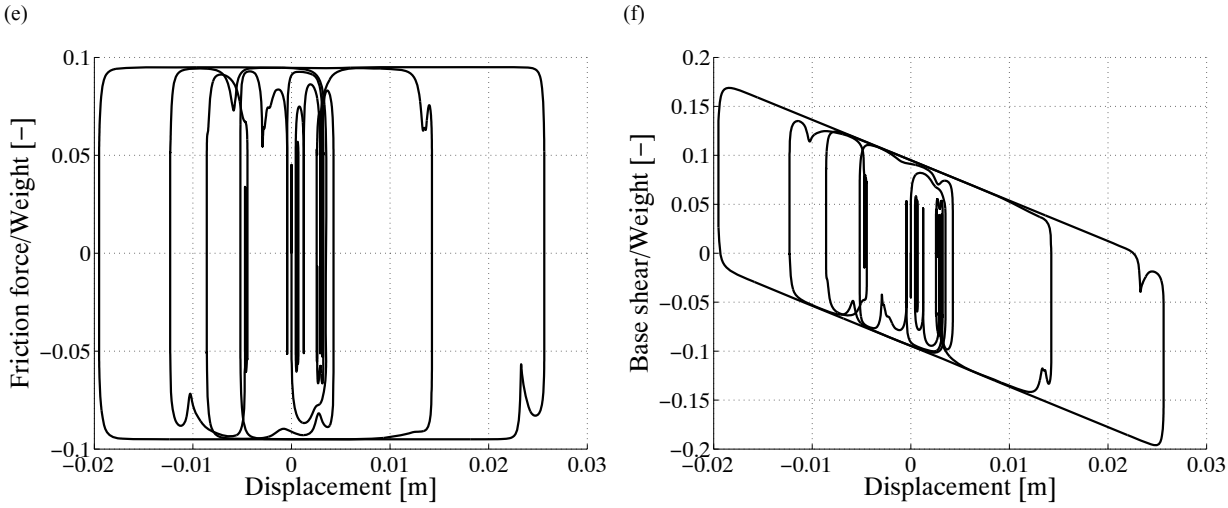

Figure 8.41 Structural response to Pacoima earthquake S74W component (a) base (bearing) displacement, (b) drift at the top of the structure (sixth floor), (c) base shear, (d) structural shear (measured at its first floor), (e) Friction force, and (f) restoring force versus sliding displacement.

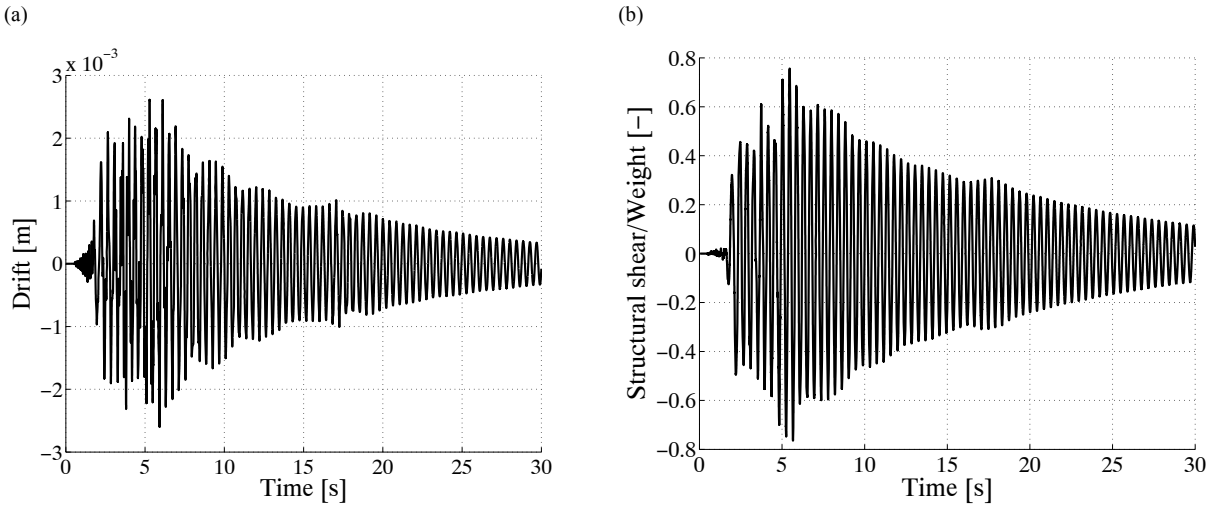

Figure 8.42 Structural response of the fixed-base structure to Pacoima earthquake S74W component: (a) drift at the top of the structure (sixth floor), and (b) structural shear (measured at its first floor).

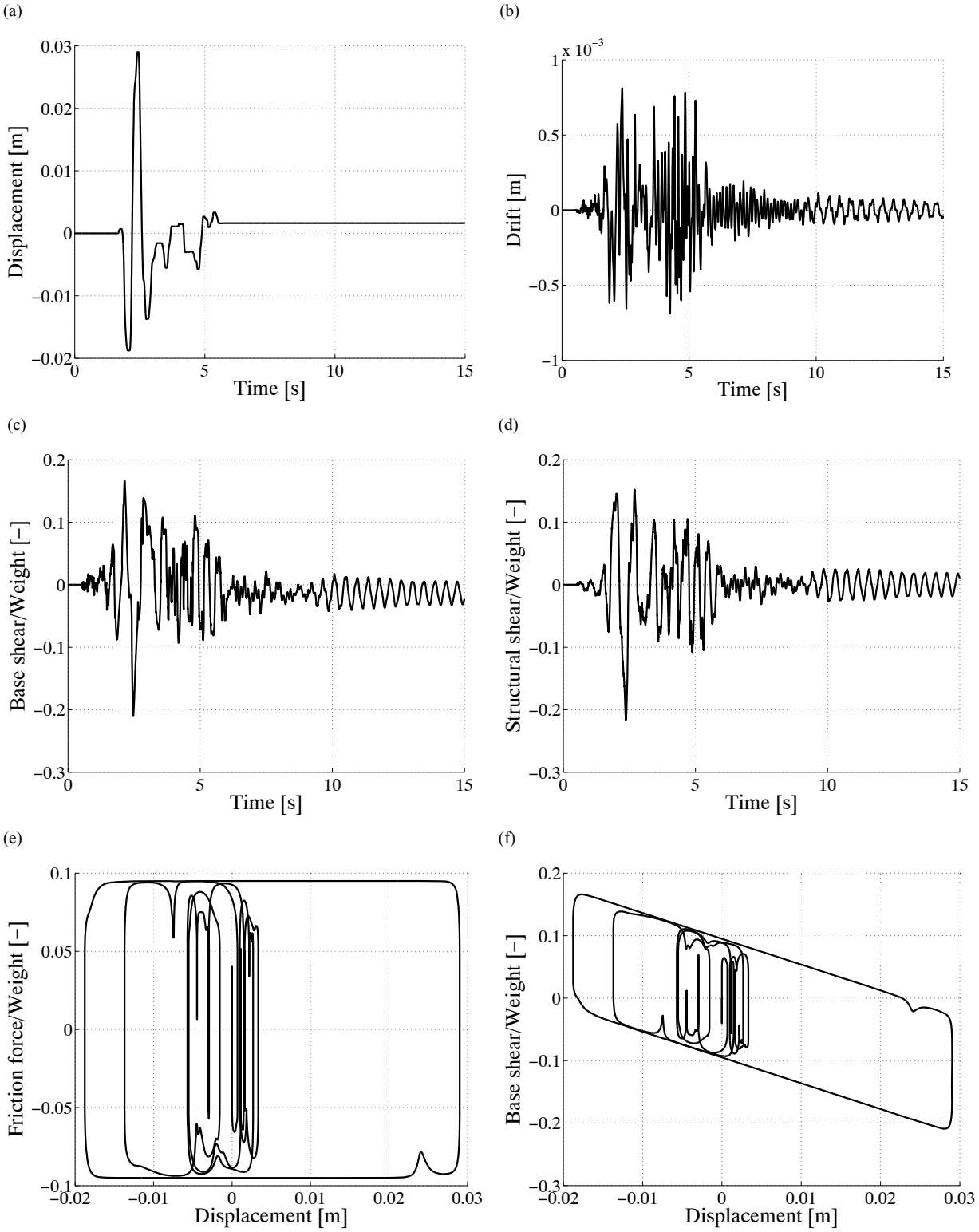

Figure 8.43 Strcutural response to Pacoima earthquake S16E component 50% (a) base (bearing) displacement, (b) drift at the top of the structure (sixth floor), (c) base shear, (d) structural shear (measured at its first floor), (e) Friction force, and (f) restoring force versus sliding displacement.

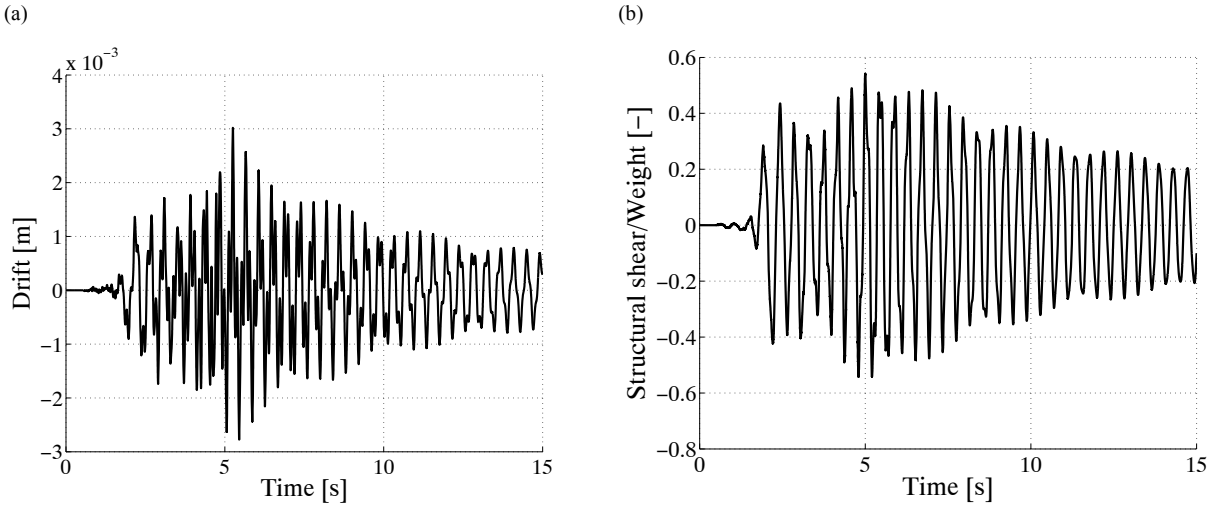

Figure 8.44 Structural response of the fixed-base structure to Pacoima earthquake S16E component 50%: (a) drift at the top of the structure (sixth floor), and (b) structural shear (measured at its first floor).

The next simulation is done with Manjil earthquake (Figures 8.45 and 8.46). Although the maximum ground acceleration is almost in the same range as the one in the analysis with Pacoima earthquake, the maximum sliding displacement and base shear are considerably larger than those computed in that analysis. It is mainly because of a larger input energy imbedded in the time history of Manjil earthquake in comparison to Pacoima earthquake (Figure 8.38). Besides, a very low frequency content of excitations, as seismic waves passed through thick layers of sedimentary soils of north of Iran, has increased the sliding displacement of the isolated structure considerably. With a higher friction coefficient and additional damping mechanism it is possible to reduce base shear and sliding displacement at the cost of a larger structural response.

The time history of the Kobe earthquake used in this analysis has a peak ground acceleration of 3.34 m/s^2 (0.34 *g*), which is almost the same as El Centro. It has a form similar to Pacoima S74W component (Figure 8.38 and Table 8.4). Both base and structural shear are less than 15% of the total weight of the structure. The same structure with a fixed foundation would experience a shear force as much as 60% of the structural weight, considering an elastic response for the structure (Figures 8.47 and 8.48).

The devastating Bam earthquake was a near source excitation with a very large maximum ground acceleration of 7.75 m/s^2 (0.79 *g*). It has a strong impulse effect on the isolated structure in a very short period of time (Figure 8.49.a). Apart from the first four seconds, the response is almost the same as the response to other motions studied here. Base isolated structures are susceptible to impulse-shape loads. An additional damping mechanism dissipates to some extent the energy and gives the system more time to react more smoothly. With a larger value of friction coefficient it is possible to restrict the maximum sliding displacement.

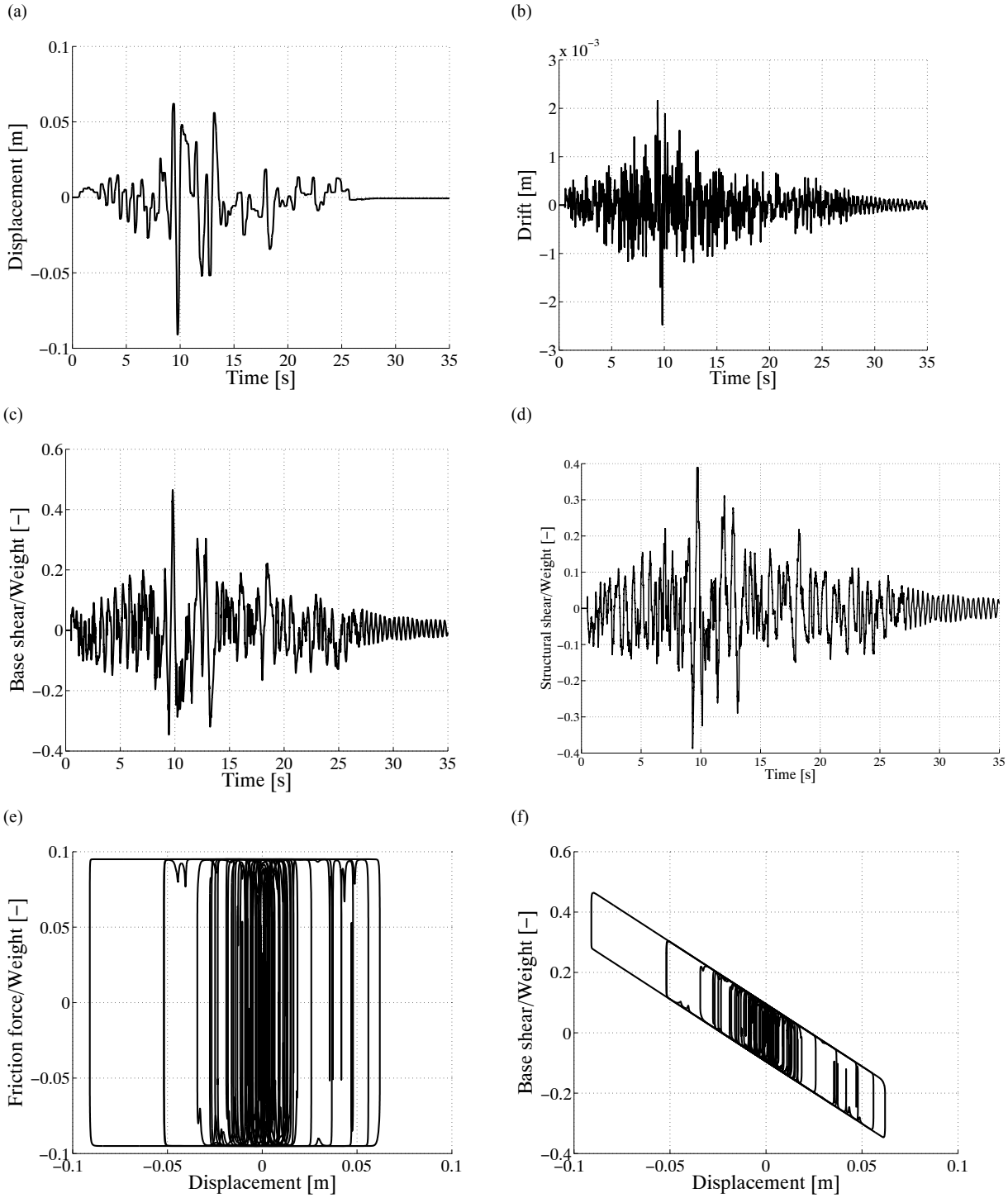

Figure 8.45 Structural response to Manjil earthquake: (a) base (bearing) displacement, (b) drift at the top of the structure (sixth floor), (c) base shear, (d) structural shear (measured at its first floor), (e) Friction force, and (f) restoring force versus sliding displacement.

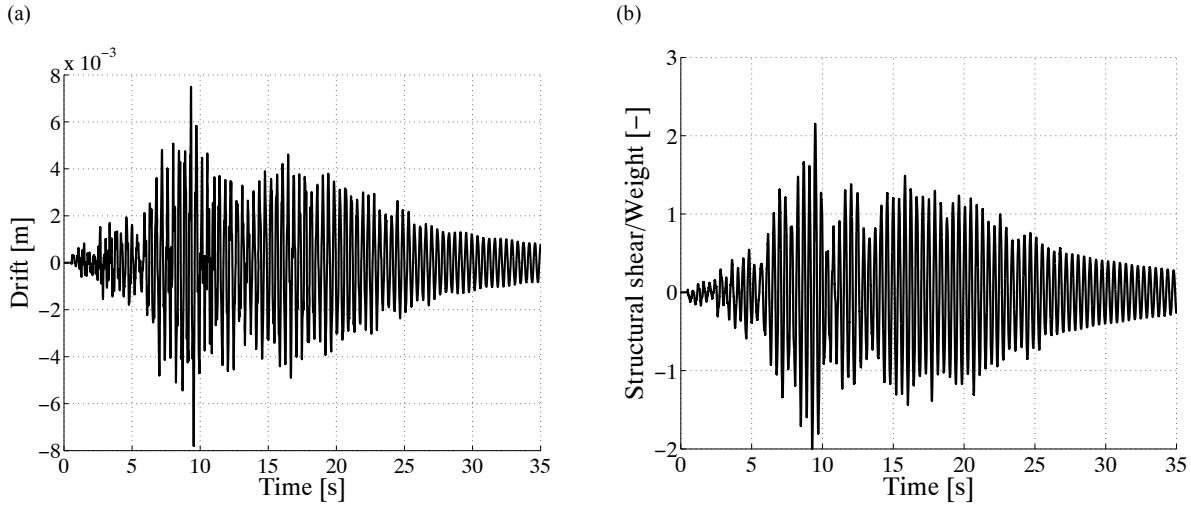

Figure 8.46 Structural response of the fixed-base structure to Manjil earthquake: (a) drift at the top of the structure (sixth floor), and (b) structural shear (measured at its first floor).

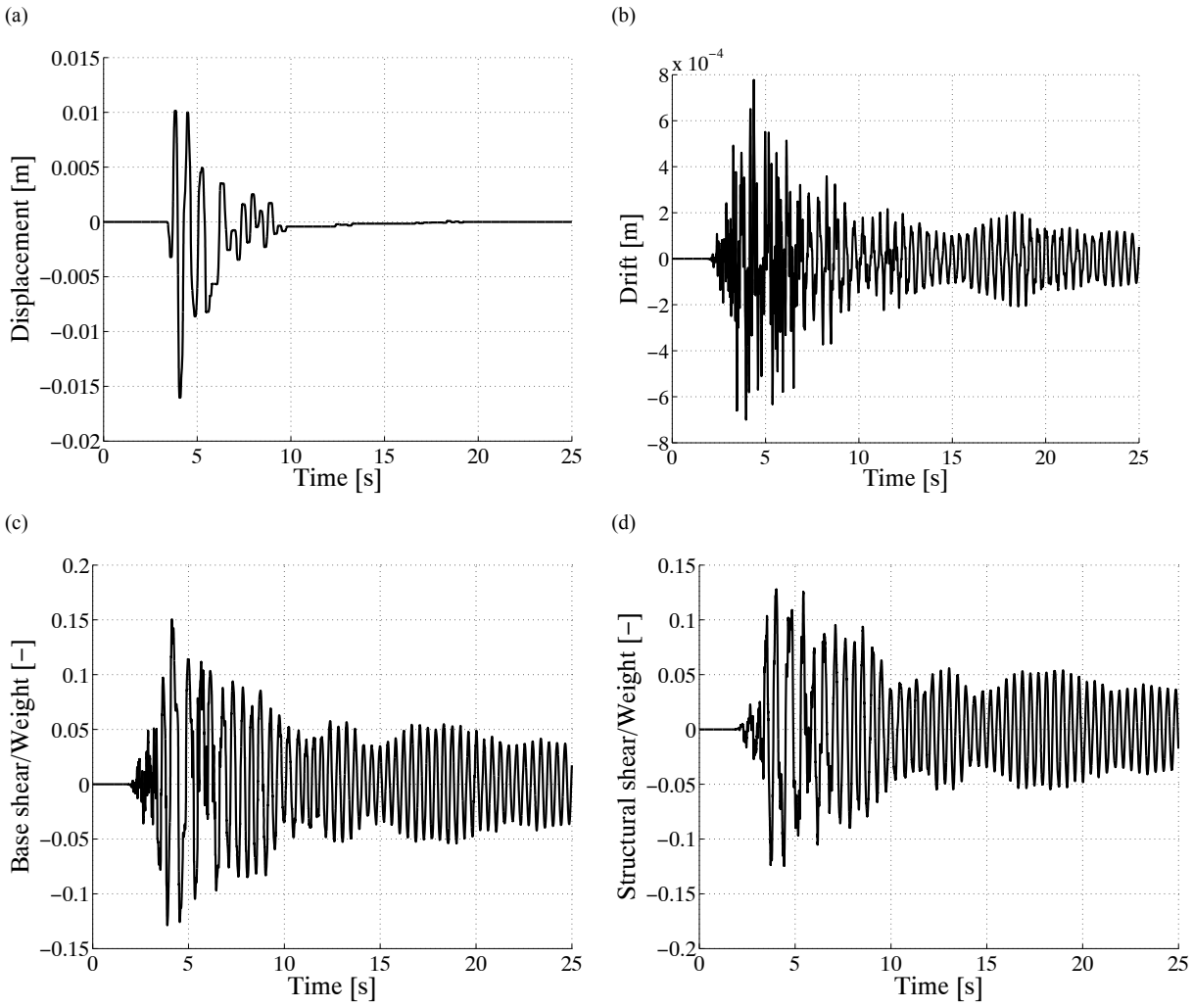

Figure 8.47 Structural response to Kobe earthquake: (a) base (bearing) displacement, (b) drift at the top of the structure (sixth floor), (c) base shear, (d) structural shear (measured at its first floor), (e) Friction force, and (f) restoring force versus sliding displacement.

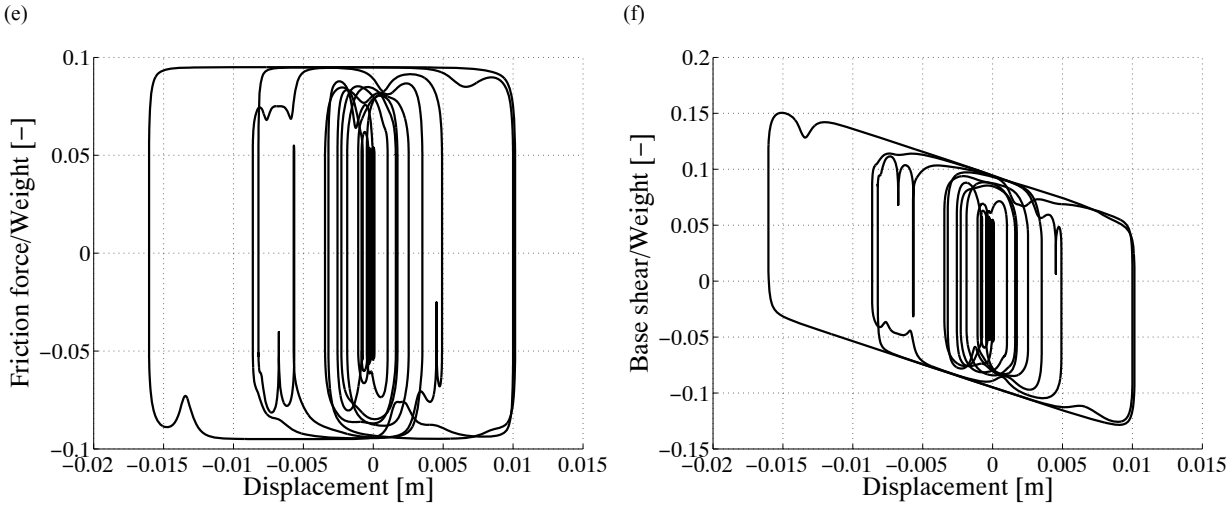

Figure 8.47 Structural response to Kobe earthquake: (a) base (bearing) displacement, (b) drift at the top of the structure (sixth floor), (c) base shear, (d) structural shear (measured at its first floor), (e) Friction force, and (f) restoring force versus sliding displacement.

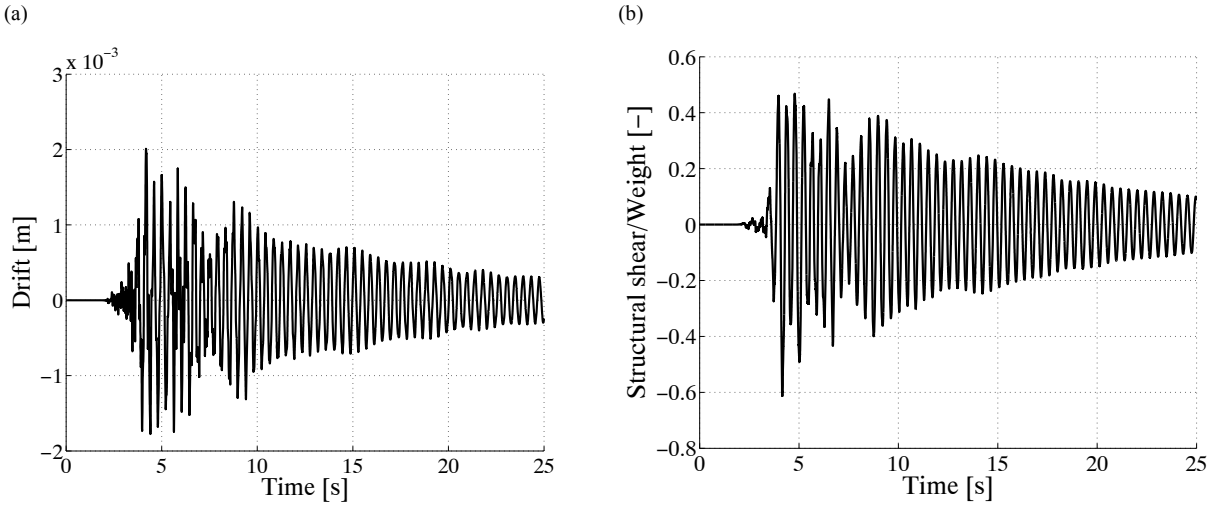

Figure 8.48 Structural response of the fixed-base structure to Kobe earthquake: (a) drift at the top of the structure (sixth floor), and (b) structural shear (measured at its first floor).

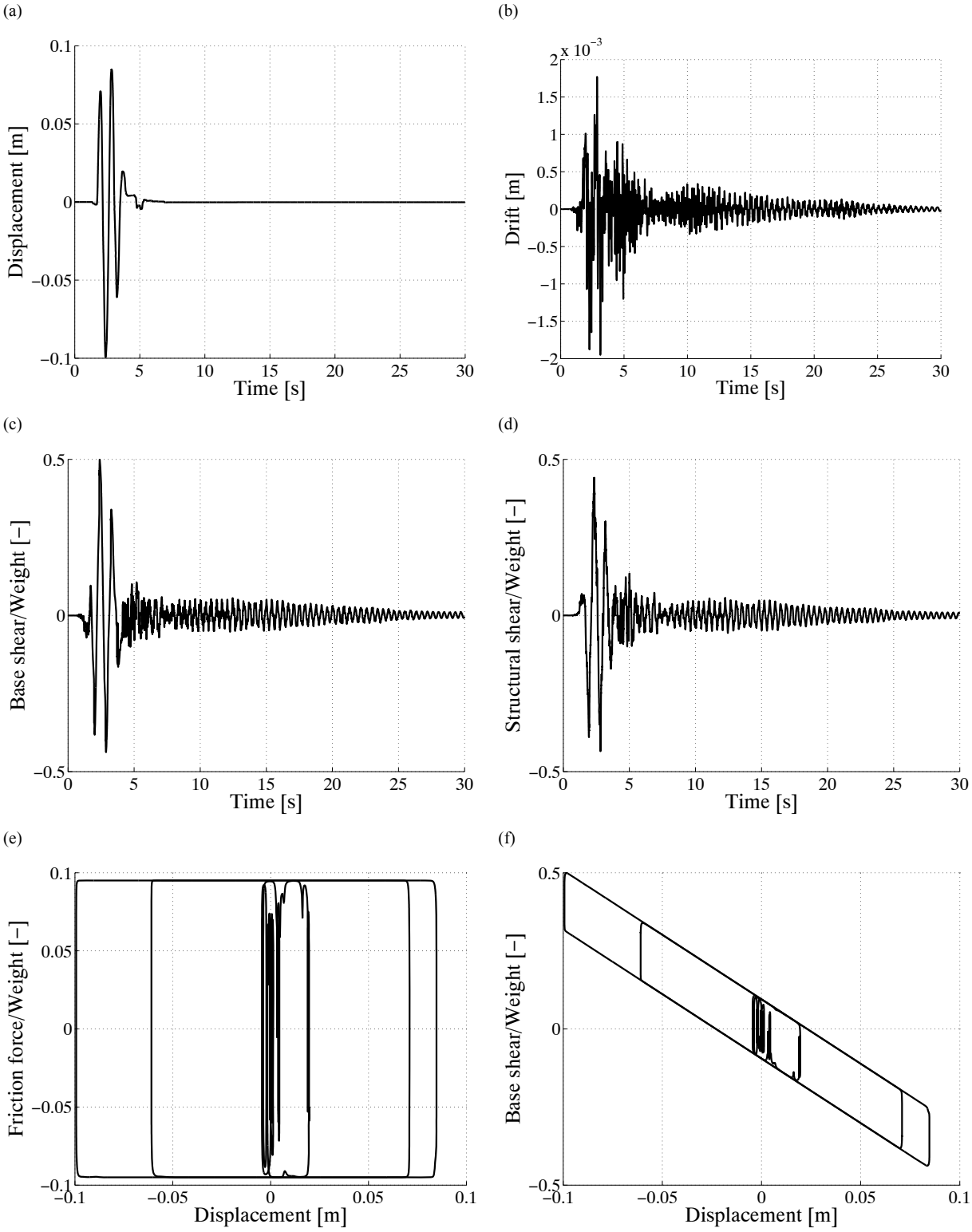

Figure 8.49 Structural response to Bam earthquake: (a) base (bearing) displacement, (b) drift at the top of the structure (sixth floor), (c) base shear, (d) structural shear (measured at its first floor), (e) Friction force, and (f) restoring force versus sliding displacement

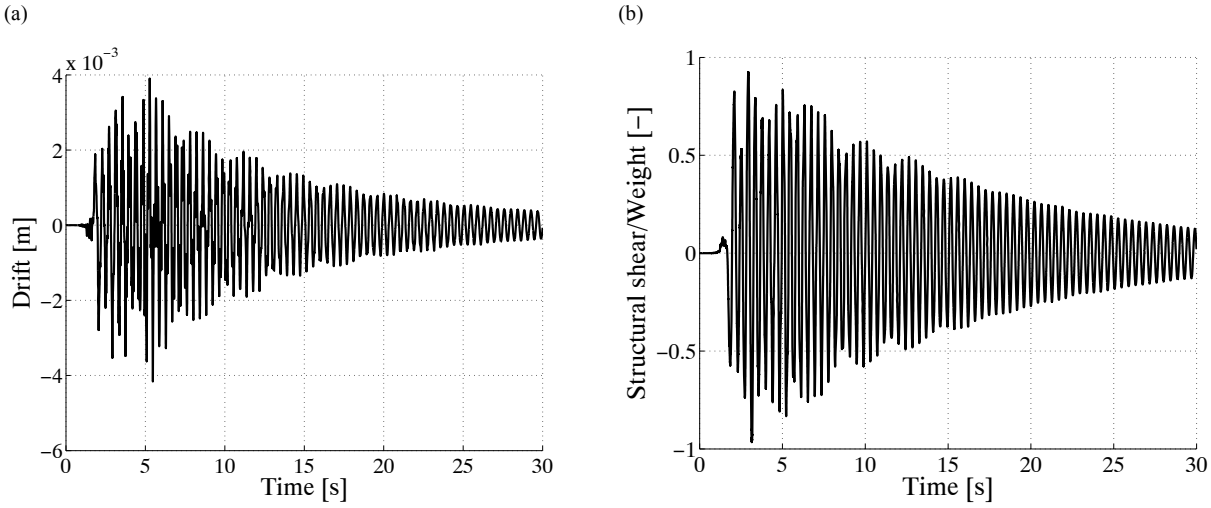

Figure 8.50 Structural response of the fixed-base structure to Bam earthquake: (a) drift at the top of the structure (sixth floor), and (b) structural shear (measured at its first floor).

Results of the first three analyses are in good agreement with those reported by [Mokha et al., 1990]. It proves that it is possible to simulate the response of friction-isolated systems with the developed model based on the modal analysis.

8.6 Conclusions

In this chapter, first of all a one degree-of-freedom model is presented and its response to harmonic and non-harmonic loads have been studied. Parameters influencing the dynamic response of such a system, as for example the intensity of input excitations, frequency content of the excitation, and friction coefficient between sliding layers, are then introduced and their effects are discussed.

To study the interaction between structural and bearing modules a two degrees-of-freedom model is developed and its response to a triangular excitation is then investigated. To prove the efficiency of sliding bearings the response of such a system is compared with the response of a fixed-base two-degree-of-freedom system. It has been shown that as a result of isolation, base shear acting on the first degree-of-freedom and drift in the second degree-of-freedom are reduced considerably.

An isolated steel structure built on a shaking table is then simulated using a multi-degree-of-freedom planar model developed in this research. To study the response of such a system comprehensively, several accelerogram with different characteristics, as for example the max peak ground acceleration, duration of the excitation, frequency content, etc. have been considered. Results of the numerical simulation are then compared with results of the experiment.

It has been shown that base shear in a sliding-based isolated system is three to five times smaller than the one in a fixed-base structure. This can be achieved at the cost of a sliding displacement in bearings.

As the magnitude of an earthquake increases, the sliding displacement becomes larger. For near source cases, to restrict the maximum sliding displacement, a higher amount of friction

coefficient or an extra damping source is required. The sliding displacement anticipated by simulation matches the result reported by the experiment very well.

As a result of concavity of sliding plates in all investigated cases, bearings return back to their original configurations with a good degree of precision. This complies with results of shaking table tests done by [Mokha et al., 1990].

Permitting a structure sliding over its foundation distracts earthquake-induced forces from the structural system. In this way, drift in isolated systems is much smaller in comparison with the classical fixed-base systems. Drifts anticipated by the numerical simulation here are smaller than those reported by the experiment, mainly due to a stiffer numerical model for the structural system.

Chapter 9

Conclusions and Further Works

In friction pendulum systems, the structure is decoupled from its foundation by several sliding bearings. They can slide over a concave surface coated with a material with a very low friction coefficient. The response of such systems is complicated and combined of two phases of sticking and sliding. Numerical simulation of these systems is a challenging task because of their nonlinearity. In this chapter, firstly a brief review of numerical models developed, will be presented. Then main results of the study will be discussed. At last, some topics for further research have been proposed.

9.1 A review of modelling and results

The main goal of this study was to propose a numerical model to simulate the response of friction-isolated structures, in which the model must be simple, accurate, and practical. To this end three types of models are proposed, which will be reviewed here briefly.

A very large participation factor of the first mode of vibration in base-isolated systems motivated the idea to simulate the dynamic response of such systems with a simple one degree-of-freedom model. Differential equation governing the response of such a system is solved with a piecewise exact solution. The solution is composed of two parts: transient and particular solutions. Regarding initial conditions in each time step, unknown parameters of the solution can be calculated. As the closed form solution has been applied, it is not required to use very short time steps. In case of possibility of a phase change, however, very short time steps must be applied, so that the exact point of a phase change can be found within the desired accuracy. Phase changes are controlled by means of a stick-slip criterion that is based on forces acting on the mass, namely inertial and restoring forces as a result of the geometrical stiffness (if it exists). This kind of model implies a rigid structural response. This is a logical assumption, as seismic forces transmitted to an isolated structure are much smaller than those transferred into a classical fixed-base structure. Results simulated with this model are then compared with those reported elsewhere as for instance by [Petersen, 2005], in which there is a good agreement.

To study the interaction between an isolation block (sliding bearing) and the structure over it in a friction-isolated system, the model is developed into a two degree-of-freedom system, in which the first degree-of-freedom is corresponding the isolation module and the second one is for the structural block. In an iterative process, two differential equations governing the response of the system are solved. To decrease computational costs of the simulation an adaptive time digitization algorithm has been developed.

At last, the model is generalized to simulate a planar MDOF system, in which by the initiation of sliding several new elements are activated, regarding the number of sliding bearings in the system. In sticking phases, however, added elements are deactivated and the rest of the

system is simulated as a classical fixed-base structure. As the nonlinearity of the response of such a system is restricted only to phase changes and in every single time step, system properties do not change, it is possible to apply modal analysis to simulate the response of such systems. First few mode shapes of isolated systems govern the main part of the structural response. Because of orthogonality of mode shapes in the modal space, it is possible to consider only these mode shapes instead of taking all of them as what is done in direct integration method. This reduces computational costs of simulation considerably.

The set of differential equations controlling such a system must be written in a matrix form, so that it can be transformed into the modal space. Then the desired decoupled differential equations can be solved easily. Subsequently, results must be transformed back into the original space, as they cannot be interpreted in the modal space. For instance, it cannot be determined whether a phase change has happened or not. After controlling the possibility of a phase change in the original space, if no phase change has happened the same process will be done again for next time steps. Otherwise, time steps must be refined to fine the exact point of the phase change within the desired accuracy to activate/deactivate extra degrees-of-freedom.

To simulate these systems more realistically, a velocity-dependent friction coefficient is applied (in sliding phases only).

Results of numerical simulations with the developed numerical model are in good agreement with those cited in reports. Forces in a friction-isolated system are three to four times smaller than those in a fixed-base structure. The amount of the base sliding displacement depends on the intensity of excitations and the frequency content of the loading.

It has been shown that the efficiency of the isolation method is a function of the earthquake's magnitude (level of loading). Low levels of excitations activate sliding bearings too late or even not at all. As far as no sliding has been initiated, i.e. sticking phase, the structural response of an isolated system is the same as a fixed-base set.

The friction coefficient is the other factor controlling the initiation of sliding in an isolated set (stick-slip criterion). Sliding bearings with larger friction coefficients are activated later than those with a lower friction coefficient. Hence, it is quite important to keep the friction coefficient for the whole life-time of an isolated structure in the same range as it is designed for. Therefore, isolation modules must be kept in a closed environment, preventing dust and water to gather in the bearing's module.

The frequency content of excitations plays an important role in the structural response of isolated structures. Isolated structures are susceptible to long-period waves with a dominant frequency of vibration near the isolation frequency. Impulse-shape waves can produce large sliding displacements. An additional damping mechanism or a larger friction coefficient avoids large sliding displacement and reduces base shear in bearings.

The concavity of the sliding base plates in friction pendulum systems produces a restoring force, which creates a tendency in the set to come back to its original configuration after cessation of excitations. It has been shown that it does not have any negative effect on the efficiency of the isolation method. The choice of using a flat surface instead of a concave one depends mainly on the nature of local excitations. For instance, sites near an active fault are not appropriate for this choice. It depends also on the arrangement of neighbouring structures.

The proposed multi-degree-of-freedom model in this study is much simpler in theory rather than the existing numerical model simulating the response of sliding-based isolated structures with a contact element, which makes this model more practical. Numerical results, at the same time, are in good agreement with results of practical tests. Because of application of modal analysis an adaptive time digitization process, numerical simulation with this model is

not time consuming. All these make this model an appropriate means to simulate the response of low-rise isolated buildings, in which uplifting is not a critical issue.

9.2 Outlook

Based on the numerical model proposed in this study several recommendations for further research can be made, among them:

- Development of a numerical model to simulate the response of highly damped friction-isolated structures to restrict sliding displacement in case of excitations with a very low frequency content or impulse shape waves. Off-diagonal terms of the damping matrix in a heavily damped structure are large and may not be neglected. So modal analysis may not be directly applicable and the model must be modified.
- Computation of axial force in sliding bearings to simulate frictional properties of bearings more realistically, as several experiments have proved that the friction coefficient between layers of Teflon and polished steel depends not only on the sliding velocity but also on the contact pressure.
- Adding a gap element to the model; so that uplifting can be simulated as well. In this way the model may be applied to high-rise buildings too.

Appendix A

Major Earthquakes since 1900

Year	Day-Month	Location	Latitude	Longitude	Deaths	M
1902	19-Apr	Guatemala	14.0N	91.0W	2000	7.5
	16-Dec	Turkestan	40.8N	72.6E	4500	-
1903	19-Apr	Turkey	39.1N	42.4E	1700	-
	28-Apr	Turkey	39.1N	42.5E	2200	6.3
1905	04-Apr	India	33.0N	76.0E	19000	8.6
	08-Sep	Italy, Calabria	39.4N	16.4E	2500	7.9
1906	31-Jan	Colombia	01.0N	81.5W	1000	8.9
	16-Mar	Taiwan	23.6N	120.5E	1300	7.1
	18-Apr	USA, San Francisco	38.0N	123.0W	2000+	8.3
	17-Aug	Chile, Santiago	33.0S	72.0W	20000	8.6
1907	14-Jan	Jamaica, Kingston	18.2N	76.7W	1600	6.5
	21-Oct	Central Asia	38.0N	69.0E	12000	8.1
1908	28-Dec	Italy, Messina	38.0N	15.5E	70000	7.5
1909	23-Jan	Iran, Silakhor	33.4N	49.1E	5500	7.3
1912	09-Aug	Turkey	40.5N	27.0E	1950	7.8
1915	13-Jan	Italy, Avezzano	42.0N	13.5E	29980	7.5
1917	21-Jan	Indonesia, Bali	08.0S	115.4E	15000	-
	30-Jul	China	28.0N	104.0E	1800	-
1918	13-Feb	China, Canton	23.5N	117E	10000	7.3
1920	16-Dec	China, Gansu	35.8N	105.7E	200000	8.6
1923	24-Mar	China	31.3N	100.8E	5000	7.3
	25-May	Iran, Torbateheydaria	35.3N	59.2E	2200	5.7
	01-Sep	Japan, Kanto	35.0N	139.5E	143000	8.3
1925	16-Mar	China, Yunnan	25.5N	100.3E	5000	7.1
1927	07-Mar	Japan, Tango	35.8N	134.8E	3020	7.9
	22-May	China	36.8N	102.8E	200000	8.3
1929	01-May	Iran, Koppe Dagh	38.0N	58.0E	3300	7.4

Year	Day-Month	Location	Latitude	Longitude	Deaths	M
1930	06-May	Iran, Salmas	38.0N	44.5E	2500	7.2
	23-Jul	Italy	41.1N	15.4E	1430	6.5
1931	31-Mar	Nicaragua	13.2N	85.7W	2400	5.6
1932	25-Dec	China, Gansu	39.7N	97.0E	70000	7.6
1933	02-Mar	Japan, Sanriku	39.0N	143.0E	2990	8.9
	25-Aug	China	32.0N	103.7E	10000	7.4
1934	15-Jan	India	26.6N	86.8E	10700	8.4
1935	20-Apr	Formosa	24.0N	121.0E	3280	7.1
	30-May	Pakistan, Quetta	29.6N	66.5E	30000	7.5
	16-Jul	Taiwan	24.4N	120.7E	2700	6.5
1939	25-Jan	Chile, Chillan	36.2S	72.2W	28000	8.3
	26-Dec	Turkey, Erzincan	39.6N	38.0E	30000	8.0
1940	10-Nov	Romania	45.8N	26.8E	1000	7.3
1942	26-Nov	Turkey	40.5N	34.0E	4000	7.6
	20-Dec	Turkey, Erbaa	40.9N	36.5E	3000	7.3
1943	10-Sep	Japan, Tattori	35.6N	134.2E	1190	7.4
	26-Nov	Turkey	41.0N	33.7E	4000	7.6
1944	15-Jan	Argentina, San Juan	31.6S	68.5W	5000	7.8
	01-Feb	Turkey	41.4N	32.7E	2800	7.4
	07-Dec	Japan	33.7N	136.2E	1000	8.3
1945	12-Jan	Japan	34.8N	137.0E	1900	7.1
	27-Nov	Pakistan	25.0N	60.5E	4000	8.2
1946	31-May	Turkey	39.5N	41.5E	1300	6.0
	10-Nov	Peru	08.3S	77.8W	1400	7.3
	20-Dec	Japan	32.5N	134.5E	1330	8.4
1948	28-Jun	Japan, Fukui	36.1N	136.2E	5390	7.3
	05-Oct	Turkmenistan	38.0N	58.3E	110000	7.3
1949	05-Aug	Ecuador, Ambato	01.2S	78.5E	6000	6.8
1950	15-Aug	India, Assam; Tibet	28.7N	96.6E	1530	8.7
1954	09-Sep	Algeria	36.0N	1.6E	1250	6.8
1957	27-Jun	USSR (Russia)	56.3N	116.5E	1200	-
	02-Jul	Iran, Mazandaran	36.2N	52.7E	1200	7.4
	13-Dec	Iran, Sahneh	34.4N	47.6E	1130	7.3
1960	29-Feb	Morocco	30.0N	9.0W	10000	5.9
	22-May	Chile	39.5S	74.5W	4000	9.5
1962	01-Sep	Iran, Qazvin	35.6N	49.9E	12230	7.3
1963	26-Jul	Yugoslavia, Skopje	42.1N	21.4E	1100	6.0
1966	19-Aug	Turkey, Varto	39.2N	41.7E	2520	7.1

Year	Day-Month	Location	Latitude	Longitude	Deaths	M
1968	31-Aug	Iran, Dasht e Bayaz	34.0N	59.0E	12000	7.3
1969	25-Jul	Eastern China	21.6N	111.9E	3000	5.9
1970	04-Jan	China, Yunnan	24.1N	102.5E	10000	7.5
	28-Mar	Turkey, Gediz	39.2N	29.5E	1100	7.3
	31-May	Peru	09.2S	78.8W	66000	7.8
1972	10-Apr	Iran, Southern (Fars)	28.4N	52.8E	5054	7.1
	23-Dec	Nicaragua	12.4N	86.1W	5000	6.2
1974	10-May	China	28.2N	104.0E	20000	6.8
	28-Dec	Pakistan	35.0N	72.8E	5300	6.2
1975	04-Feb	China	40.6N	122.5E	10000	7.4
	06-Sep	Turkey	38.5N	40.7E	2300	6.7
1976	04-Feb	Guatemala	15.3N	89.1W	23000	7.5
	06-May	Italy	46.4N	13.3E	1000	6.5
	25-Jun	New Guinea	04.6S	140.1E	422	7.1
	27-Jul	China, Tangshan	39.6N	118.0E	255000	8.0
	16-Aug	Philippines	06.3N	124.0E	8000	7.9
	24-Nov	Iran	39.1N	44.0E	5000	7.3
1977	04-Mar	Romania	45.8N	26.8E	1500	7.2
1978	16-Sep	Iran, Tabas	33.2N	57.4E	15000	7.8
1980	10-Oct	Algeria, El asnam	36.1N	1.4E	3500	7.7
	23-Nov	Italy, southern	40.9N	15.3E	3000	7.2
1981	11-Jun	Iran, Southern	29.9N	57.7E	3000	6.9
	28-Jul	Iran, Southern	30.0N	57.8E	1500	7.3
1982	13-Dec	W. Arabian Peninsula	14.7N	44.4E	2800	6.0
1983	30-Oct	Turkey	40.3N	42.2E	1342	6.9
1985	19-Sep	Mexico, Michoacan	18.2N	102.5W	9500	8.1
1986	10-Oct	El Salvador	13.8N	89.2W	1000	5.5
1987	06-Mar	Colombia	00.2N	77.8W	1000	7.0
1988	20-Aug	Nepal	26.8N	86.6E	1450	6.6
	07-Dec	Armenia, Spitak	41.0N	44.2E	25000	7.0
1990	20-Jun	Iran, western	37.0N	49.4E	40000	7.7
	16-Jul	Philippines, Luzon	15.7N	121.2E	1621	7.8
1991	19-Oct	India, northern	30.8N	78.8E	2000	7.0
1992	12-Dec	Indonesia, Flores	08.5S	121.9E	2500	7.5
1993	29-Sep	India, southern	18.1N	76.5E	9748	6.3
1995	16-Jan	Japan, Kobe	34.6N	135.0E	6000	6.9
	27-May	Sakhalin Island	52.6N	142.8E	1989	7.5
1997	10-May	Iran, Manjil	33.9N	59.7E	1560	7.5

Year	Day-Month	Location	Latitude	Longitude	Deaths	M
1998	04-Feb	Afghanistan	37.1N	70.1E	2323	6.1
	30-May	Afghanistan	37.1N	70.1E	4000	6.9
	17-Jul	Papua New Guinea	2.96S	141.9E	2183	7.1
1999	25-Jan	Colombia	4.46N	75.8W	1185	6.3
	17-Aug	Turkey	40.7N	30.0E	17118	7.4
	20-Sep	Taiwan	23.7N	121.0E	2297	7.6
2001	26-Jan	India, Bhuj	23.3N	70.3E	19988	7.7
2002	25-Mar	Afghanistan	35.9N	69.2E	1000	6.1
2003	21-May	Algeria	36.9N	3.71E	2266	6.8
	26-Dec	Iran, Bam	29.0N	58.3E	31000	6.6
2004	26-Dec	Sumatra	03.3N	95.9E	227898	9.1
2005	28-Mar	Indonesia	02.1N	97:0E	1313	8.6
	08-Oct	Pakistan	34.5N	73.6E	86000	7.6
2006	26-Jun	Indonesia	07.0N	110.5E	5749	6.3
				Total Death	**2115000**	

Source: National Earthquake Information Center, Golden, CO, http://neic.usgs.gov/neis/eqlists/eqsmajr.html.

Appendix B

Modified Mercalli Intensity Scale

Intensity level	Reaction of observers and types of damage
I	Not felt except by a very few people under especially favourable circumstances. No damage.
II	Felt only by a few persons at rest, especially on upper floors of buildings. Many people do not recognize it as an earthquake. No damage. Delicately suspended objects may swing.
III	Felt quite noticeably indoors, especially on upper floors of buildings. The vibration is like the passing of a truck, and the duration of the earthquake may be estimated. However, many people do not recognize it as an earthquake. No damage. Standing motor cars may rock slightly.
IV	During the day, felt indoors by many, outdoors by a few. At night, some people are awakened. The sensation is like a heavy truck striking the building. Dishes, windows, and doors are disturbed. Walls make a creaking sound. Standing motor cars rock noticeably.
V	Felt by nearly everyone, many awakened. Some dishes, windows, etc., broken. A few instances of cracked plaster and unstable objects overturned. Disturbances of trees, poles, and other tall objects sometimes noticed. Pendulum clocks may stop.
VI	Felt by everyone. Many people are frightened and run outdoors. There is slight structural damage. Some heavy furniture is moved, and there are a few instances of fallen plaster or damaged chimneys.
VII	Everyone runs outdoors. It is noticed by persons driving motor cars. Negligible damage in buildings of good design and construction, slight to moderate damage in well-built ordinary structures, and considerable damage in poorly built or badly designed structures. Some chimneys are broken.
VIII	Persons driving motor cars are disturbed. Slight damage in specially designed structures. Considerable damage in ordinary substantial buildings, with partial collapse. Great damage in poorly built structures. Panel walls are thrown out of frame structures. There is the fall of chimneys, factory stacks, columns, monuments, and walls. Heavy furniture is overturned. Sand and mud are ejected in small amounts, and there are changes in well-water levels.
IX	Considerable damage in specially designed structures. Well-designed frame structures are thrown out of plumb. There is great damage in substantial buildings with partial collapse. Buildings are shifted off of their foundations. The ground is conspicuously cracked, and underground pipes are broken.
X	Some well-built wooden structures are destroyed. Most masonry and frame structures are destroyed, including the foundations. The ground is badly cracked. There are bent train rails, a considerable number of landslides at river banks and steep slopes, shifted sand and mud, and water is splashed over their banks.
XI	Few, if any, masonry structures remain standing. Bridges are destroyed, and train rails are greatly bent. There are broad fissures in the ground, and underground pipelines are completely out of service. There are earth slumps and landslips in soft ground.
XII	Waves are seen on the ground surface. The lines of sight and level are distorted. Total damage with practically all works of construction greatly damaged or destroyed. Objects are thrown upward into the air.

Appendix C

2-DOF Model Algorithm

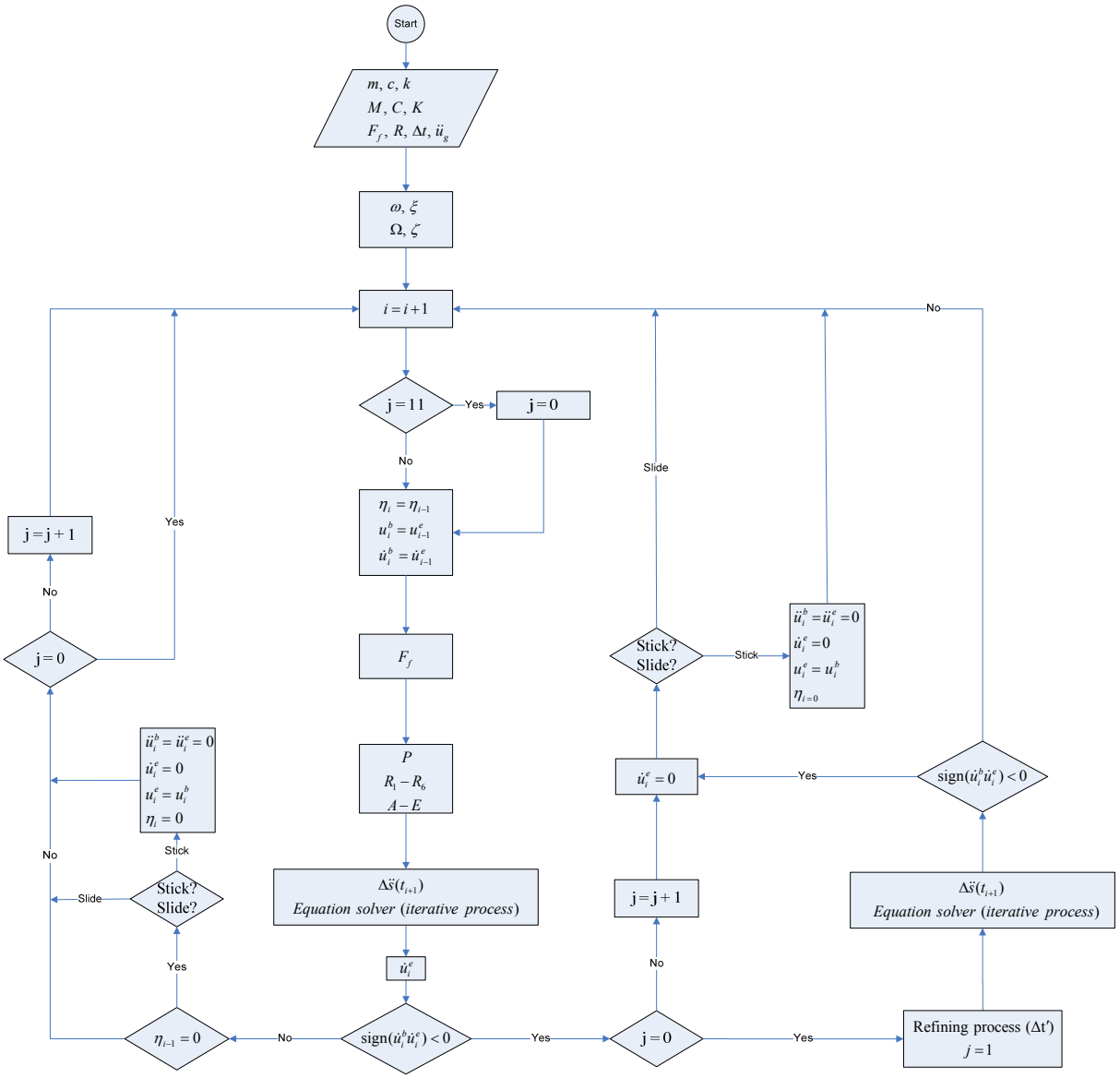

m	Structural mass	M	Base mass
c	Structural damping	C	Base damping
k	Structural stiffness	K	Base stiffness
R	Radius of curvature of the sliding surface	F_f	Friction force
ω	Structural natural frequency	Ω	Base natural frequency
ξ	Structural damping ratio	ζ	Base damping ratio
i	Time counter	j	Time counter for refined time steps
u_i^b	Base displacement at the beginning of the time step *Nr. i*	$\dot{u}_i^b$	Base velocity at the beginning of the time step *Nr. i*
u_{i-1}^e	Base displacement at the end of the time step *i-1*	$\dot{u}_{i-1}^e$	Base velocity at the end of the time step *i-1*
η_i	Phase state variable of the current time step (zero for sticking and one for sliding)	η_{i-1}	Phase state variable of the previous time step (zero for sticking and one for sliding)
Δt	Time step	$\Delta\ddot{s}$	Variation of the calculated structural acceleration in two consecutive iterations
P	The known part of the loading (Equation 7.58)	$\ddot{u}_g$	Ground acceleration

Appendix D

MDOF Model Algorithm

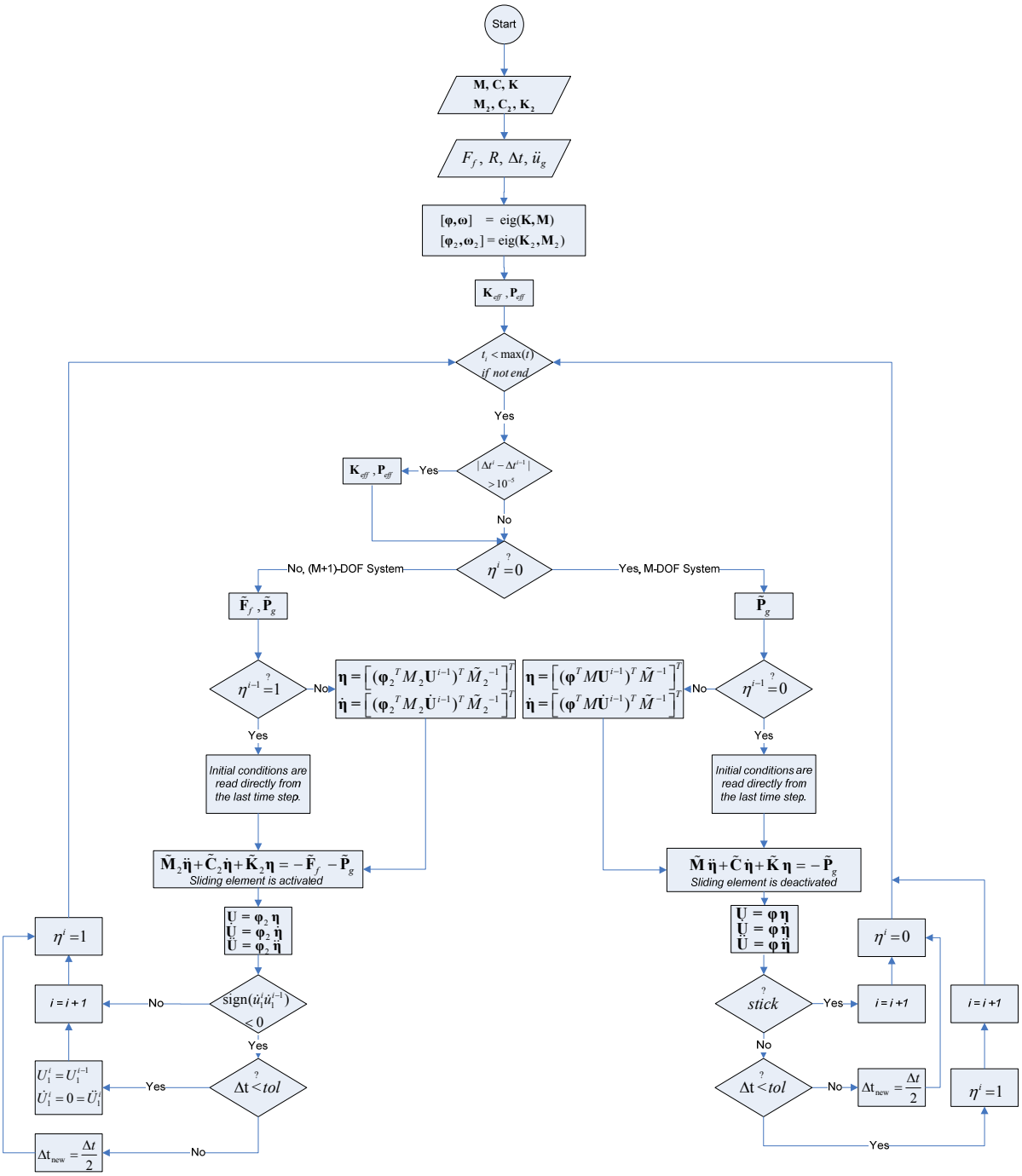

$\mathbf{M}$	Mass matrix of the Superstructure	$\mathbf{M_2}$	Mass matrix of the whole set
$\mathbf{C}$	Damping matrix of the Superstructure	$\mathbf{C_2}$	Damping matrix of the whole set
$\mathbf{K}$	Stiffness matrix of the Superstructure	$\mathbf{K_2}$	Stiffness matrix of the whole set
$\tilde{\mathbf{M}}$	Modal mass matrix of the super-structure	$\tilde{\mathbf{M}}_2$	Modal mass matrix of the whole set
$\tilde{\mathbf{C}}$	Modal damping matrix of the super-structure	$\tilde{\mathbf{C}}_2$	Modal damping matrix of the whole set
$\tilde{\mathbf{K}}$	Modal stiffness matrix of the super-structure	$\tilde{\mathbf{K}}_2$	Modal stiffness matrix of the whole set
$\boldsymbol{\omega}$	Eigenfrequencies of the superstructure	$\boldsymbol{\omega_2}$	Eigenfrequencies of the whole set
$\boldsymbol{\varphi}$	Eigenvector of the superstructure	$\boldsymbol{\varphi_2}$	Eigenvector of the whole set
i	Time counter	*tol*	Tolerance (10^{-6})
Δt	Time step	Δt_{new}	Refined time step
$\boldsymbol{\eta}$	Modal displacement	$\mathbf{U}$	Displacement matrix of the whole set
$\dot{\boldsymbol{\eta}}$	Modal velocity	$\dot{\mathbf{U}}$	Velocity matrix of the whole set
$\ddot{\boldsymbol{\eta}}$	Modal acceleration	$\ddot{\mathbf{U}}$	Acceleration matrix of the whole set
$\mathbf{F}_f$	Friction force matrix	$\mathbf{P}_g$	Matrix of the inertial force
$\tilde{\mathbf{F}}_f$	Modal friction force matrix	$\tilde{\mathbf{P}}_g$	Matrix of the modal inertial force
η^i	Phase state variable of the current time step (zero for sticking and one for sliding)	η^{i-1}	Phase state variable of the previous time step (zero for sticking and one for sliding)
$\mathbf{K}_{eff}$	Effective stiffness (CAA method)	$\mathbf{P}_{eff}$	Effective load (CAA method)

Bibliography

Al Hussaini, T., Zayas, V., Constantinou, M. C. (1994), ''Seismic isolation of multi-storey frame structures using spherical sliding isolation system'', *National Centre for Earthquake Engineering Research*, Report Nr. NCEER-94-0007, State Univ. of New York, Buffalo, USA.

Almazan, J. L., Llera, J. C., Inaudi, J. A. (1998), ''Modelling aspects of structures isolated with the friction pendulum systems'', *Earthquake engineering and structural dynamics*, 27, 845-867.

Almazan, J. L., Llera, J. C. (2002), ''Analytical model of structures with frictional pendulum isolators'', *Earthquake engineering and structural dynamics*, 31, 305-322.

Almazan, J. L., Llera, J. C. (2003), ''Physical model for dynamic analysis of structures isolated with FPS isolators'', *Earthquake engineering and structural dynamics*, 32, 1157-1184.

Bachmann, H. (1995), *Erdbebensicherung von Bauwerken*, Birkhaeuser Verlag, in German, Basel.

Berberian, M., *Earthquakes in Iran*, Encyclopedia Iranica, *www.iranica.com*.

Beucke, K. E., Kelly, J. M. (1985), ''Equivalent linearizations for practical hysteretic systems'', *Int. J. Non-linear Mechanics*, Vol. 23, No. 4, 211-238.

Bozorgnia, Y., Bertero, V. V. (2004), *Earthquake Engineering: From Engineering Seismology To Performance-Based Engineering*, CRC Press, USA.

Brüggemann, M. (2002), *Zur nichtlinearen Zeitbereichssimulation flüssigkeitsgefüllter Tankbauwerke unter Erdbebenanregung*, Dissertation, in German, Wuppertal University, Germany.

Chalhoub, M. S., Kelly, J. M. (1990),''Earthquake simulator testing of a combined sliding bearing and rubber bearing isolation system'', *Earthquake Engineering Research Centre*, Report Nr. UCB/EERC-87/04, University of California, Berkeley, CA.

Chen, W. F. (1999), *Structural Engineering Handbook*, CRC Press, USA.

Chen, W. F., Scawthorn, C. (2003), *Structural Engineering Handbook*, CRC Press, USA.

Chopra, A. (2001), *Dynamics of Structures: Theory and Applications to Earthquake Engineering*, 2nd edition, Prentice Hall, New Jersey.

Clough, R. W., Penzien, J. (2003), *Dynamics of Structures*, McGraw-Hill.

Constantinou, M. C., Adnan, M. A. (1987), ''Dynamic of soil-based-isolated structure systems: Evaluation of two models for yielding systems'', Report to the *National Science Foundation*, Dept. of Civil Eng., Drexel University, PA.

Constantinou, M. C., Caccese, J., Harris, H. (1987), ''Frictional characteristics of Teflon-Steel interfaces under dynamic conditions'', *Earthquake engineering and structural dynamics*, 15, 751-759.

Constantinou, M. C., Mokha, A., Reinhorn, A. M. (1990), ''Teflon bearings in base isolation II: Modelling'', *J. Struc. Eng.*, 116 (2), 455-473.

Cook, R.D. (1995), *Finite Element Modelling for Stress Analysis*, John Wiley & Sons, University of Wisconsin-Madison, USA.

Day, R. W. (2002), *Geotechnical Engineering Handbook*, McGraw-Hill, New York.

Den Hatog, J. P. (1956), *Mechanical vibration*, 4th edition, McGraw-Hill, USA.

Derham, C. J., Kelly, J. M. (1985), ''Non-linear natural rubber bearings for seismic isolation'', *Nuclear Eng. Design*, Vol. 84, No. 3, 417-428.

Fan, F. G., Ahmadi, G. (1990), ''Floor response spectra for base-isolated multi-storey structues'', *Earthquake engineering and structural dynamics*, 19, 377-388.

Hamidi, M., El Naggar, M. H., Vafai, A., Ahmadi, G. (2003), ''Seismic isolation of buildings with sliding concave foundation'', *Earthquake engineering and structural dynamics*, 32, 15-29.

Hosseini, S. B. (1999), *Neue Planungskonzepte für ländliche Siedlungen in Erdbebengefährdeten Gebieten im Nordiran*, Dissertation, in German, Stuttgart University, Germany.

Iran Daily (2006), *www.iran-daily.com*.

Jamali, N., Zahlten, W. (2006), ''Numerical simulation of base-isolated systems sliding on concave surfaces'', *1st European Conference on Earthquake Engineering and Seismology*, Geneva, Switzerland.

Jamali, N., Zahlten, W., Neuhaus, C. (2007) ''Modal analysis of friction based-isolated structures'', *5th International Conference on Seismology and Earthquake Engineering*, Tehran, Iran.

Jamali, N., Zahlten, W., Neuhaus, C. (2008), ''Modal analysis of isolated structures with friction pendulum systems'', *7th European Conference on Structural Dynamics*, Southampton, England.

Kanamori, H. (1977), ''The energy release in great earthquakes'', *Journal of geophysical research*, 82, 2981-2987.

Kelly, J. M. (1988), ''Base isolation in Japan, 1988'', *Earthquake Engineering Research Centre*, Report Nr. UCB/EERC-88/20, University of California, Berkeley, CA.

Kelly, J. M. (1996), *Earthquake resistant design with rubber*, Springer, 2nd edition, London.

Kelly, J. M. (1999), ''The roll of damping in seismic isolation'', *Earthquake engineering and structural dynamics*, 28, 3-20.

Lin, S., Tadjbakhsh, I. C., Papageorgian, A. S., Ahmadi, G. (1990), ''Performance of earthquake isolation systems'', *J. of Eng. Mech.*, ASCE, 116, 446-461.

Lin, S., Ahmadi, G., Tadjbakhsh, I. C. (1991), ''Performance of sliding resilient–friction base isolation systems'', *J. of Struc. Eng.*, ASCE, 117, 165-181.

Lin, T. W., Hone, C. C. (1993), ''Base isolation by free rolling rods under basement'', *Earthquake engineering and structural dynamics*, 22, 261-273.

Makris, N., Chang, S. P. (1998), ''Effects of damping mechanisms on the response of seismically isolated structures'', *Pacific Earthquake Engineering Research Center*, University of California, Berkeley, CA.

MATLAB, *reference guide*, The Mathworks Inc., Natick, MA.

Meskouris, K. (1999), *Baudynamik: Modelle, Methoden, Praxisbeispiele*, Ernst & Sohn, in German, Germany.

Meskouris, K., Hinzen, K. G. (2003), *Bauwerke und Erdbeben: Grundlage, Anwendung, Beispiele*, Vieweg, in German, Germany.

Mistler, M., Butenweg, C., Meskouris, K. (2006), ''Modeling methods of historic masonry buildings under seismic excitation'', *Journal of Seismology*, 10(4), 497-510.

Mohasseb, S. (1988), ''Non-linear seismic analysis of fully base isolated structures on flexible soils'', *Institute für Baustatik und Konstruktionn*, Report Nr. 162, Zürich, Switzerland.

Mokha, A. S., Constantinou, M. C., Reinhorn, A. M. (1990), ''Experimental study and analytical prediction of earthquake response of a sliding isolation system with a spherical surface'', *National Centre for Earthquake Engineering Research*, Report Nr. NCEER-90-0020, State University of New York, Buffalo, USA.

Mokha, A. S., Constantinou, M. C., Reinhorn, A. M. (1990), ''Teflon bearings in base isolation I: Testing'', *J. Struc. Eng.*, 116 (2), 438-454.

Mokha, A. S., Constantinou, M. C., Reinhorn, A. M. (1991), ''Further results on frictional properties of Teflon bearings'', *J. Struc. Eng.*, 117 (2), 622-626.

Mokha, A. S., Constantinou, M. C., Reinhorn, A. M. (1993), ''Verification of friction model of Teflon bearings under triaxial load'', *J. Struc. Eng.*, 119 (1), 240-261.

Mokha, A. S., Amin, N., Constantinou, M. C., Zayas, V. (1996), ''Seismic isolation retrofit of large historic buildings'', *Earthquake engineering and structural dynamics*, 122, 298-307.

Mostaghel, N., Hejazi, M., Tanbakuchi, J. (1983), ''Response of sliding structures to harmonic support motion'', *Earthquake engineering and structural dynamics*, 11, 355-366.

Mostaghel, N., Tanbakuchi, J. (1983), ''Response of sliding structures to earthquake support motion'', *Earthquake engineering and structural dynamics*, 11, 729-748.

Mostaghel, N., Khodaverdian, M. (1987), ''Dynamic of resilient friction base isolator (R-FBI)'', *Earthquake engineering and structural dynamics*, 15, 379-390.

Mostaghel, N., Khodaverdian, M. (1988), ''Seismic response of structures supported on R-FBI system'', *Earthquake engineering and structural dynamics*, 16, 839-854.

Mostaghel, N., Davis, T. (1997), ''Representation of Coulomb friction for dynamic analysis'', *Earthquake engineering and structural dynamics*, 26, 541-548.

Naeim, F., Kelly, J. M. (1999), *Design of Seismic Isolated Structures from Theory to Practice*, John Wiley & Sons, New York.

Nawrotzki, P. (2001), ''Seismic protection of structures by viscoelastic elements'', *The 8th east Asia-Pacific conference on structural engineering and construction*, Nanyang Technological University, Singapore.

Park, Y. J., Wen, Y. K., Ang, A. H. (1986), ''Random vibration of hysteretic systems under bi-directional ground motions'', *Earthquake engineering and structural dynamics,* 14, 543-557.

Petersen, C. (1996), *Dynamik der Baukonstruktion*, Vieweg Verlag, in German, Wiesbaden, Germany.

Petersen, C. (2005), ''Studien zum Einsatz von Erdbebenschutzsystemen'', *Berichte aus dem konstruktiven Ingenieurbau ISSN 1431-5122*, Universität der Bundeswehr München, in German, München, Germany.

Pocanschi, A., Phocas, M. C. (2003), ''Kräfte in Bewegung, die Techniken des Erdbebensicheren Bauens'', Teubner Verlag, in German, Germany.

Richter, C. F. (1935), ''An instrumental earthquake magnitude scale'', *Bulletin of seismological society of America*, 25, 1-32.

Roussis, P. C., Constantinou, M. C. (2006), ''Experimental and analytical studies of structures seismically isolated with an uplift-restraining friction pendulum system'', *Earthquake engineering and structural dynamics,* 35, 595-611.

Roussis, P. C., Constantinou, M. C. (2006), ''Uplift-restraining friction pendulum seismic isolation system'', *Earthquake engineering and structural dynamics,* 35, 577-594.

Shabana, A. (2001), *Computational Dynamics*, John Willey & Sons, 2nd edition,USA.

Shampione, L. F. (1994), *Numerical Simulation of Ordinary Differential Equation*, Chapman & Hall.

Soong, T. T., Constantinou, M. C. (1994), *Passive and Active Structural Vibration Control in Civil Engineering*, Springer, Wien.

Su, L., Ahmadi, G., Tadjbakhsh, I. G. (1989), ''A comparative study of performances of various base isolation systems'', *Earthquake engineering and structural dynamics,* 18, 11-32.

Suy, H. M. R. (2005), *Nonlinear Dynamic Analysis of a Structure with a Friction-Based Seismic Base Isolation System*, Master thesis, Eindhoven University of Technology, Netherland.

Tsai, C. S, Chen, B. J., Chiang, T. C. (2003), ''Experimental and computational verification of reasonable design formulae for base-isolated structures'', *Earthquake engineering and structural dynamics*, 32, 1389-1406.

Tsai, C. S, Chiang, T. C. (2005), ''Experimental evaluation of piecewise exact solution for predicting seismic response of spherical sliding type isolated structure'', *Earthquake engineering and structural dynamics*, 34, 1027-1046.

United States Geological Survey (USGA), *www.usgs.org*.

Wen, Y. K. (1976), ''Method for random vibration of hysteretic systems'', *J. of Eng. Mech.*, ASCE, 102, 249-263.

Wenk, T. (1992), ''Studien zu Zeitverläufen der Bodenbewegung und zu der Antwortspektren'', Institut für Baustatik und Konstruktion, ETH Zürich, in German.

Westermo, B., Udwadia, F. (1983), ''Periodic response of a building to harmonic excitations'', *Earthquake engineering and structural dynamics*, 11, 135-146.

Yang, Y. B., Lee, T. Y., Tsai, I. C. (1990), ''Response of multi-degree-of-freedom structures with sliding supports'', *Earthquake engineering and structural dynamics*, 19, 739-752.

Zayas, V., Low, S., Mahin S. (1987), ''The FPS earthquake protection system: experimental report'', *Earthquake Engineering Research Centre*, Report Nr. UCB/EERC-87/01, Univ. California, Berkeley, CA.

Zhao, B., Lu, X., Wu, M., Mei, Z. (2000), ''Sliding mode control of buildings with base isolation hybrid protective system'', *Earthquake engineering and structural dynamics*, 29, 315-326.

Zhou, Q., Lu, X., Wang, Q., Feng, D., Yao, Q. (1998), ''Dynamic analysis on structures base-isolated by a ball system with restoring property'', *Earthquake engineering and structural dynamics*, 27, 773-791.

Berichte aus dem Konstruktiven Ingenieurbau
Bergische Universität Wuppertal

Heft 1 Andres, M.: Zum Stabilitätsnachweis von Schalentragwerken aus Hochleistungsbeton, 2004.

Heft 2 Wörmann, R.: Zur Erfassung hygrothermischer Einflüsse auf das nichtlineare Trag- und Schädigungsverhalten von Stahlbetonflächentragwerken, 2004.

Heft 3 Piel, W.: Zur Erhöhung der Durchstanztragfähigkeit von Flachdecken mit Stahlverbundsystemen, 2004.

Heft 4 Mahran, E.: Finite-Infinite-Elemente-Modellierung zur Simulation der Boden-Bauwerk-Flüssigkeit-Interaktion unter dynamischer Anregung, 2004.

Heft 5 Eusani, R.: Zur numerischen Zeitbereichssimulation der Aeroelastischen Instabilität bei Seilbrücken, 2005.

Heft 6 Stracke, J.: Flachdecken aus Konstruktions - Leichtbeton, 2005.

Heft 7 Hanswille, G., Porsch, M., Üstündağ, C.: Versuchsbericht über die Durchführung von 77 Push-Out-Versuchen im Rahmen des Forschungsprojektes „Modellierung von Schädigungsmechanismen zur Beurteilung der Lebensdauer von Verbundkonstruktionen aus Stahl und Beton“, Projekt C8 im Sonderforschungsbereich 398, 2007.

Heft 8 Schäfer, M.: Zum Tragverhalten von Flachdecken mit integrierten hohlkastenförmigen Stahlprofilen, 2007.

Heft 9 Üstündağ, C.: Beitrag zur Bemessung von Verbundträgern unter ermüdungswirksamen Beanspruchungen, 2007.

Heft 10 Hanswille, G., Porsch, M.: Versuchsbericht über die Durchführung von 36 Push-Out-Versuchen.

Heft 11 Hanswille, G., Porsch, M.: Metallurgische Untersuchungen an Schweißnahtverbindungen.

Heft 12 Jamali, N.: On the Numerical Simulation of Friction-Isolated Structures.